ResearchGate

See discussions, stats, and author profiles for this publication at: https://www.researchgate.net/publication/234009982

SERS Tags: Novel Optical Nanoprobes for Bioanalysis

ARTICLE *in* CHEMICAL REVIEWS · DECEMBER 2012

Impact Factor: 46.57 · DOI: 10.1021/cr300120g · Source: PubMed

CITATIONS
235

READS
452

3 AUTHORS:

Yunqing Wang
Chinese Academy of Sciences
26 PUBLICATIONS **918** CITATIONS
SEE PROFILE

Bing Yan
Shandong University
187 PUBLICATIONS **4,612** CITATIONS
SEE PROFILE

Lingxin Chen
Chinese Academy of Sciences
216 PUBLICATIONS **4,820** CITATIONS
SEE PROFILE

Available from: Yunqing Wang
Retrieved on: 20 January 2016

CHEMICAL REVIEWS

Review

pubs.acs.org/CR

SERS Tags: Novel Optical Nanoprobes for Bioanalysis

Yunqing Wang,[†] Bing Yan,[‡] and Lingxin Chen*,[†]

[†]Key Laboratory of Coastal Zone Environmental Processes, Yantai Institute of Coastal Zone Research, Chinese Academy of Sciences, Yantai 264003, China

[‡]School of Chemistry and Chemical Engineering, Shandong University, Jinan 250100, China

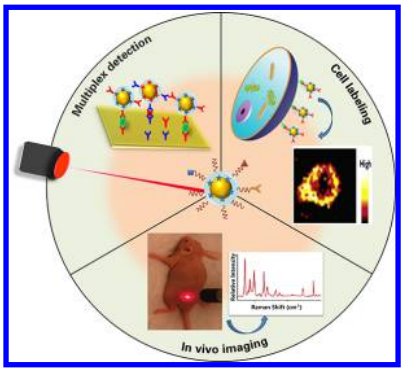

CONTENTS

1. Introduction 1391
1.1. Fundamental Theory of Surface-Enhanced Raman Scattering 1392
1.2. Optical Properties of SERS Tags 1392
2. Synthesis of SERS Tags 1393
2.1. Noble Metal Nanosubstrates 1393
2.1.1. Single Particle-Based SERS Substrates 1393
2.1.2. Nanoparticle Cluster-Based Substrates 1396
2.2. Raman Reporter Molecules 1396
2.2.1. Selection Principles and Reporter Types 1396
2.2.2. Self-Assembled Monolayer Coverage Strategy 1397
2.3. Surface Coating for Protection 1397
2.3.1. Biomolecule Coating 1397
2.3.2. Polymer Coating 1397
2.3.3. Liposome Coating 1398
2.3.4. Silica Coating 1399
2.4. Attachment of Targeting Molecules 1400
3. Bioanalysis Applications 1401
3.1. Ionic and Molecular Detection 1401
3.2. Pathogen Detection 1402
3.3. Live-Cell Imaging 1404
3.3.1. Cancer Marker Detection 1404
3.3.2. Intercellular Microenvironment Sensing 1405
3.4. Tissue SERS Imaging 1406
3.5. *In Vivo* SERS Imaging 1407
4. Challenges and Perspectives 1409
4.1. Reproducible Signal of SERS Tags 1409
4.1.1. Precisely Controlled Hot Spots for Nanosubstrates 1409
4.1.2. Calibration of SERS Intensities and Enhancements 1413
4.2. Improving Multiplexing Capability 1415
4.3. Reduced Size for Subcellular Imaging 1417
4.4. Development of Multifunctional Nanoplatforms 1418
4.4.1. Magnetic SERS Dots 1418
4.4.2. Multimodal Imaging Dots 1418
4.4.3. SERS Tag-Based Therapeutic Systems 1420
4.5. Biocompatibility 1422
5. Conclusions and Remarks 1422
Author Information 1423
Corresponding Author 1423
Notes 1423
Biographies 1423
Acknowledgments 1423
References 1423

1. INTRODUCTION

Surface-enhanced Raman scattering (SERS) is an ultrasensitive vibrational spectroscopic technique to detect molecules on or near the surface of plasmonic nanostructures, greatly extending the role of standard Raman spectroscopy.[1] Since its discovery in the 1970s,[2−4] SERS has been applied to many analyses, especially in biochemistry and life sciences.[5−11] The classic application is the direct sensing of various analytes attached to a metallic SERS substrate, yielding both qualitative and quantitative information based on the analytes' SERS spectra.[12]

More recently, this technique has been used to design novel nanoprobes named "SERS tags" that combine metallic nanoparticles (NPs) and specific organic Raman reporter molecules. Such SERS-active nanoprobes produce strong, characteristic Raman signals and can be used to indirectly sense the target molecules by using laser Raman spectrometry or SERS microscopy, demonstrating optical labeling functions similar to those of external chromophores such as organic dyes and fluorescent quantum dots (QDs). However, this kind of probe has the ultrasensitivity, multiplexing, and quantitative abilities of the SERS technique, and it shows extraordinary features for bioanalysis.

Despite tremendous interest in developing SERS tags, research in this area has fallen behind that of other nanoprobes such as QDs and dye-doped nanobeads.[13] One reason for this is that early Raman instrumentation is expensive and can be locally set up only by specialized experts, with fair optical performance. The other is that the mechanisms and fundamental principles of SERS are not as well understood as those of fluorescence. Recent advances in commercial Raman spectrometers and Raman microscopes make it possible to acquire sensitive and reproducible Raman signals and have greatly increased the widespread use of Raman-based detection

Received: March 21, 2012
Published: December 28, 2012

 © 2012 American Chemical Society dx.doi.org/10.1021/cr300120g | *Chem. Rev.* 2013, 113, 1391−1428

techniques. Meanwhile, theoretical and experimental investigations of the relationship between noble metal nanosubstrates and SERS' enhancement ability (especially the discovery of single-molecule SERS),[14,15] as well as the related analytical technique advances, have been reported within the past few years.[13] These developments offer a platform for the growing application of SERS tags.

In this review, we will focus on the most recent advances in the use of SERS tags. First, we will give a brief overview of SERS mechanism and the basic concept of SERS tags. Next, we will discuss the synthesis and development of SERS tags and the tags' growing popularity for bioanalysis at different levels of molecular multiplex detection, for pathogen and live-cell sensing, and for tissues diagnosis and *in vivo* bioimaging. Finally, we will present the challenges and future perspectives of the field, such as creating reproducible signals for single-SERS tags, multifunctional nanoplatforms, and biocompatibility research.

1.1. Fundamental Theory of Surface-Enhanced Raman Scattering

SERS theory has been studied by many scientists, and several excellent reviews and books exist.[1,14−23] Here, two primary theoretical mechanism models, long-range electromagnetic (EM) enhancement and short-range chemical enhancement (CE), will be briefly introduced.

It is commonly thought that EM enhancements make a major contribution to the SERS phenomenon.[17,19] When incident light illuminates a noble metal NP, it causes collective oscillations of the NP's surface electrons, which is termed surface plasmon resonance (SPR).[12] When the frequency of incident light is resonant with a plasmon, then the metal NP will radiate a dipolar field and be coherent with the exciting electric field. This process leads to redistribution of the local field and a great enhancement of the EM field at a specific position around the NP (called a "hot spot"). A molecule near or adsorbed at the hot spot will experience much-enhanced incident intensity that excites its Raman mode. The scattered Raman signal will be further magnified in the same way, resulting in a greater increase in the total output. When both the incident light and the scattered signal of molecules are in resonance with the plasmon frequency, then the SERS signal is maximized, leading to the $|E|^4$ enhancement.[19] EM enhancement provides the same enhancement for any type of molecule; thus, it is chemically nonselective. This enhancement also has a strong analyte distance-dependence feature: Only molecules on or very close to the metal surface experience the enormous field enhancement.[1]

The EM enhancement mechanism does not totally explain the SERS phenomenon. Researchers have thus proposed a CE mechanism, which provides an order or two of magnitude of enhancement to the Raman signal intensity.[24−26] CE refers to the interaction between chemisorbed molecules and a metal surface and has mainly been described in two ways. The first explanation is that the molecule−surface interaction induces novel charge-transfer intermediates that have higher Raman scattering cross sections than do those of the analyte that is unadsorbed and on the surface.[15] The other explanation is that when the lowest unoccupied molecular orbital (LUMO) and highest occupied molecular orbital (HOMO) of the chemisorbed molecules fall symmetrically about the Fermi level of the metal surface, then the excitation of half the energy can make the transition. Thus, charge transfer between a metal surface and adsorbate can produce Raman excitation photons.[13,14,27]

It can be concluded that the EM enhancement emphasizes the role of the nanosubstrate providing the long-range electromagnetic fields, which depends on the nanosubstrate's inherent properties (such as material type, size, and shape).[10] However, CE is achieved by changing the scattering cross section of the analytes attached on a metal surface; thus, the extent of enhancement is determined by the chemical features of the analytes themselves.[19] Together, the two primary mechanisms contribute to the total enhancement. In 1997, Nie[28] and Kneipp[29] separately reported the use of single-molecule SERS for dye molecules in Ag colloids. In the single-molecule detection cases, the combined Raman signal enhancement was nearly 14 orders of magnitude greater than those obtained in the absence of a metal substrate;[27,30] this high sensitivity laid the foundation for future studies of SERS tags.

To give a brief theoretical guideline for the design and synthesis of SERS tags with high signal intensity, we shall present an equation proposed by Kneipp,[15,17,30] in which the SERS Stokes signal, $P^{\mathrm{SERS}}(\nu_{\mathrm{S}})$, can be estimated:

$$P^{\mathrm{SERS}}(\nu_{\mathrm{S}}) = N\sigma^{\mathrm{R}}_{\mathrm{ads}}|A(\nu_{\mathrm{L}})|^2|A(\nu_{\mathrm{S}})|^2 I(\nu_{\mathrm{L}}) \quad (1)$$

Here, $I(\nu)_{\mathrm{L}}$ is the excitation laser intensity; $\sigma^{\mathrm{R}}_{\mathrm{ads}}$ is the Raman cross section of the adsorbed molecule, possibly increased due to chemical enhancement; N is the number of molecules that undergo the SERS process; and $A(\nu)_{\mathrm{L}}$ and $A(\nu)_{\mathrm{S}}$ are laser and Raman scattering field enhancement factors, respectively. From this equation, one can deduce that the SERS-active nanosubstrate, type of attached molecules, and molecule numbers will all determine the optical quality of SERS tags. Later sections contain detailed discussions of these issues.

1.2. Optical Properties of SERS Tags

A SERS tag is created by attaching intrinsically strong Raman scattering molecules (called Raman reporters) to the surface of plasmon-resonant Ag or Au NPs, thereby creating a known SERS spectrum of the Raman reporter. Once this basic structure is established, a protective shell and a biorecognition element such as an antibody may be added to render the tags with biostability, biocompatibility, and a specific binding feature.

The development of SERS tags can be considered a significant step forward in the spectroscopic analysis of biological samples because these tags offer four main advantages over other optical probes, such as organic fluorescence dyes and QDs.[31,32] First, SERS tags can provide sufficient sensitivity for trace analysis. Several groups reported that the great SERS enhancement factor led to signals at levels similar to or better than those generated from fluorescence.[27,29,33] Second, Raman produces vibrational spectral bands with narrow line widths (~1 nm),[34] and fluorescent bands can be as wide as 50 nm;[35] thus, Raman-based probes are inherently suitable for advanced multiplex analysis. Third, the extremely short lifetimes of Raman scattering prevent photobleaching, energy transfer, or quenching of reporters in the excited state,[36] rendering high photostability to SERS tags. And fourth, optimal contrast can be achieved by using red to near-infrared (NIR) excitation to minimize the disturbing autofluorescence of cells and tissues, enabling SERS tags to be used for noninvasive imaging in living subjects.[37] The comparison of SERS tags, QDs, and conventional dyes is summarized in Table 1.

dx.doi.org/10.1021/cr300120g | *Chem. Rev.* 2013, 113, 1391−1428

Table 1. Comparison of SERS Tags, Quantum Dots, and Conventional Dyes

properties	SERS tags	quantum dots	conventional dyes
physical principle	Raman scattering	fluorescence emission	electronic absorption/ fluorescence emission
core composition	Au and Ag based NPs	CdSe and CdTe based NPs	organic compounds
size	~50 nm	~10 nm	~1 nm
bandwidth	less than 2 nm	~30−50 nm	usually more than 50 nm
structural information	fingerprint	nonfingerprint	nonfingerprint
multiplexing capacity[1]	~10−100	~3−10	~1−3
photostability	antiphotobleaching	decay under strong laser	decay under weak excitation
toxicity	not toxic	toxic	toxic

2. SYNTHESIS OF SERS TAGS

A typical SERS tag is composed of four parts: a metal nanosubstrate, an organic Raman reporter molecule, a protection shell, and targeting molecules. Various metal nanostructures can provide strongly enhanced spectroscopic signals due to the local optical fields at metal surfaces, which provide rigid foundations for the tags. Manipulation of the metal core's chemical composition, size, and structure can greatly affect the SERS properties of the tags. Furthermore, Raman reporter molecules should be attached to the metal nanostructure to generate SERS fingerprint signatures. However, this simple metal NP−Raman reporter structure usually lacks stability, and the signal is easily disturbed by surrounding interference. Hence, carefully designed coating materials and procedures are essential to improve the tags' biocompatibility and reducing their nonspecific binding and aggregation. Further, adding targeting molecules to the SERS tags imparts biofunctionality. Therefore, preparing SERS tags requires a multistep process, which is similar to that of fluorescent QDs probes.[38] Each step is guided by individual design principles aimed at controlling the optical, physical, and chemical properties of the final probe (Figure 1).

2.1. Noble Metal Nanosubstrates

Metal nanosubstrates act as structural scaffolds and a Raman signal amplifier for engineering of nanotags. In general, their size distribution, geometry, chemical composition, and surface chemistry can influence the Raman enhancement ability. As illustrated in Figure 2, various kinds of metal NPs and nanocluster-based SERS substrates have been reported: Their unique optical properties are explained in the following sections.

2.1.1. Single Particle-Based SERS Substrates. According to the EM enhancement theory, SERS intensity is dependent on the resonance frequency of the noble metal substrate. The field enhancement is greatest when the plasmon frequency of NPs is in resonance with the laser radiation. When designing SERS tags, it is important to select a NP composition and geometry that can be used under the desired laser wavelength. In the next section, we will discuss several typical noble NPs, focusing on how their size, shape, and composition affect their plasmon frequency and Raman enhancement ability and on suitable applications of each tag type.

2.1.1.1. Au and Ag Nanosphere. Gold and silver nanospheres (NSs) are the most widely used Raman enhancing platforms. Typical gold NSs are synthesized by the reduction of $HAuCl_4$ with citrate acid as described by Frens.[39] These NSs have many advantages, including having an easily controlled size distribution, long-term stability, and significantly high biocompatibility. Therefore, basic structural studies or applications involving living organisms are usually carried out by using gold NSs.[40−42] The most frequently used silver NSs for SERS applications are usually prepared by the reduction of $AgNO_3$ either with sodium citrate acid at boiling condition (Lee−Meisel method)[43] or with hydroxylamine hydrochloride at room temperature (Leopold method).[44] As illustrated in Figure 2A, the maximum SPR position of both NS types is 400−600 nm, and this red-shifts with increasing particle size.[45,46] This SPR range is in resonance with the wavelength of common illuminating lasers. Generally speaking, silver is a much more efficient Raman signal-enhancing material and gives rise to SERS signals that are 10-fold to 100-fold higher than those of similar gold nanostructures[47] because its d-s band gap is in the UV region, causing less damping of the plasmon mode.[48,49] The size of both gold[50,51] and silver NSs[52,53] plays a crucial role in SERS signal enhancement ability. On one hand, the intensity of the EM field is strongly dependent on the number of electrons excited and, thus, on the volume of the nanostructure.[47] On the other hand, using a particle that is too large is not appropriate because the increased size results in larger radiation damping effects, decreasing the enhancement factor. The optimum size range is thought to be 30−100 nm.[16] Besides the SERS property, other features should also be considered. For instance, silver NSs have poor biocompatibility, uncontrollable size distributions, and only short-term stability;[54] hence, silver often cannot be substituted for gold in designing SERS tags, especially those for living species-labeling.

2.1.1.2. Au Nanoshell. Several types of metal nanoshell substrates, including silica-supported gold nanoshells,[55,56] hollow gold nanoshells,[57−59] and nanocages,[60,61] have been developed as single-NP SERS substrates. These individual particles have strong enhancement effects because of their capability to localize the surface electromagnetic fields through the pinholes in the hollow particle structures.[62] Individual nanoshell surfaces offer an easily accessible topology and provide average integrated SERS enhancements similar to those obtained with nanosphere dimers.[50,63] Furthermore, nanoshells have sensitive SPRs on the inner and outer shell radius and can be tuned from the visible to the NIR region.[64−66] The SPRs of hollow Au nanoshells with shell diameters around 40 nm red-shift from about 610 to 820 nm by decreasing the shell-wall thickness from 6.8 to 3 nm (Figure 2B).[67] This fact is of particular importance for *in vivo* imaging because long-wavelength laser excitation minimizes cellular or tissue autofluorescence, increasing the signal-to-background ratio and image contrast.[68,69]

2.1.1.3. Au Nanorod. Unlike Au NSs and nanoshells, which have one SPR band, gold nanorods (Au NRs) have two: a weak transverse band in the visible region with a position similar to that of gold NSs that corresponds to electron oscillations along the short axis and a strong longitudinal band in the longer wavelength region that corresponds to electron oscillation along the long axis.[70] Au NRs have attracted much attention because of the tunable, longitudinal plasmon resonance that can be engineered by changing the aspect ratio.[71] By simply varying the silver nitrate concentration during the growth process, the

dx.doi.org/10.1021/cr300120g | Chem. Rev. 2013, 113, 1391−1428

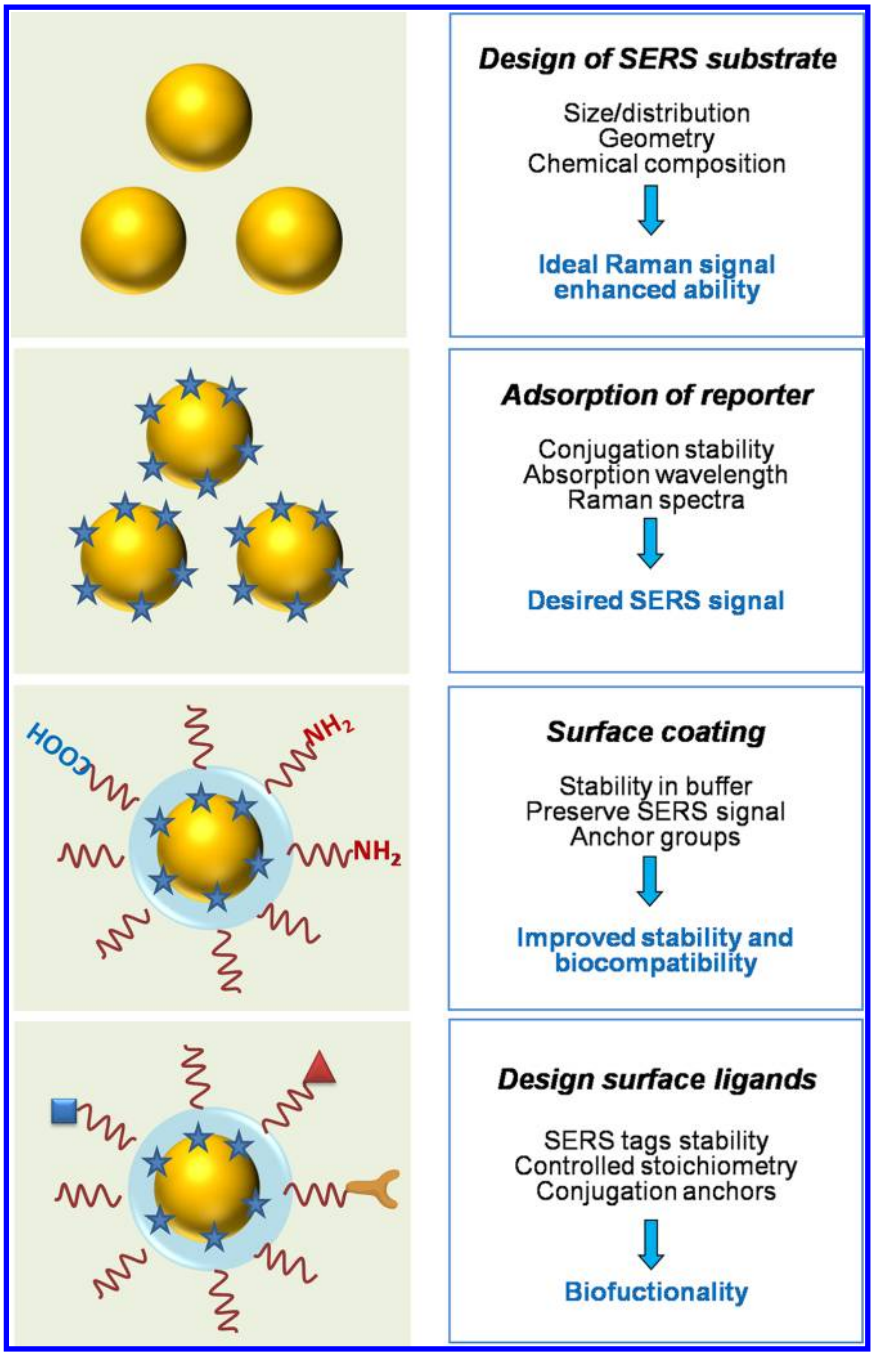

Figure 1. General steps and design criteria in engineering of SERS tags for biomedical applications.

longitudinal plasmon resonance shifts from the visible to the NIR region as the rod's aspect ratio increases from 2.4 to 5.6 (Figure 2C).[72] Besides, Au NRs have a high theoretical per-micrometer absorption coefficient that is more than an order of magnitude higher than that of nanoshells.[73] These advantages have enabled Au NRs to be used in Raman scattering probes for bioapplications, including molecular and cell imaging,[74−76] *in vivo* tumor detection, and photothermal therapy.[73,75,76] The aspect ratio also plays an important role in the Raman enhanced effect: The SERS signals of 4-mercaptopyridine attached on Au NRs with an aspect ratio of 1.6 are much stronger than those of Au NRs with an aspect ratio of 4.5 when using a 632.8 nm laser as the excitation source.[77]

2.1.1.4. Multibranched Metal Nanoparticle. A new class of multibranched metal NPs, referred to as nanostars[78−82] (Figure 2D), nanoflowers[83−86] (Figure 2E), or gold lace shells,[87] has more surface roughness than do spherical particles of similar size. The extremely small radii of curvature in this class of NPs result in strong electric field enhancement and subsequently large SERS enhancement factors per surface molecule, which is referred to as a "sharp tip effect".[88−90] Additionally, surface plasmons originating from the hybridization of individual tips and cores give rise to a further increase in the local electric field. Furthermore, the increased surface area relative to that of a sphere of equivalent size allows more Raman reporter molecules to be attached on multibranched NPs than on smooth-shaped NPs.

2.1.1.5. Au−Ag Bimetallic Nanoparticle. Besides the monometallic NPs mentioned above, multicomponent architectures have also become attractive candidates because of their

dx.doi.org/10.1021/cr300120g | *Chem. Rev.* 2013, 113, 1391−1428

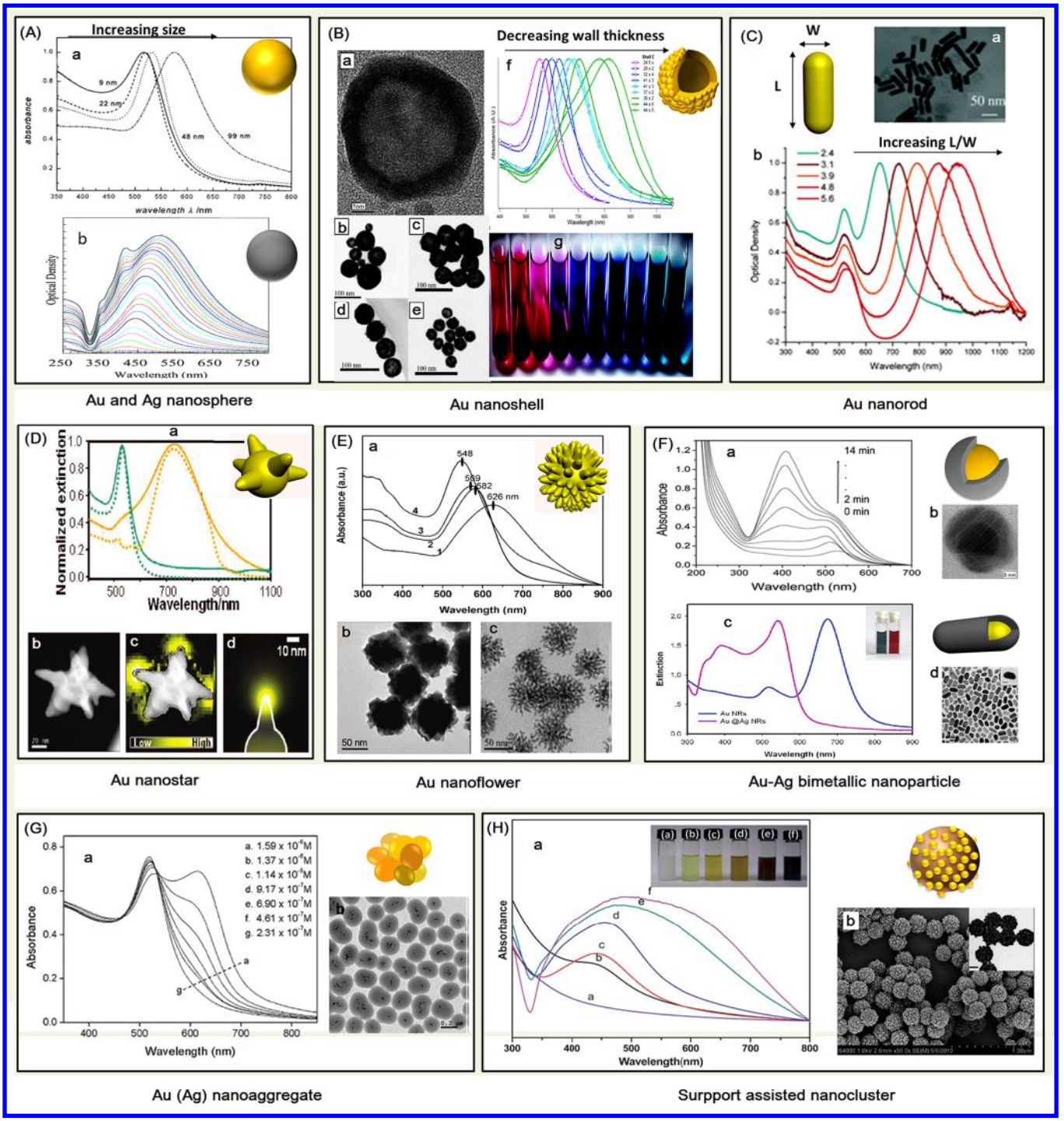

Figure 2. Representative nanosubstrates for synthesis of SERS tags. (A) (a) UV−vis absorption spectra of different sized gold nanoparticles (NPs) in water. The particle size is 9, 22, 48, and 99 nm, respectively. Reproduced with permission from ref 45. Copyright 1999 American Chemical Society. (b) Extinction spectra of different sized silver NPs. The particle size is 29, 34, 37, 44, 48, 52, 58, 61, 75, 78, 92, 97, 105, 113, 120, and136 nm, respectively. Reproduced with permission from ref 46. Copyright 2004 American Chemical Society. (B) (a) High-resolution transmission electron micrographs (TEM) of a single 30 nm hollow Au nanoshell (HGN) with a wall thickness of approximately 4 nm. (b−e) Low-resolution TEM images of particles of 71 ± 17 nm (b), 50 ± 5 nm (c), 40 ± 3.5 nm (d), and 28 ± 2.3 nm (e), respectively. (f) UV−vis absorption spectra of nine HGN samples with varying diameters and wall thicknesses, and (g) the color range of HGN solutions. Reproduced with permission from ref 67. Copyright 2006 American Chemical Society. (C) (a) TEM image of gold nanorods (AuNRs) of aspect ratio 3.9. Surface plasmon absorption spectra of AuNRs of different aspect ratios (b), showing the sensitivity of the strong longitudinal band to the aspect ratios of the nanorods. Reproduced with permission from ref 72. Copyright 2006 American Chemical Society. (D) (a) Experimental (solid curves) and calculated (broken curves) extinction spectra in water for spherical (46 ± 4 nm) and star-shaped (41 ± 8 nm) Au colloids. All spectra are normalized to their maximum value. (b) High-resolution scanning transmission electron microscopy dark-field image of a single Au nanostar. (c) Electron energy-loss spectroscopy (EELS) intensity mapping of the same particle. (d) Calculated EELS intensity map of the plasmon resonance in a particle tip, showing high localization near the tip apex, in agreement with the observed EELS image. Reproduced with permission from ref 81. Copyright 2009 American Chemical Society. (E) Au nanoflowers' UV−vis spectra formed by reducing $HAuCl_4$ with different concentrations of 4-(2-hydroxyethyl)-1-piperazineethanesulfonic acid

dx.doi.org/10.1021/cr300120g | Chem. Rev. 2013, 113, 1391−1428

Figure 2. continued

(HEPES) solutions (a) and a typical TEM image (b). Reproduced with permission from ref 83. Copyright 2008 American Chemical Society. (c) Au nanoflowers of another morphology synthesized by using $HAuCl_4$ and pyrrole. Reproduced with permission from ref 84. Copyright 2010 IOP Publishing Ltd. (F) Time-dependent absorption spectra of an Au@Ag bimetallic nanosphere during the Ag shell coating (a) and the high resolution TEM image (b). Reproduced with permission from ref 92. Copyright 2007 American Chemical Society. (c) UV−vis spectra of Au NRs and Au@Ag NRs. The inset shows the photograph of Au NRs (left) and Au@Ag NRs (right) solution. (d) TEM image of Au@Ag NRs. Reproduced with permission from ref 96. Copyright 2012 American Chemical Society. (G) (a) TEM images of Au nanoaggregate-embedded beads with silica coating. (b) UV−vis spectra of Au NP solutions at pH 10.0 after being mixed with an increasing concentration of Raman reporter of X-rhodamine-5- (and 6)-isothiocyanate. Reproduced with permission from ref 113. Copyright 2009 John Wiley & Sons, Inc. (H) (a) UV−vis absorption spectra of the poly(styrene-*co*-acrylic acid) (PSA)@Ag NPs composite microspheres with increasing size of Ag NPs. Inset: photographs of solutions corresponding to the curves. (b) SEM and TEM images of typical PSA@Ag NPs composite microspheres. Reproduced with permission from ref 116. Copyright 2011 Royal Society of Chemistry.

composition-dependent physicochemical properties.[91] Taking advantage of the higher SERS activity of silver and the homogeneous superiority of gold, researchers have coated silver layers over gold colloid seeds to prepare bimetallic Au@Ag core−shell NPs, including Au@Ag NSs,[92−95] Au@Ag NRs,[91,94,96,97] Au@Ag shells,[68,98] and Au@Ag nanocages.[99] During the Ag-coating process, the SPR wavelength of the bimetallic NPs can be continuously tuned in a wide range covering that of Au cores and Ag shells, which is a benefit for making a match with the given laser excitation wavelength to achieve the strongest SERS enhancement (Figure 2F).

A novel bimetallic NP architecture in which the Raman reporter molecules are placed between layers of gold cores and silver shell yields a dramatic signal enhancement.[100−103] The metal−reporter−metal sandwich assembly mode is an important complement to the classic SERS tag structure, as is detailed in section 4.3.

2.1.2. Nanoparticle Cluster-Based Substrates. Mild aggregation of metallic NPs generates intense EM field enhancement at the junctions between nanoparticle dimers and small clusters, which are commonly called "hot spots".[13,27,104,105] The enhancement factor at hot spots can be greater than 10^{10}, which is enough for single-molecule detection.[106] Therefore, metal NP aggregates have also been developed to produce highly sensitive substrates for SERS tags. Moreover, the aggregated NPs have new absorption bands toward the long-wavelength region for Ag clusters around 500−600 nm and Au clusters around 700−900 nm,[91] and the latter is coincident with the longer laser wavelengths used for *in vivo* investigations. Precise control of the shape and size of the aggregated NPs is essential to fabricate homogeneous, nano-sized probes with reproducible signals. Therefore, the moderate aggregation strategy has been widely investigated.

2.1.2.1. Direct Nanoparticle Aggregation. Salt-induced aggregation is the most common aggregation method.[107,108] To obtain SERS tags with the desired extent of aggregation, the amount of salt added should be precisely controlled. Moreover, polymers are usually applied to quench the aggregation process by forming a shell on the particle's surface. For instance, Tan et al.[108] used polyvinylpyrrolidone (PVP) to control the aggregation and improve the tags' chemical stability. Braun et al.[109] used PVP or polyvinylpyrrolidone−poly(acrylic acid) (PVPA) followed by polyethylene glycol (PEG)-thiol to achieve the same goal.

An alternative way to form nanoaggregates is by dye-induced aggregation.[110] Upon adsorption of Raman reporters, the capping agent (such as citrate) on the surface of metal NPs is replaced, which decreases the electrostatic repulsion between particles and therefore induces the formation of closely adjacent NPs[111,112] (Figure 2G). The pH of a NP's colloid helps to regulate this process. For example, when adding a strong-binding dye of X-rhodamine-5-(and-6)-isothiocyanate (XRITC) to citrate-adsorbed Au NPs, small aggregates appear at pH 7.0 and pH 10.0, and large aggregates form at pH 5.0.[113]

2.1.2.2. Support-Assisted Nanoclusters. Support-assisted nanoclusters contain high densities and reproducible hot spot structures. Silica, polystyrene, and polymer beads are commonly used as support materials for depositing much smaller metal NPs (Figure 2H).[114−116] After being functionalized with 3-mercaptopropyltrimethoxysilane (MPTMS) or treated with sulfuric acid, the support bead can adsorb noble metal salts, and the noble NPs are *in situ*-synthesized and compactly spread on the bead's surface. The amount and size of the coating NPs can be adjusted by changing the concentration of metal salts and the reaction time.[117] Therefore, the finely formed NP junctions or aggregates can produce intense Raman signatures of reporters with high reproducibility. An alternative method is to assemble the as-prepared metal NPs on silica beads based on covalent linkage or electrostatic interaction. For example, researchers have developed compatible and multiplex SERS tags that are composed of silica particles and subsequently coated with Au NRs and organic Raman reporters.[118]

2.2. Raman Reporter Molecules

2.2.1. Selection Principles and Reporter Types. The second step in preparing SERS tags is to conjugate SERS-active nanosubstrates to Raman reporter molecules with a characteristic Raman spectral signature. Several principles apply to the selection of Raman reporters and the deposition method used to prepare tags with strong, stable multiplex signals: (1) Generally, optical enhancement requires that Raman reporter molecules be attached on or near the surface of SERS substrates because CE requires chemical bonding and EM enhancement is strongly distance-dependent. Meanwhile, the interaction between the reporters and metals should be strong enough to prevent desorption during further modification or use. Therefore, nitrogen- or sulfur-containing molecules are often used because of their high affinity to silver and gold. (2) The reporter molecules must have a relatively large Raman scattering cross section, which helps produce strong SERS signals. (3) When the excitation-laser's wavelength matches the optical absorption of Raman reporters, then surface-enhanced resonant Raman scattering (SERRS) occurs, and the enhancement factor may be further enhanced 100 times.[119] So, in some circumstances, the absorption wavelength should also be taken into consideration when choosing an ideal reporter. (4) The signal level is also influenced by the number of reporters encapsulated in the tag. Good coating methods that can form a

Table 2. Typical Raman Reporters Used for SERS Tag Preparation

type	example	linking mode	advantages	disadvantages
nitrogen-containing cationic dye	crystal violet	electrostatic force	cheap	weak affinity to metal
	rhodamine B rhodamine 6G	N−Au(Ag) interaction	large Raman cross section	weak signal stability
	nile blue		ready for SERRS	hard for further tag surface coating
sulfur-containing dyes	3,3′-diethylthiadicarbocyanine iodide	S−Au(Ag) interaction	large Raman cross section	expensive
	malachite green isothiocyanate		strong binding affinity to metal	limited types
	tetramethylrhodamine-5-isothiocyanate		suitable for further tag coating and modification	hard to form SAM
	rhodamine-5-(and-6)-isothiocyanate		ready for SERRS	
thio-small molecules	4-aminothiophenol	S−Au(Ag) interaction	cheap	small Raman cross section
	4-methylbenzenethiol		strong binding affinity to metal	not ready for SERRS
	2-naphthalenethiol		few Raman peaks is beneficial for multiplexing	
	benzenethiol			

dense, uniform reporter layer on the substrates will result in a higher signal. (5) A simple Raman spectrum with relatively few characteristic peaks is essential for preparing tags for multiplex labeling to avoid signal overlap of the tags. Representative types of Raman reporters with nitrogen-containing cationic dyes, sulfur-containing dyes, and thio-small molecules are summarized in Table 2 along with their SERS features.

Although the reporter molecule is a major factor that influences the quality of SERS tags, it has not been studied as extensively as metal substrates. One key problem is that most researchers have directly applied the ready-made molecules as reporters. Rational design, screening, and systematic characteristic investigation of novel reporters are rarely reported. Recently, Olivo's group[120−124] reported on the combinatorial synthesis and screening of a triphenylmethane dye library for the development of highly sensitive SERS tags: At least 13 compounds had a stronger SERS signal than did the general reporter crystal violet. After modifying lipoic acid to obtain strong binding to the gold surface, the novel reporters were used to produce tags that had better signal stability than those modified with the currently popular Raman reporter malachite green isothiocyanate (MGITC).[121,122] Endeavors were also made to discover novel Raman-active compounds in the NIR region, where the availability of reporters is restricted to fewer molecules. The synthesis and screening of an 80-member tricarbocyanine library led to the identification of CyNAMLA-381 as a NIR SERS reporter with 12-fold higher sensitivity than the standard 3,3′-diethylthiatricarbocyanine (DTTC) (Figure 3), validating its advantages for the synthesis of ultrasensitive *in vivo* SERS tags.[123] As a proof of concept for multiplex targeted in vivo detection, simultaneous sensing of cancer in living mouse using three bioconjugated tags was successfully demonstrated.[124] These results showed the importance of designing and screening novel Raman reporters.

2.2.2. Self-Assembled Monolayer Coverage Strategy. As illustrated in the equation in section 1.1, the SERS intensity of each tag is proportional with the number of Raman reporters attached to the nanosubstrates. Therefore, increasing the number of labeling reporters is an effective way to obtain sensitive probes. However, it is difficult to coat high density, uncharged reporter molecules on NPs without inducing severe aggregation. Recently, the self-assembled monolayer (SAM)[67,125−127] structure of Raman reporters on metal NPs surface was developed. These Raman reporters have the structure of the thio group to anchor them to the metal surface and the carboxyl group to generate a negative charge in solution. Therefore, this kind of molecule acts as both signal generator and NP stabilizer, enabling their high-coating density on tags. The SAM-coating strategy has several significant advantages: (1) the maximum surface coverage with reporter molecules will provide a high SERS sensitivity; (2) the uniform orientation of Raman reporters leads to defined and reproducible spectral signatures; (3) the dense packing structure avoids coadsorption of other molecules with unwanted spectral signals; and (4) quantitative coadsorption of various Raman reporter molecules on one surface of the metal colloid provides multicoded tags for multiplexing analysis, as detailed in section 4.2.

2.3. Surface Coating for Protection

Attaching Raman reporters onto metal substrates can produce probes with SERS signals that are ready for biological labeling. However, the efficiency and reliability of such "bare" tags are often compromised by ligand dissociation of the reporters. In addition, the exposed surface of the metal substrate easily adsorbs interfering molecules in the chemical or biological environment, which may cause variations of the original SERS signals and induce biotoxicity. To overcome these problems, a variety of surface coating materials and encapsulation methods were developed to enhance the stability and biocompatibility of the tags.

2.3.1. Biomolecule Coating. Bovine serum albumin (BSA) is the most commonly used surface-coating biomolecule. After being mixed with an NP's colloid, BSA can absorb on the metal surfaces via weak interaction and produce a protective shell.[98,108,128] Adding glutaraldehyde to the BSA-coated tags forms a more compact cross-linked encapsulation layer.[129] Because most of the surface amino groups on the protein are removed in this process, the encapsulated tags have a net negative charge from the carboxylic acid groups. Denatured BSA (*d*BSA) is another satisfactory biomolecule that has been used to stabilize Au nanoflowers based SERS tags, with embedded rhodamine B used as the Raman reporters.[83] A layer of *d*BSA can be formed via strong binding of thiol groups originating from the 35 cysteine residues in each BSA molecule (Figure 4a).

2.3.2. Polymer Coating. SH-PEG is an ideal polymer protector because the pegylated colloidal NPs are nontoxic and have an adjustable coating shell thickness, weak affinity to interference molecules, and excellent *in vivo* biodistribution and pharmacokinetic properties[37,63,130,131] (Figure 4b). PVP,[108]

dx.doi.org/10.1021/cr300120g | *Chem. Rev.* 2013, 113, 1391−1428

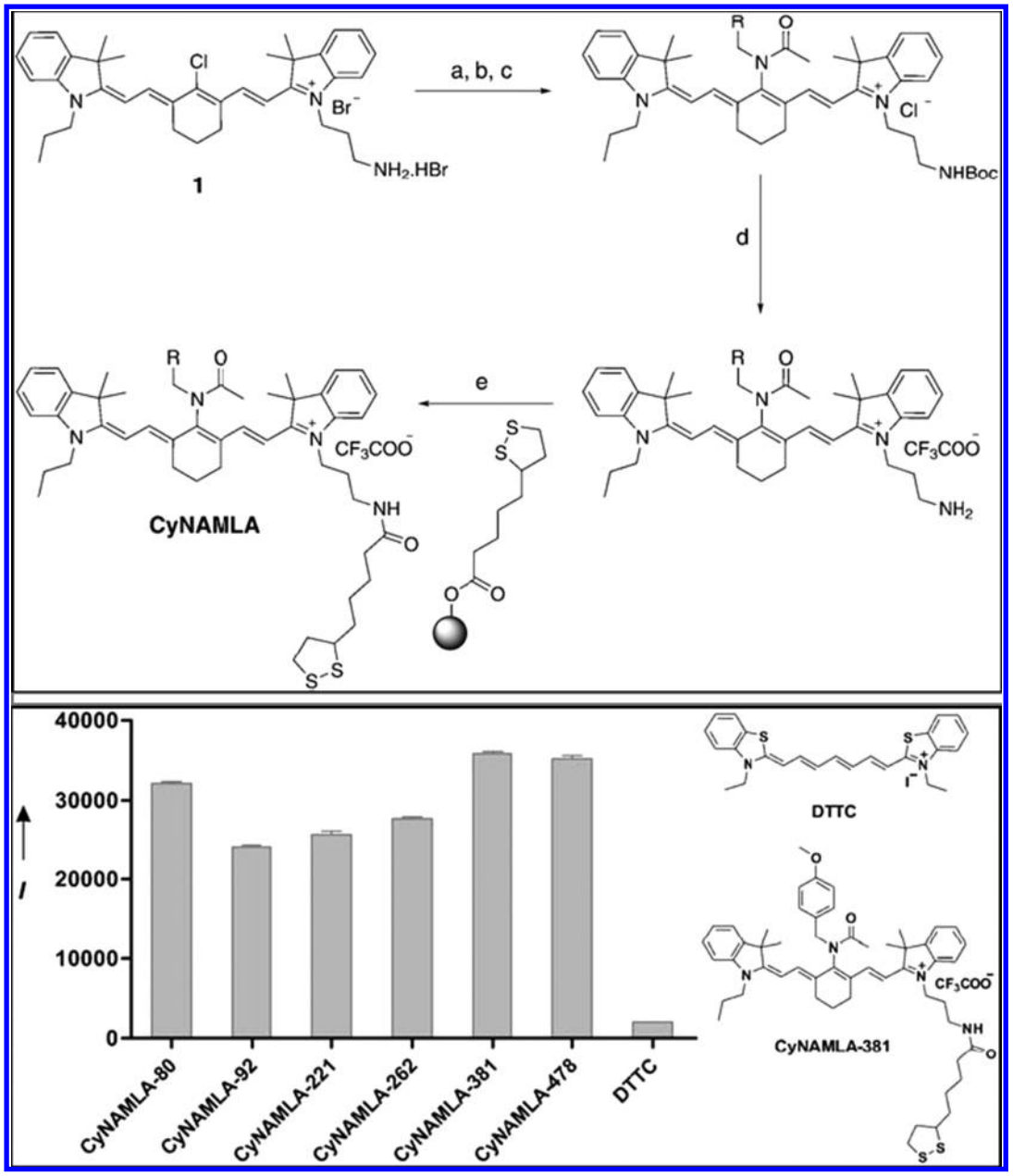

Figure 3. Synthesis of lipoic acid-containing amine acetylated tricarbocyanines (CyNAMLA) (top) and SERS intensities of the selected BSA-encapsulated CyNAMLA-AuNPs (bottom). SERS spectra were measured in a Renishaw Raman microscope (excitation: 785 nm). Reproduced with permission from ref 123. Copyright 2011 John Wiley & Sons, Inc.

chitosan,[84,132] and sulfur-containing reversible addition–fragmentation chain transfer polymers[133] have also been widely used for their biocompatibility, biodegradability, and complexation with metal ions. Recently, a facile preparation method for a new class of SERS tag–coating was reported that used an amphiphilic diblock copolymer, polystyrene block-poly(acrylic acid) (PS154-b-PAA60), for thermodynamically controlled self-assembly (Figure 4c).[134] The process was advantageous in that polymer shells with uniform thickness were easily prepared without meticulous control, requiring only a one-pot synthesis that involved simple heating and cooling.

2.3.3. Liposome Coating. Liposomes are promising coatings for particles because of their inherent biocompatibility and ability to self-assemble into organized structures. Furthermore, the stability and targeting properties of liposomes can be provided by the lipid vesicle itself and by the targeting molecules bound to lipid anchors.[135,136] Some strategies used to address these functions for liposome drug-delivery can be applied to lipid-coated metal NPs for diagnostics and therapeutics if a Raman reporter can be incorporated. Tam et al.[137] first synthesized 60 nm Au NS-based SERS tags with a nonthiol phospholipid coating composed of double-chain (1,2-dimyristoyl-*sn*-glycero-3-phosphocholine, DMPC) and single-chain (1-myristoyl-2-hydroxy-*sn*-glycero-3-phosphocholine, MHPC) phospholipids. The Raman reporter-labeled Au NSs were stirred and gradually heated to 65 °C while the phospholipid solution was added dropwise. Immediate evaporation of the organic solvents formed liposome-like structures (Figure 4d). More recently, Walker's group[138] showed that liposome-coated SERS tags incorporate three Raman-active species of MGITC, L-tryptophan, and rhodamine lissamine DSPE via three variations of the same aqueous

dx.doi.org/10.1021/cr300120g | *Chem. Rev.* 2013, 113, 1391–1428

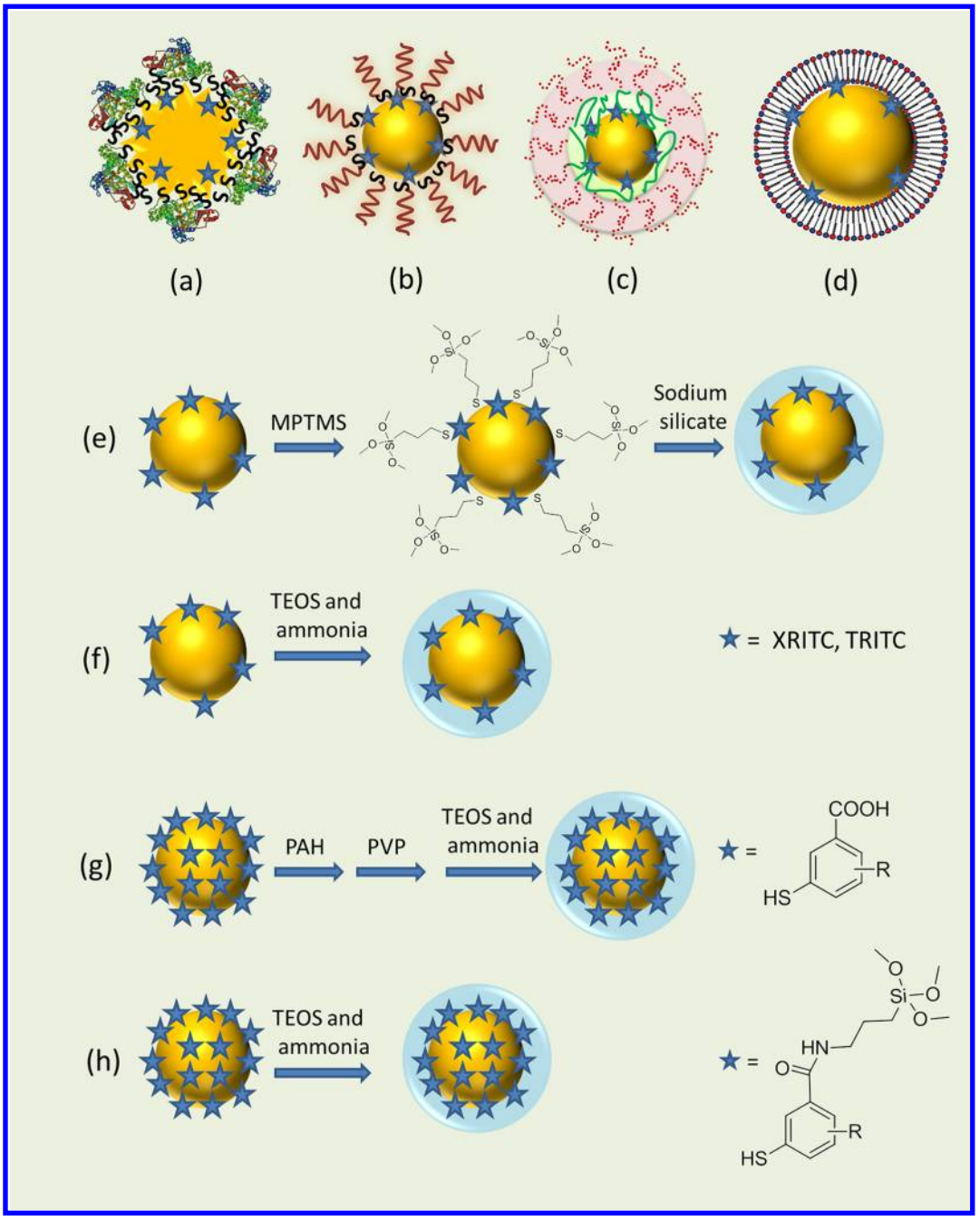

Figure 4. Strategies for surface-coating SERS tags include coating with denatured BSA (a), SH-PEG (b), amphiphilic diblock copolymer (c), liposome (d), and silica shells via different encapsulation routes (e–h).

method. The encapsulation is achieved in aqueous solution, avoiding phase transfer and possible contamination from organic solvents. A porphyrin-phospholipid conjugate was also applied to serve as both the Raman dye and a biocompatible surface coating material for SERS tags.[139]

2.3.4. Silica Coating. Silica coating is another attractive encapsulation method, providing high stability, good water solubility, low nonspecific binding, and ease of further modification in biological systems. In 2003, two groups simultaneously reported creating silica-coated, dye-linked, gold NSs for use as SERS tags by hydrolysis of sodium silicate.[36,140] As shown in Figure 4e, after attaching reporter molecules on NPs, a silane that can act as a vitrophilic (i.e., "affine to silica") agent for a later glass shell should be introduced. Typically, either 3-aminopropyltrimethoxysilane (APTMS) or MPTMS is used as the functionalized silane because the terminal amine/thiol has an affinity for metal that leaves the trimethoxysilane group exposed to the surrounding solution. Once both dye and silane are present, sodium silicate is added to produce a thin glass shell. For obtaining tags with stronger SERS signals, silica-coated metal nanoclusters were prepared in the same way.[141] This sodium silicate hydrolysis method advantageously produces an ultrathin silica layer. However, it requires troublesome pretreatment steps such as dialysis, ion-exchange, and preparation time exceeding 30 h.[142]

Haisch and co-workers[143] described a fast, daily use method without the need for vitrophilic pretreatment. As shown in Figure 4f, the coating method involves generating silica sols

dx.doi.org/10.1021/cr300120g | Chem. Rev. 2013, 113, 1391–1428

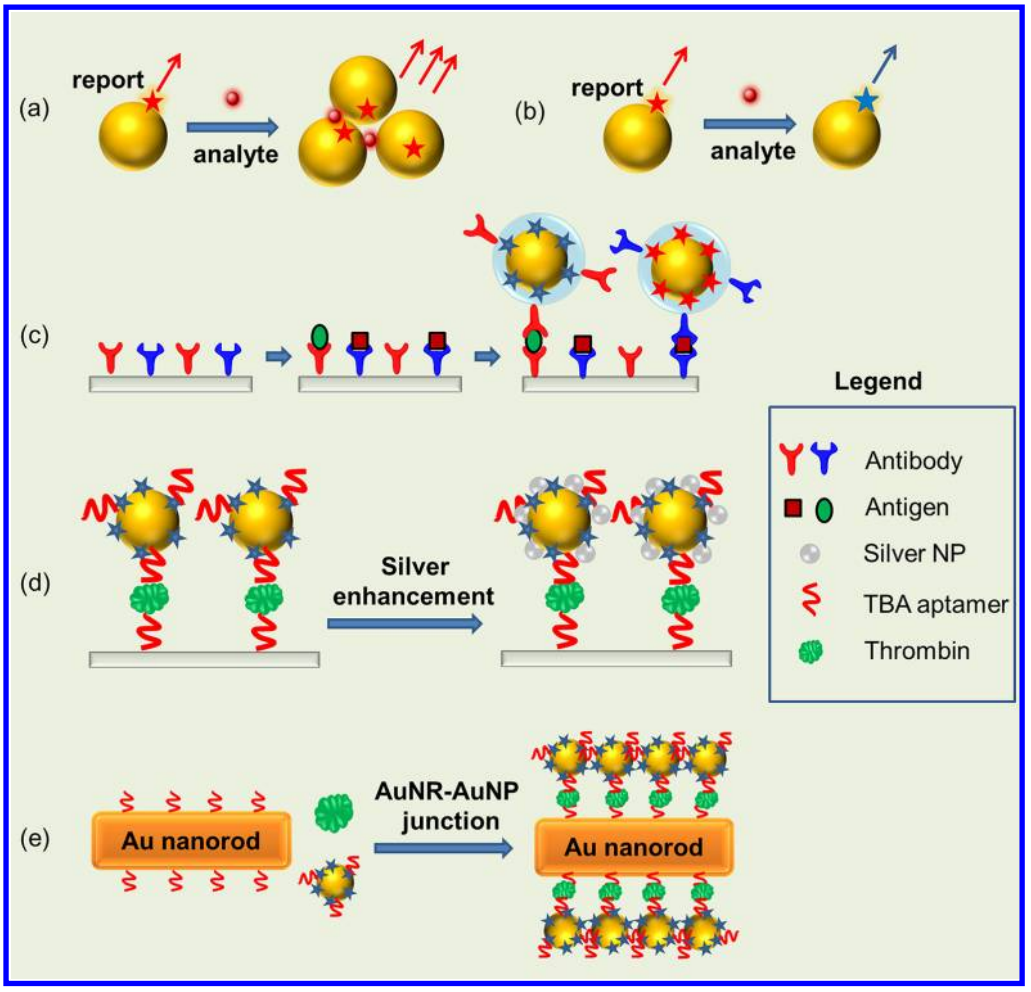

Figure 5. Schematic illustration of ionic and molecular detection by using SERS tags. (a) Analyte-induced SERS tag aggregation; (b) analytes changing the Raman signature of the reporter; (c) immunosandwich assay using SERS tags for protein analyte detection; (d) the fabrication process of SERS aptasensor for protein recognition and signal enhancement with silver; and (e) fabrication of AuNR-AuNP junctions for protein detection.

with ammonia-catalyzed hydrolysis of tetraethyl orthosilicate (TEOS) followed by nucleation and condensation of these sols onto the surface of tagged core particles. In this case, strong-binding reporter molecules with isothiocyanate groups or multiple sulfur atoms were required to prevent desorption from the metal surface after the basic media for TEOS hydrolysis was added.

Recently, Schlücker's group designed a novel silica-coated SERS tag with a stable and reproducible signal that was based on SAM of Raman reporter molecules on the NPs (Figure 4g).[68] With the aid of the polyelectrolyte layer-by-layer deposition technique, poly(allylamine hydrochloride) (PAH) was first coated on a monolayer of the 4-mercaptobenzoic acid (MBA) reporter via electrostatic interaction and then absorption of PVP rendered the particles vitreophilic. Growth of the silica shell was achieved by using an ammonia/2-propanol mixture and TEOS. A similar method uses poly(acrylic acid) to protect SAM reporter-coated Au nanoshells and further adsorb coupling agents of MPTMS.[62] An alternative approach was designed to silica-encapsulate a SAM, independent of the constraint of SAM's surface charge.[126] As shown in Figure 4h, MBA used as the Raman reporters and amino alkylalkoxysilanes (such as APTMS) used as SiO_2 precursors were covalently bound to form Ra-SiO_2; that is, both functions were merged into a single molecular unit. The further addition of TEOS forms a silica shell because Ra-SiO_2 is already vitreophilic.

2.4. Attachment of Targeting Molecules

Water-soluble SERS tags must be cross-linked to antibodies, aptamers, or small-molecule ligands to render them specific to biological targets. SERS tags can be functionalized via sulfhydryl group-containing molecules. For instance, after incubation of thiolated aptamers, the metal surface reaches equilibrium, resulting in partial substitution of the initial coating molecules such as citrate.[144,145] Stable covalent bonds can also be formed by coating the tags with ortho-pyridyldisulfide-polyethylene glycol-*N*-succinimidyl propionate (OPSS-PEG-NHS).[100,130] The mercapto groups can bind to the metal NP's surface, and *N*-succinimidyl can form stable amide bonds with amines in various biomolecules. Similarly, with the aid of coupling reagents such as 1-ethyl-3-(3-dimethylaminopropyl) carbodiimide (EDC) and *N*-hydroxysuccinimides (NHS), carboxylic acid groups on the surface-coating molecules (such as BSA) are activated for the reaction with the amine groups in the antibody.[129] Biotin-modified tags can also be used for coating because they can easily be linked to streptavidin-tagged biomolecules.[146] Additionally, electrostatic interactions between the negative polyelectrolyte (such as poly(4-styrene sulfonate, PSS)-coated NPs and positive antibodies can also provide an easy way to add modifications.[77] A variety of organic

dx.doi.org/10.1021/cr300120g | *Chem. Rev.* 2013, 113, 1391−1428

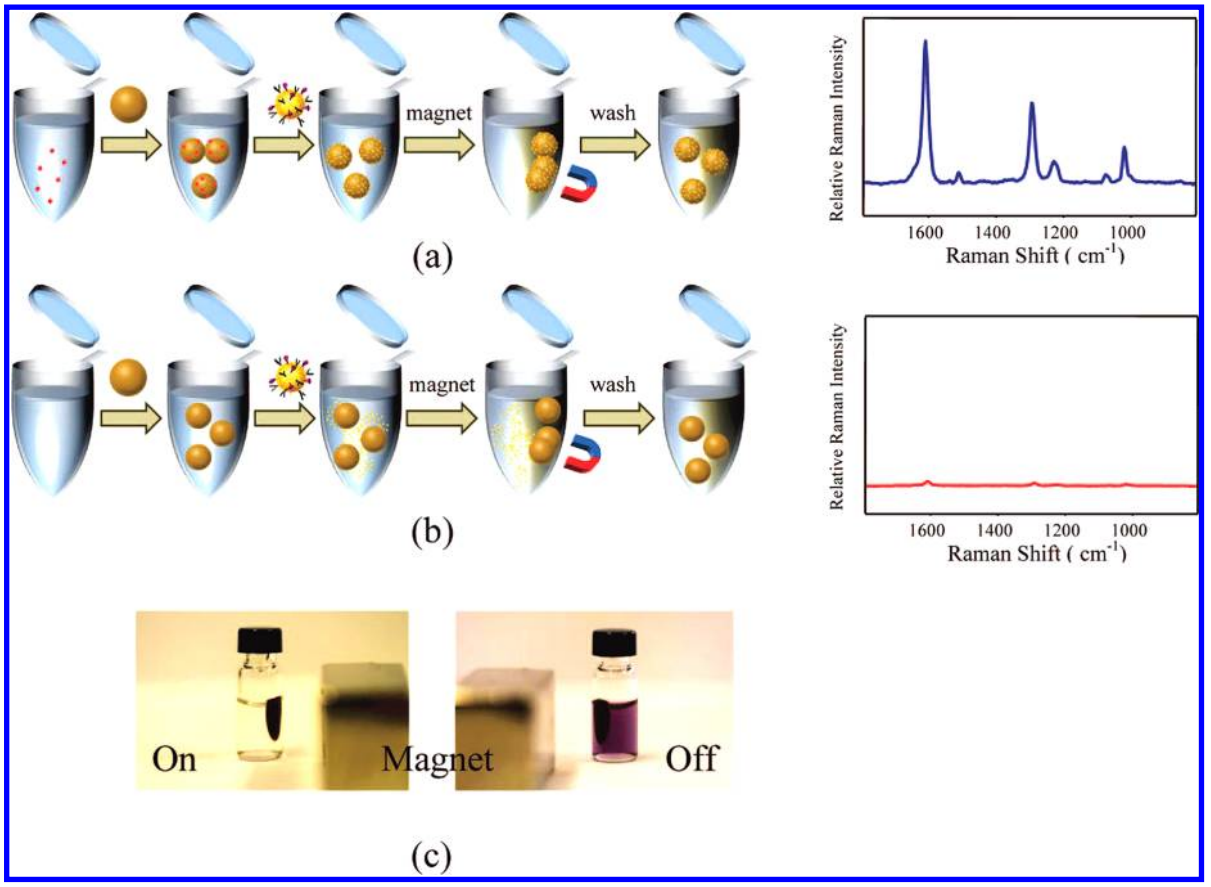

Figure 6. Schematic illustration of immunoassay processes and corresponding Raman spectra: (a) with CEA antigens and (b) without CEA antigens. (c) Photographs showing suspended magnetic beads attracted to the wall of a microtube by a bar magnet: with CEA (left) and without CEA (right). Reprinted with permission from ref 58. Copyright 2009 American Chemical Society.

functionalities can be readily attached to SERS tags encapsulated in silica shells by using well-developed silane chemistry.[143]

3. BIOANALYSIS APPLICATIONS

3.1. Ionic and Molecular Detection

Several strategies, including analyte-induced SERS tag aggregation, SERS-tag based immunoassays, and analytes-induced alteration of the reporter's Raman signature, have been developed to detect ions and biomolecules. The idea of tag aggregation (Figure 5a) originated from noble metal NP-based colorimetric methods based on two mechanisms. The first mechanism is that coordinating interactions will neutralize the tags and lead to dramatic aggregation after addition of certain kinds of analytes with high affinity to metal surfaces.[147] This method is sensitive but lacks selectivity. The second mechanism is to comodify the Raman reporter and selective ligand on SERS tags. Only target analytes can induce aggregation, and the Raman scattering signal of reporters is greatly increased. The signal "turn on" mode offers a possible approach for the rapid and sensitive assay of the analytes.[148,149] On the contrary, if the analytes have enough affinity with metal nanosubstrates to replace preadsorbed Raman reporters, then their addition will decrease SERS tag signals. This idea was successfully used to analyze thio-containing small molecules.[150]

In another circumstance, SERS tags can be designed as chemical sensors, relying on the changeable SERS profiles of Raman reporters upon binding events with analytes (Figure 5b). Specifically, the vibrational modes of certain chemical ligands are very sensitive to ion coordination, and the SERS response of such ligands when associated with metal NPs provided a powerful strategy to be explored in analytical chemistry.[151,152]

Taking advantage of the richness of Raman signatures and the single-molecule-level detection sensitivity, researchers successfully used SERS tags for more complicated multiplex and ultrasensitive immunoassays of biomolecules. Antigen identification was first demonstrated with different tags. Generally, polyclonal antibodies (PAbs) are immobilized on a solid substrate and then antigen and monoclonal antibody (mAb)-conjugated SERS tags are added in sequence. After washing away nonspecific binding antigens and free tags, the antigen can be identified by the measurement of SERS signals[140] (Figure 5c). For example, multiplex detection of human interleukin (IL)-2 and IL-8 was achieved via this method.[110] The binding event of target molecules and the type of ligand could be simultaneously recognized with a single laser-line excitation.

This sandwich immunoassay format was further developed for quantitative analysis of tag-attached targets.[93,118,153] Wang and colleagues used goat anti-hIgG and hIgG as a model system for protein detection.[118] A substrate coated with goat anti-hIgG was exposed to a solution containing different concentrations of hIgG. After incubation, the sample was immersed into a solution of goat anti-hIgG-anchored, Au NR-embedded, silica SERS tags. The hIgG first bound to the corresponding goat anti-hIgG that was previously immobilized on the substrate.

dx.doi.org/10.1021/cr300120g | Chem. Rev. 2013, 113, 1391−1428

Then, it could capture the same antibody that was labeled on the SERS tags. Thus, the amount of hIgG could be reflected by the SERS signal with a limit of detection (LOD) of 0.01 ng mL^{-1}.

Certain approaches were used to further enhance the tags' signals, increasing detection sensitivity.[154−156] In an a-thrombin assay (Figure 5d), one thrombin molecule could bind two 15-mer thrombin-binding aptamers (TBAs) simultaneously; thus, a sensing interface with a sandwich-type TBA/thrombin/TBA-Au SERS tag could be fabricated. Then, Ag NPs were deposited on the Au SERS tags. Taking advantage of this hot spot-generating process, a detection limit of 0.5 nM was achieved.[155] Similar signal enhancement effects could be achieved by self-assembly of multicomponent metal nanostructures.[156] As illustrated in Figure 5e, AuNPs were labeled by TBA and the Raman reporter MBA, forming modified SERS tags. Thrombin was then allowed to bind with AuNRs through antibody−antigen interactions and with AuNP-tags through aptamer−protein binding to form AuNR−AuNP junctions, giving rise to an enhanced Raman signal as a measure of the bound protein.

A SERS tag-based immunoanalysis technique using magnetic separation has been developed. This method does not use an immobilization procedure on a solid substrate; instead, it uses magnetic NPs as antibody-supporting materials. The magnetic NPs permit the rapid concentration of the plasmonic hybrid material within a small region (i.e., facilitate the formation of hot spots) prior to SERS analysis; thus, it is possible to obtain more reproducible and sensitive signals. Choo's group reported a quick and reproducible carcinoembryonic antigen (CEA) immunoanalysis method that integrates magnetic beads and SERS tags.[58]

Figure 6 shows a schematic diagram for the formation of a sandwich immunocomplex and its SERS immunoassays that requires magnetic beads as separation agents. As shown in Figure 6a, sandwich immunocomplexes were generated via a two-step process. In the first step, mAb-conjugated magnetic beads were added in a PBS buffer solution containing CEA. Next, the CEA-captured magnetic beads were isolated by a magnetic bar and then the solution was washed. In the second step, the obtained particles were further reacted with mAb-conjugated SERS tags in a shaker. The sandwich immunocomplexes were isolated by using a magnetic bar, causing the residual solution to become colorless, as shown in the left picture of Figure 6c. The residual solution was washed, and the immunocomplexes were redispersed in the PBS solution before SERS measurements. An LOD of 1−10 pg/mL was obtained, approximately 100 to 1000 times more sensitive than that of enzyme-linked immunosorbent assays. Furthermore, the assay took less than 1 h. Subsequently, taking advantage of the multiplex-labeling ability of SERS tags, the researchers accurately and sensitively detected CEA and another cancer marker protein, α-fetoprotein, in blood sera from clinical patients.[157]

A model paramagnetic NP assay was also demonstrated for SERS detection of DNA oligonucleotides derived from the West Nile virus (WNV) genome.[158] The detection was based on the capture of WNV target sequences by hybridization with complementary oligonucleotide probes covalently linked to the magnetic NPs and SERS tags. The resultant SERS tag−target sequence-magnetic NP complexes were removed from solution by an externally applied magnetic source. Laser excitation of the pelleted material provided a signature SERS spectrum that was diagnostic for the reporter, 5,5′-dithiobis(succinimidy-2-nitrobenzoate), and restricted to hybridization reactions containing WNV target sequences. The LOD for target sequences in buffer was 10 pM. A similar strategy was used to detect rabbit IgG via immuno-γ-Fe_2O_3/Au, MBA-labeled immunogold in concentrations from 10 pg/mL to 0.1 fg/mL.[159] The applications of SERS tags for ionic and molecular detection are summarized in Table 3.

3.2. Pathogen Detection

The rapid screening of pathogen remains a key issue in food safety, public health assurance, and diagnosis of infectious diseases.[175] Routine analyses of pathogens typically involve time-consuming biochemical characterization of cultured bacteria taken from contaminated sources.[176] Advances in SERS tags offer new possibilities for rapid screening and detection. For example, by combining the high sensitivity of SERS tags with the high specificity of single-domain antibodies (sdAbs), the targeted detection of a single bacterial pathogen *S. aureus* was achieved.[176] Microagglutination assay results and SEM images show that adding antibody-modified tags induces the agglutination of the bacteria, and their SERS intensity maps were clearly resolved. Goat anti-*Salmonella*-conjugated silver-silica core−shell SERS tags were prepared and used in a typical sandwich immunoassay to bioimage *Salmonella* bacteria.[143] Three successful surface conjugation strategies were used to conjugate silica-encapsulated SERS tags to the *Salmonella*-specific tail spike protein, allowing the detection of a single bacterium using SERS.[112] The selective detection of the multiple drug-resistant bacteria *Salmonella typhimurium DT104* was demonstrated by using M3038 monoclonal antibody-conjugated, popcorn-shaped gold tags, and an LOD of 10 cfu mL^{-1} was achieved.[177]

In another example, rhodamine B isothiocyanate (RBITC)- and MGITC-labeled SERS tags were conjugated with antibodies specific to *Giardia lamblia* cysts and *Cryptosporidium parvum* oocysts for simultaneous detection of these two waterborne pathogens.[178] Having diameters between 3 and 13 μm, these organisms were large enough to be identified by using an optical microscope if they were fixed to glass microscope slides (Figure 7). After incubation with the tags, the organisms could be easily measured and differentiated by using Raman spectroscopy. The results suggested that this SERS tag-based strategy could readily be used to simultaneously detect numerous waterborne organisms.

Charan and co-workers designed a simple, sensitive, and highly specific lipid-targeting SERS tag (Nile red-coated Ag NPs) to image living nematode *Caenorhabditis elegans* (*C. elegans*).[179] This tag would be incorporated into the intracellular intestinal granules of *C. elegans* after coincubation, thus allowing fast visualization of lipid droplets through a confocal Raman imaging technique.

The separation and detection of multiple pathogens in a food matrix by using magnetic SERS tags was also reported.[180] In this scheme, pathogens were first immunomagnetically captured with magnetic NPs, and pathogen-specific SERS tags were functionalized with corresponding antibodies to allow the formation of a sandwich assay. The detection of multiple pathogens in selected food matrices could be achieved by simply changing the kind of Raman reporters on the SERS tags. *Salmonella enterica* serovar Typhimurium and *Staphylococcus aureus* were used to illustrate the probability of using this scheme to detect multiple pathogens. The lowest cell concentration detected in a spinach solution was 10^3 cfu

dx.doi.org/10.1021/cr300120g | *Chem. Rev.* 2013, 113, 1391−1428

Table 3. Ionic and Molecular Detection Using SERS Tags[a]

samples	substrates	Raman reporters	detection limits	sensing properties	ref
Ions					
Hg^{2+}, Cd^{2+}	Au NPs	2,4,6-trimercapto-1,3,5-triazine		vibrational modes of ligands are sensitive to the metal ion coordination	151
Cd^{2+}	Au NPs	BGLA	8 μM	a layer of Cd^{2+}-chelating polymer grafted on Au NPs to render the selectivity	148
As^{3+}	Ag NPs	4-MPY	0.76 ppb	glutathione is used as selective ligand for its specific binding with As^{3+} ions through As−O linkage	160
Ni^{2+}	Au and Ag NPs	NIR-797 isothiocyanate	0.5 ppm	Ni^{2+}-nitrilotriacetic acid chemistry is applied to ensure the sensitivity	149
Hg^{2+}	Au nanopopcorn	tryptophan	5 ppb	a SERS signal turn-off mode and tryptophan acts as both Raman reporter and selectivity agent	161
Cl^-	Au@Ag NPs coating silica beads	amino-MQAE	20 pM	quantification is demonstrated by monitoring the vibrational changes of Cl-sensitive dye	152
Small Molecules					
glutathione	Ag NPs	rhodamine 6G, crystal violet, and 5,5′-dichloro-3,3′-disulfopropylthiacyanine	1 μM	thiol group containing analyte replaces the reporters and reduces the SERS signal	150
glucose, lactose, and glucuronic acid	Ag NPs	rhodamine B	1 nM	ratiometric SERS carbohydrate quantification using glucose labeled with rhodamine tag (RT) and RTd4	162
melamine	Au NPs	4-MPY	0.1 ppb	enhanced SERS signal due to the melamine induced aggregation of MPY-labeled gold nanoparticles	147
	Au NRs	DNBA	0.38 mg L^{-1}	enhanced SERS signal due to the melamine induced aggregation of magnetic-core Au shell NPs and Au NR based SERS tags	163
adenosine triphosphate	Au nanostar	MGITC	12.4 pM	the targets dissociate the duplex DNA structure and thereby removal of the SERS probe, reducing the Raman signal	164
Protein					
rabbit IgG	Au NPs	4-MBA	1−0.1 fg mL^{-1}	direct magnetic−immunoassay without requiring the assembly of sandwich structure onto a solid surface	159
mouse IgG	Au−Ag−C core−shell NPs	4-MBA	100−10 ng mL^{-1}	nontoxic carbon shell coated tags for ultrasensitive detection of biomolecules	93
	Ag@Au	*p*-aminothiophenol, thiophenol		the specificity of the labeled SERS tag was tested by control experiments using human IgG and PBS buffer	165
thrombin	Ag NPs	DBDT	100 pM	SERS aptatag components in an idealized dimer configuration	153
	Au NPs	rhodamine 6G	0.5 nM	hot spots can be further fabricated by deposition of Ag NPs on Au NPs based SERS tags	155
	Au NPs	4-MBA, 4-MPY, and RBITC	220 pM	fabrication of AuNR−AuNP junctions to enhance SERS signals	156
	Au−Ag−C core−shell NPs	4-MBA	10 fM	sandwich type of SERS immunoassay applied to detect α-thrombin in plasma	166
	Ag NPs	DBDT, BDT, and 2,6-NDT	100 pM	Ag NP dimers based aptatags for multiplexed heterogeneous bioassay	167
prostate-specific antigen	Au NPs	DNBA, Rhodamine G	1 pg mL^{-1}	sandwich type of SERS immunoassay	168
Interleukin-2 (IL-2) and IL-8	Ag NPs	8-azaadenine, benzoyladenine		composite organic−inorganic NPs (COINs) were designed for multiplex detection	110
avidin	Ag NPs	Coomassie brilliant blue dyes		Coomassie brilliant dyes can stain proteins and have strong Raman activity	169
human IgG	Au NR cluster	4-aminothiophenol	0.1 ng mL^{-1}	Raman tags of SiO_2@GNRs@SiO_2 provide better sensitivity than SiO_2@GNSs@SiO_2	118
	Au NP nanocluster	4-MBA	100 fg mL^{-1}	SERS-active immune substrate made a certain contribution to the highly sensitive immunoassay	170
mucin protein MUC4	Au NPs	4-nitrobenzenethiol	1 ng mL^{-1}	sera from cancer patients produced a higher SERS response compared to sera from benign diseased patients	171
carcinoembryonic antigen	SiO_2@$(AgNPs/PEI)_5$	4-aminobenzenethiol (4-ABT)	0.1 pg mL^{-1}	uniform SERS tags with reproducible signals were developed by the layer-by-layer assembly and cross-linkage of small Ag NPs at the surface of silica particles	172

dx.doi.org/10.1021/cr300120g | Chem. Rev. 2013, 113, 1391−1428

Table 3. continued

samples	substrates	Raman reporters	detection limits	sensing properties	ref
DNA					
oligonucleotides derived from West Nile virus genome	Au NPs	DSNB	10 pM	magnetic pull-down and concentration of hybridization complexes	158
multiple pathogen DNAs	Au NPs	Cy5 and TAMRA	10 pM to 10 nM	reproducible SERS signals by using nanoscale gaps between Au nanowire and NPs	173
synthetic model ssDNA	Au NPs	Rox	10.0 pM	rolling circle amplification-based SERS might discriminate perfect matched target DNA from 1-base mismatched DNA with high selectivity	174

[a]Abbreviations: MGITC, malachite green isothiocyanate; BGLA, 2-(4-((bis(4-(diethylamino)phenyl)(hydroxy-methyl)phenoxy)ethyl 5-(1,2-dithiolan-3-yl)pentanoate; 4-MPY, 4-mercaptopyridine; amino-MQAE, 2-(2-(6-methoxyquinoliniumchloride)ethoxy)-ethanamine-hydrochloride; 4-MBA, 4-mercaptobenzoic acid; DBDT, biphenyl-4,4′-dithiol; MGITC, malachite green isothiocyanate; RBITC, Rhodamine B isothiocyanate; BDT, 1,4-benzenedithiol; 2,6-NDT, 2,6-naphthalenedithiol; DNBA, 5,5′-dithiobis(2-nitrobenzoic acid); DSNB, 5,5′-dithiobis(succinimidyl-2-nitrobenzoate); TAMRA, carboxytetramethylrhodamine.

mL^{-1}: The results of a blind test in peanut butter validated that this LOD was achieved with high specificity, demonstrating the potential of this approach in complex matrices. Similarly, a specific method was developed to enumerate *Escherichia coli* in water samples with a linear range of 10^1−10^4 cfu mL^{-1} and an LOD of 8 cfu mL^{-1}.[181]

3.3. Live-Cell Imaging

SERS tags are increasingly being used in live-cell studies. The SERS technique fulfills the requirements of live-cell imaging in the following aspects.[182−184] First, the use of low laser powers can produce strong signals; therefore, SERS imaging avoids light-induced injury of the cells. Second, the excitation laser spot of the Raman microscope can be focused in a micrometer scale. Together with the nanosized SERS tags, the method can provide high-resolution images that reflect the microenvironment in cells. Third, data acquisition time is short when using the Raman system, enabling real-time and dynamic monitoring of biological processes.

3.3.1. Cancer Marker Detection. One key use of SERS tags in living cells is for multiplex, highly sensitive detection of cancer biomarkers on the cell membrane, demonstrating the potential for high-throughput screening of cancer cells. Kim et al.[117] synthesized silica-coated silver NPs with 4-mercaptotoluene (4-MT) or thiophenol (TP) used as reporters. After surface modification, the antibody-conjugated SERS tags (SERS $tag_{4MT\text{-}HER2}$ and SERS $tag_{TP\text{-}CD10}$) were used to reorganize HER2 and CD10 on cellular membranes. Similarly, Choo's group developed antibody-modified Au NR-based[77] and Au/Ag bimetallic NP-based[100] tags to monitor MCF7 cells overexpressing the breast cancer marker HER2 and HEK293 cells overexpressing phospholipase PLCγ1. SERS tags' sensing was compatible with traditional pathology stains. Raman signals were not disrupted by pathology stains such as eosin, hematoxylin, and Giemsa, indicating advantages over fluorescence methods for multiplex pathology diagnosis.[130]

An interesting and novel type of stand-alone cellular SERS tag called a nanocoral was reported.[185] As shown in Figure 8, half of the nanocoral's surface was coated with highly roughened gold to increase its reporter adsorption capacity and create a high density of SERS hot spots, and the blank polystyrene hemisphere could be functionalized with targeting moieties to specific cells. Therefore, the targeting and sensing mechanisms for a particular experiment could be separately engineered. By incubating reporter-labeled nanocoral suspensions with anti-HER2 antibodies, specific targeting and SERS detection of breast cancer cells (BT474 cell line, ATCC) were both achieved.

SERS tags can be used to identify cancer cells in biological samples via specific membrane cancer marker binding. Sha et al.[186] reported detecting circulating breast cancer cells in the blood by using a combination of epithelial cell-specific, antibody-conjugated, magnetic nanoprobes and anti-HER2 antibody-conjugated SERS tags. Because the breast cancer cell is of epithelial origin, the magnetic nanoprobes can specifically bind to this tumor cell but not to regular blood cells. Furthermore, because the HER2 receptor is highly expressed on the breast cancer cell membrane, the SERS tags will specifically recognize these tumor cells. Thus, the cancer cells could be detected rapidly and with good sensitivity. Similarly, SERS tags with epidermal growth factor (EGF) peptide as a targeting ligand have been put into practical use to identify circulating tumor cells (CTCs) in the peripheral blood of 19

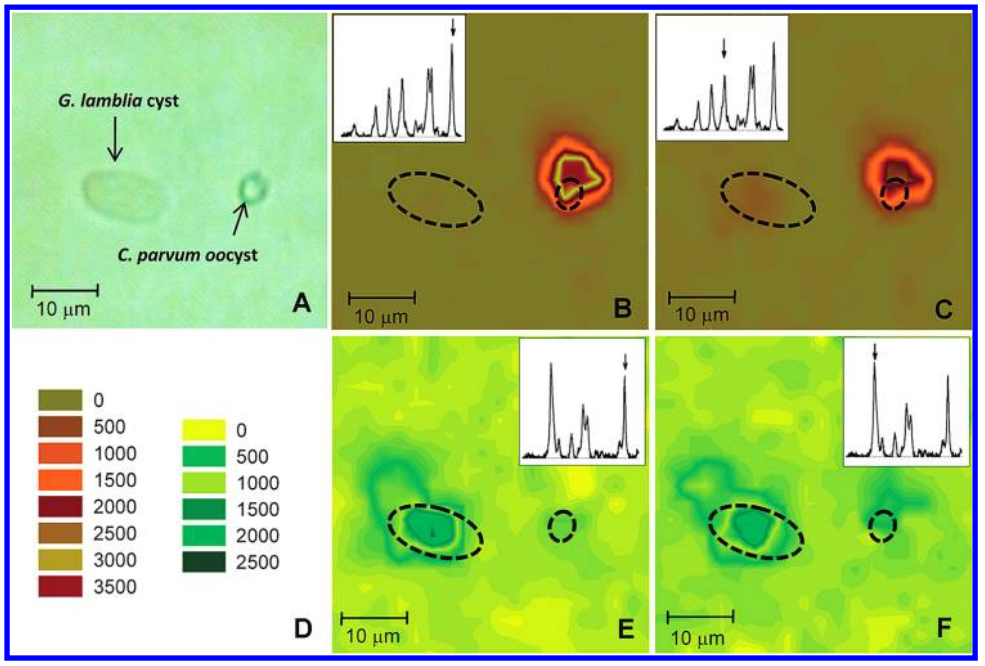

Figure 7. Raman $x-y$ maps of a *G. lamblia* cyst and a *C. parvum* oocyst. (A) Optical microscope image of a cyst and an oocyst. (B) Raman map of the 1647 cm^{-1} RBITC peak. Inset: RBITC SERRS spectrum with the arrow identifying the 1647 cm^{-1} peak. (C) Raman map of the 1360 cm^{-1} RBITC peak. Inset: RBITC SERRS spectrum with the arrow identifying the 1360 cm^{-1} peak. (D) Raman intensity key. (E) Raman map of the 1618 cm^{-1} MGITC peak. Inset: MGITC SERRS spectrum with the arrow identifying the 1618 cm^{-1} peak. (F) Raman map of the 1175 cm^{-1} MGITC peak. Inset: MGITC SERRS spectrum with the arrow identifying the 1175 cm^{-1} peak. Reprinted with permission from ref 178. Copyright 2009 American Chemical Society.

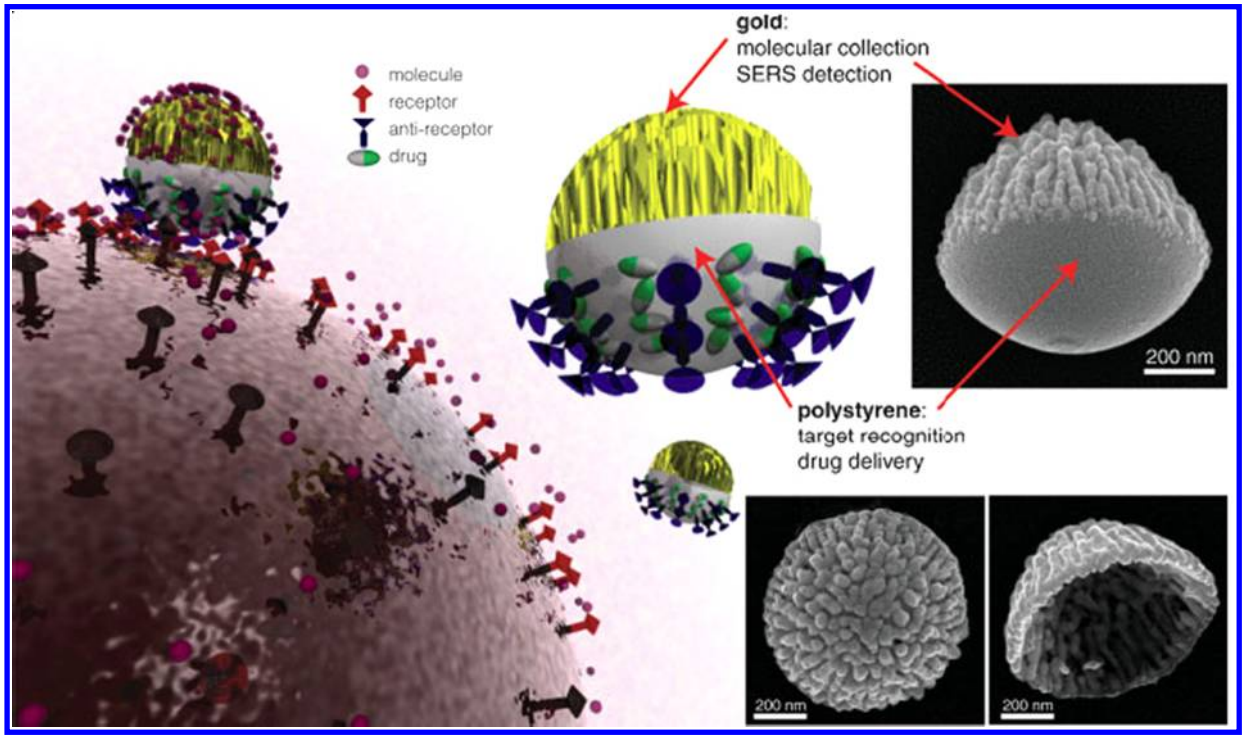

Figure 8. Schematic of nanocorals as multifunctional nanoprobes for targeting, sensing, and drug delivery; insets show scanning electron microscopy images of fabricated nanocoral probes; the polystyrene template has been etched in the bottom right inset. Reprinted with permission from ref 185. Copyright 2010 John Wiley & Sons, Inc.

patients with squamous cell carcinoma of the head and neck, with a range of 1−720 CTCs per milliliter of whole blood.[187]

3.3.2. Intercellular Microenvironment Sensing. SERS tags are also powerful tools for studying local chemistry and changes in the cellular microenvironment. The huge enhancements of the Raman signal induced by the noble metal NPs make SERS ideal for the nondestructive, ultrasensitive detection of intrinsic chemical species in living cells. By monitoring and analyzing the signal variations of the SERS tags, rare chemicals

dx.doi.org/10.1021/cr300120g | *Chem. Rev.* 2013, 113, 1391−1428

and important cellular parameters such as pH levels can be measured.

Kneipp's group performed a serial of pioneered work in this field.[17,182,184,188−190] They designed indocyanine green (ICG)-,[190] rose bengal-, or crystal violet-labeled[182] Ag and Au NPs as SERS tags. After internalization, the tags not only exhibited the characteristic SERS signatures of dyes but also delivered spatially localized chemical information about intercellular components by using SERS in the local optical fields of the NPs. Figure 9 showed examples of SERS spectra measured in single Dunning R3327 rat prostate carcinoma cells incubated with the ICG-gold SERS tag at 830 nm excitation.[190] Trace A was an ICG SERS spectrum measured from a bare dye-gold tag. Traces B, D, and E showed relatively weak spectral signatures of ICG and several Raman lines originating from the cellular surroundings of the Au NPs. The ability to extract qualitative vibrational information about the biological matrix in trace C showed a spectrum of native cell components, which was obtained after subtracting the ICG spectrum (i.e., spectrum A) from spectrum B. The Raman lines observed could be assigned to vibrations characteristic for protein, lipid, or nucleotide molecular groups.

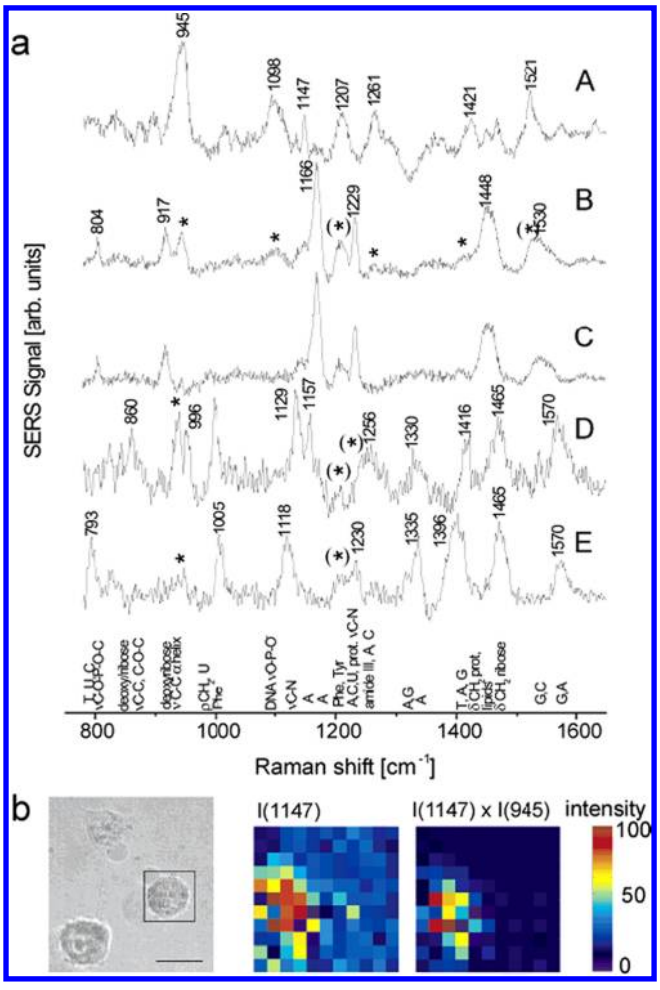

Figure 9. Examples of SERS spectra measured in single living cells incubated with the ICG-gold nanoprobe at 830 nm excitation. Trace A represents the ICG signature. Assignments of major bands in spectra B−E are given below spectrum E. ICG bands are marked with an asterisk, while an asterisk in parentheses indicates contribution of both ICG and cell. Trace C shows the difference between spectra B and A and displays only Raman lines of the cell. Abbreviations: A, adenine; G, guanine; C, cytosine; T, thymine; U, uracil; Phe, phenylalanine; Tyr, tyrosine; prot, proteins; ν, stretching; δ, deformation; ρ, rocking. (b) Spectral map of the tag in a cell based on the 1147 cm^{-1} ICG line and on the product of two ICG lines at 1147 and 945 cm^{-1}. Intensities are scaled to the highest value in each area. A photomicrograph of the cell, indicating the studied area, is shown for comparison. Scale bar 20 μm. Reprinted with permission from ref 190. Copyright 2005 American Chemical Society.

Several groups recently showed that SERS tags enable the dynamic detection of local pH in individual living cells to be followed at subendosomal resolution. The main principle for the measurement was the pH-dependent SERS spectra of reporters such as MBA[191,192] or 2-aminobenzenethiol (2-ABT)[193] due to protonation of the carboxyl or amino groups at low pH. For example, the line at 1423 cm^{-1} on gold or at 1380 cm^{-1} on silver in MBA belonged to the COO^--stretching mode and was sensitive to the dissociation of the carboxyl group. Signal ratios of the 1423 cm^{-1} or 1380 cm^{-1} line to the aromatic ring vibration at 1076 cm^{-1} could be used to sense pH variation. Therefore, SERS pH nanosensors detected information by using the relative signals of spectrally narrow "pairs" of Raman lines in the same spectrum, allowing quantitative measurement without any correction of cellular background absorption and emission signals.

Figure 10 showed typical pH imaging in a single, live NIH/3T3 cell detected by using MBA-Au SERS tags.[194] The colored portion displayed the ratio of the SERS signals at 1423 and 1076 cm^{-1} as a function of sampling position in one of the cells, that is, a pH map of the cell. After 1 h coincubation of the cell and SERS tags, the pH at different sampled spots in the cell was between 6.2 and 6.9, indicating that endosomes containing the tags had only partially spread throughout the cytoplasm. However, 4.5 h later, the images showed pH values between 6.9 and 5, indicating that the tag-containing endosomes were distributed throughout the cytosol. Using this novel pH sensor and Raman imaging technique, researchers clearly showed the NP's endocytosis process from accumulation in late endosomes to the lysosome.

The samples detected by using SERS tags for cellular imaging are summarized in Table 4.

3.4. Tissue SERS Imaging

Either frozen or formalin-fixed specimens and paraffin-embedded tissue samples can be used for specific protein localization in tissue after SERS microscopy with functionalized SERS tags: detection in embedded specimens requires paraffin removal and antigen retrieval. In 2006, Schlücker's group first demonstrated this approach:[203] They chose prostate-specific antigen (PSA) as the target because of its high expression level in prostate tissue and selective histological abundance in the epithelium of the prostate gland. After incubating primary antibody-modified Au/Ag nanoshell SERS tags with prostate tissue sections, characteristic Raman signals of the SERS tags were detected only in the PSA(+) epithelium; however, no spectral contributions were detected in the PSA(−) stroma or lumen negative controls (Figure 11). Lately, they performed the same experiment by using novel silica-coated tags with complete SAM of Raman reporters on Au/Ag nanoshells, illustrating a much better sensitivity than that obtained after submonolayer coverage of reporters on solid gold NPs.[68]

Knudsen and co-workers next reported a simultaneous double-SERS tag staining for PSA, yielding two distinct signals labeling PSA antibodies on the tissue surface.[129] The

dx.doi.org/10.1021/cr300120g | Chem. Rev. 2013, 113, 1391−1428

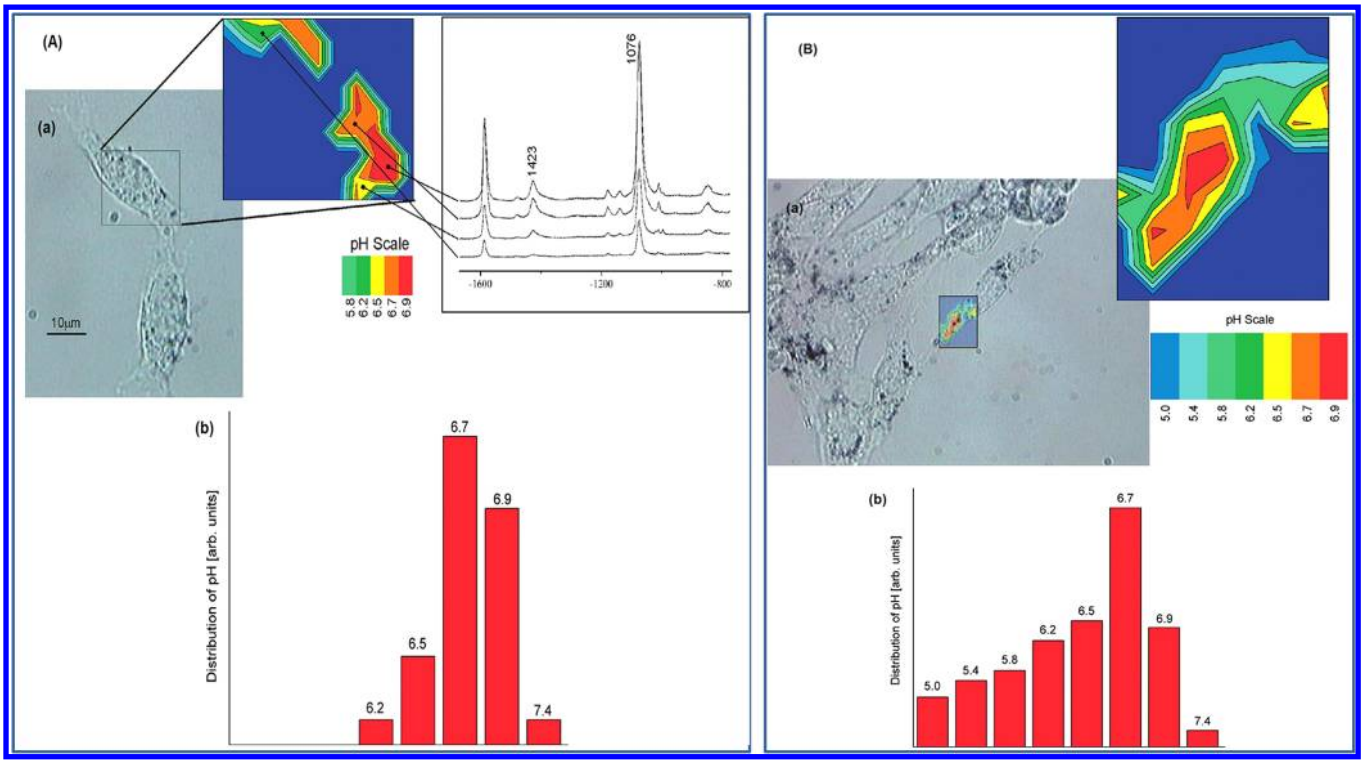

Figure 10. (A) Probing and imaging pH in single live cells after 60 min of incubation time with SERS nanosensors. (a) The bright field image shows a 3T3 cell incubated with gold NPs. The displayed SERS spectra are examples for spectra measured in different cellular compartments during a raster scan over the rectangle. The false color plot of the calibrated ratio of the Raman lines at 1423 and 1076 cm^{-1} displays a pH image of the cell. Scattering signals below a defined signal threshold, i.e., from places where no SERS signals exist, appear in dark blue. The values given in the color scale bar determine the upper end value of each respective color. (b) Distribution of pH based on SERS mapping over eight cells. (B) Probing and imaging pH in a single live 3T3 cell after 4.5 h of incubation time with SERS nanosensors. (a) pH image merged with the bright-field image of the cell. (b) Distribution of pH based on SERS mapping over five cells. Reprinted with permission from ref 194. Copyright 2010 American Chemical Society.

characteristic Raman signatures from both tags were detected at almost every location in the epithelium, suggesting that steric hindrance from tags did not represent a major problem. In a subsequent study, the same group compared the staining performance of SERS-tagged PSA antibody to that of Alexa fluorophore-tagged PSA antibody conjugates on adjacent tissue sections.[204] Both labeling methods yielded similar results, with a lower staining accuracy but similar signal intensities when using SERS tags. The spectral analysis results demonstrated the fundamental difference between SERS-based and molecular fluorophore-based detection:[205] the narrow Raman signals of the SERS probes could clearly be discriminated from background autofluorescence, which was particularly advantageous when analyzing low-abundance analytes and low-intensity signals.

3.5. *In Vivo* SERS Imaging

Many aspects of biomedical research and patient treatment rely on optical imaging of living subjects. Various imaging modalities, including NIR fluorescence,[206,207] bioluminescence,[208] and photoacoustic tomography,[209] are frequently used for small-animal models. Raman imaging has emerged as a novel and powerful tool for optical *in vivo* imaging analysis and overcomes several limitations of other imaging methods.[210] First, few types of NIR fluorescent imaging agents exist, and the spectra are likely to overlap, restricting the ability to detect multiple targets simultaneously; however, multiplexing is easily achieved with SERS tags. Second, the SERS technique can be used with NIR laser excitation, allowing it to share the advantages of fluorescence *in vivo* imaging in deep tissues. However, unlike fluorescent dyes, SERS tags have superior photostability, making them suitable for studies of prolonged duration. Third, the biosafety of SERS tags can be expected to be better than that of the heavy metal-composed NIR QDs, which are extensively used as *in vivo* fluorescence imaging probes.[211] Therefore, SERS imaging shows much more potential for real clinical application in the future than fluorescent probes do.

In 2008, Nie and co-workers[37] demonstrated the first use of SERS tags for *in vivo* tumor targeting: a single tag composed of a 60 nm Au NP, crystal violet, and thiol-PEG was approximately 200 times brighter than a NIR QD. When conjugated to tumor-targeting ligands such as single-chain variable fragment antibodies, the SERS tags could target tumor biomarkers (epidermal growth factor receptors) on human cancer cells and in xenograft tumor models. The SERS spectra obtained by using a 785 nm laser beam on the tumor site had a strong SERS-tag signature; however, anatomic locations such as the liver only yielded a low background signal.

Gambhir et al.[212] demonstrated multiplexed *in vivo* SERS imaging in mice using labeled, pegylated, or silica-coated gold particles as SERS tags, imaging four types of SERS tags that had been subcutaneously (sc) injected into mice at varying concentrations. Because the SERS tags had different Raman spectra, the concentration of each could be calculated by using the component analysis method. These researchers also demonstrated the ability of Raman spectroscopy to separate

dx.doi.org/10.1021/cr300120g | *Chem. Rev.* 2013, 113, 1391−1428

Table 4. Live-Cell Detection Using SERS Tags[a]

samples	substrates	Raman reporters	detection limits	detection properties	ref
BT474 breast cancer cell	Au coated nanocoral	Rhodamine 6G	single cell	fluorescent markers or drugs may be embedded in the PS template region to add increased functionality	185
HEK293 cell	Au@Ag NPs	Rhodamine 6G	single cell	the antibody-conjugated SERS tags were used for t bioimaging of HEK293 cells expressing PLCγ1 cancer markers	100
leukemia cell	Au NPs	MGITC	single cell	to detect CD19 antigen on leukemia cells in a spun-down whole blood sample	130
	Au NPs	MGITC	single cell	CD20 clustering within 100 nm was observed by using rituximab conjugated tags	195
gland adenocarcinoma cell	Au NRs	4-mercaptopyridine	subcellular level	GNRs-antibody conjugation was developed using the layer-by-layer deposition method	77
	hollow Au NSs	crystal violet	subcellular level	HGNs were used as multimodal sensing agents for both dark-field and SERS detection	54
	Ag NPs	4-MT, 2-NAT	subcellular level	antibody conjugated SERS dots for the targeting of HER2 and CD10 on cellular membranes	117
human hepatoma cell	Ag NPs	Carborane	subcellular level	carborane functionalized tags have a therapeutic potential in addition to imaging capabilities	196
mouse fibroblast 3T3 cell	Au NPs	Rose Bengal and crystal violet	subcellular level	provide sensitive information on the immediate molecular environment of the SERS tags	182
	Au NPs	4-MBA	subcellular level	spatially resolved probing and imaging of pH in live cells	197
R3327 rat prostate carcinoma cell	Au NPs and Ag NPs	indocyanine green	subcellular level	delivering spatially localized chemical information	190
SKBR3 breast cancer cell	Nanoplex TM biotag		10 cells mL^{-1}	nanoplex biotags for the direct detection of rare cancer cells in whole blood	186
	Au NPs	triphenylmethine derivatives	single cell	nanotag conjugated with selective antibodies recognizing HER2 and EGFR cancer proteins found reasonably strong SERS signals	121
HeLa cell	PVP coated Ag NPs	4,4′-Bipyridine and 4-MBA		PVP shell coated tags exhibit strong SERS effect and low toxicity toward living cells	108
macrophage cell	Au nanoflowers	Rhodamine B		the nanoflower tags showed a stronger signal than that of NSs tags with similar size	83
H9c2 cardiac myocyte	Ag NPs	4-(mercaptomethyl)benzonitrile	subcellular level	report on the receptor aggregation state of specifically label β_2-adrenergic receptors based on the distance modulated SERS signal enhancement	198
MIAPaCa-2 pancreas carcinoma cell	Ag NPs	2-aminothiophenol	single cell	pH-dependent SERS spectra enable one to sense the pH over the range 3.0−8.0	193
Chinese hamster ovary cell	Ag NPs	4-MBA	subcellular level	the tag shows a characteristic response to the pH and is sensitive to pH changes in the range 6−8	199
.ymphocyte	Au NPs	Rhodamine 6G	subcellular level	the principal component analysis enabled separation of the spectral contribution of rhodamine 6G from the complex cellular matrix	200
bronchioalveolar stem cell	Ag-magnetic-SERS dots	4-methylbenzenethiol and benzenethiol		M-SERS Dots as a sorting system with very effective isolation of targeted cells	201
rat cardiomyocyte cell	Ag NPs	MMBN, DMMB, MMByne, and MMBNO	subcellular level	multiplexed imaging of β_2-adrenergic receptor and caveolin-3 on the cell surface	202

[a]Abbreviations: 4-MT, 4-mercaptotoluene; 2-NAT, 2-naphthalenethiol; MMBN, 4-(mercaptomethyl)benzonitrile; DMMB, *d*7-mercaptomethyl benzene; MMByne, 4-(mercaptomethyl)ethynylbenzene; MMBNO, 4-(mercaptomethyl)nitrobenzene.

dx.doi.org/10.1021/cr300120g | *Chem. Rev.* 2013, 113, 1391−1428

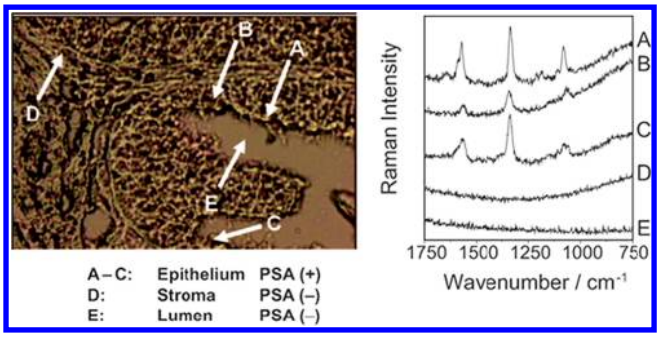

Figure 11. White light microscope image of epithelial tissue from the prostate (left) and Raman spectra (right) recorded in situ at the locations indicated by arrows: (A–C) epithelium; (D) stroma; (E) lumen. Reprinted with permission from ref 203. Copyright 2006 John Wiley & Sons, Inc.

the spectral fingerprints of up to ten different sc injected tags and five intravenous (iv) injected tags in liver (Figure 12).[213] They also linearly correlated Raman signals with SERS concentrations after sc or iv injecting four unique tags. This *in vivo* multiplex-imaging ability has great potential for use in high-throughput drug screening in living subjects. Lately, SERS tags were applied for in vivo imaging of early stage inflammation.[214] The intercellular adhesion molecule 1- (ICAM-1-) antibody-conjugated tags were able to detect ICAM-1 expression on endothelial cells. SERS based non-invasive measurement provided twice the sensitivity of two-photon fluorescence.

4. CHALLENGES AND PERSPECTIVES

Recent advances in a variety of approaches to the synthesis of SERS tags have contributed significantly to the goals of understanding the optical properties of these tags and developing them for biological analysis and imaging. Still, further advances in the use of SERS tags cannot be made until the following challenges are met: improvement of the tags' quantitative ability, expansion of their multiplex labeling ability, reduction of the tag's size for high-spatial cell imaging, ability to quickly locate their signals *in vivo*, and biocompatibility.

4.1. Reproducible Signal of SERS Tags

Signal reproducibility of SERS tags is crucial for quantitative bioanalysis. Better synthesis routes that would produce high-quality tags should fulfill the following two requirements: (1) the NPs or nanoclusters constituting the hot spots should have uniform size and morphology; (2) the number and position of Raman reporters in the hot spots should be reproducible. The second issue can be well addressed via a SAM-coating strategy, as described in section 2.2.2. Therefore, we will focus the following paragraphs on advances in the fabrication of precisely controlled nanosubstrates for SERS enhancement. Because using proper signal calibration methods can also dramatically increase the reproducibility and quantitation ability of SERS tags, we will discuss signal calibration as well.

4.1.1. Precisely Controlled Hot Spots for Nanosubstrates. Hot spots generated in the metal substrates are thought to play an important role in the Raman signal enhancement. The results of recent investigations of 10^6 SERS active sites revealed that 63 hot spot sites contributed 24% of the overall SERS intensity.[215] However, typical studies have

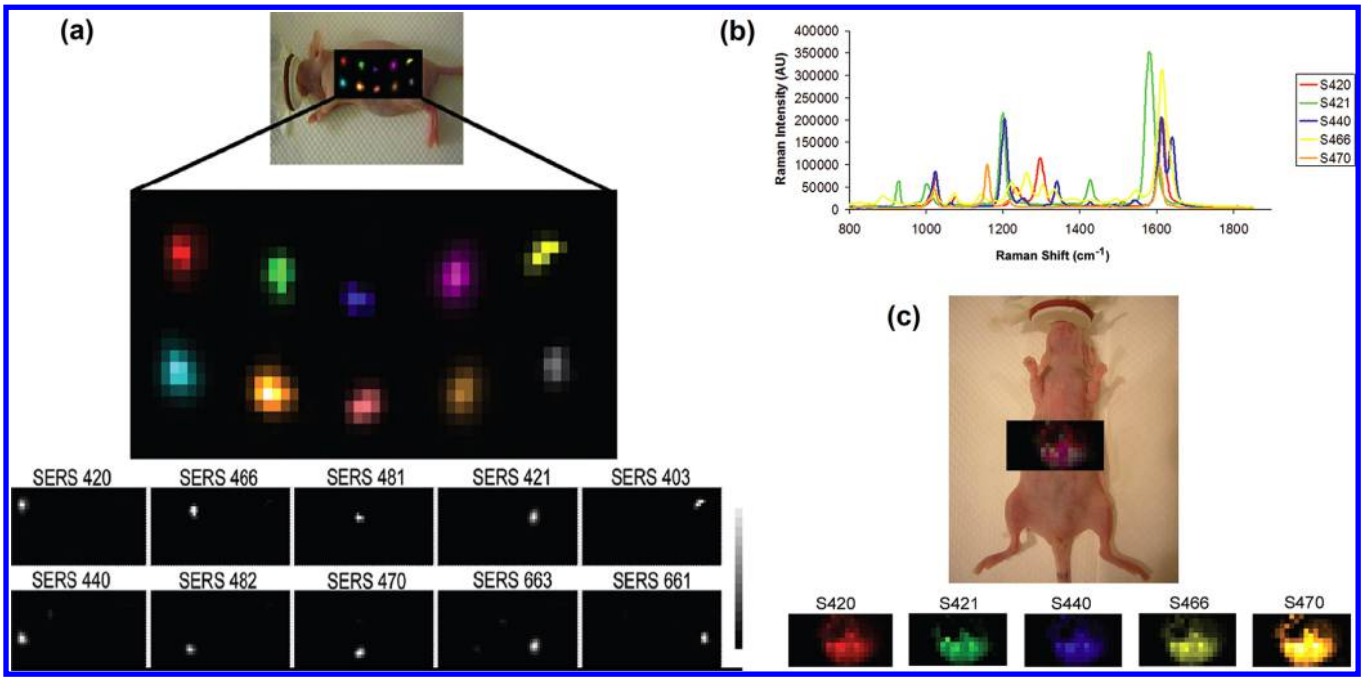

Figure 12. (a) Evaluation of multiplexing 10 different SERS NPs *in vivo*. Raman map of 10 different SERS particles injected subcutaneously in a nude mouse. Arbitrary colors have been assigned to each unique SERS NP batch injected. *Panels below* depict separate channels associated with each of the injected SERS NPs. Grayscale bar to the right depicts the Raman intensity, where white represents the maximum intensity and black represents no intensity. (b and c) Demonstration of deep-tissue multiplexed imaging 24 h after intravenous (iv) injection of five unique SERS NP batches simultaneously. (b) Graph depicting five unique Raman spectra, each associated with its own SERS batch. (c) Raman image of liver overlaid on digital photo of mouse, showing accumulation of all five SERS batches accumulating in the liver after 24 h post iv injection. *Panels below* depict separate channels associated with each of the injected SERS NP batches. Reproduced with permission from ref 213. Copyright 2009 National Academy of Sciences, USA.

dx.doi.org/10.1021/cr300120g | *Chem. Rev.* 2013, 113, 1391–1428

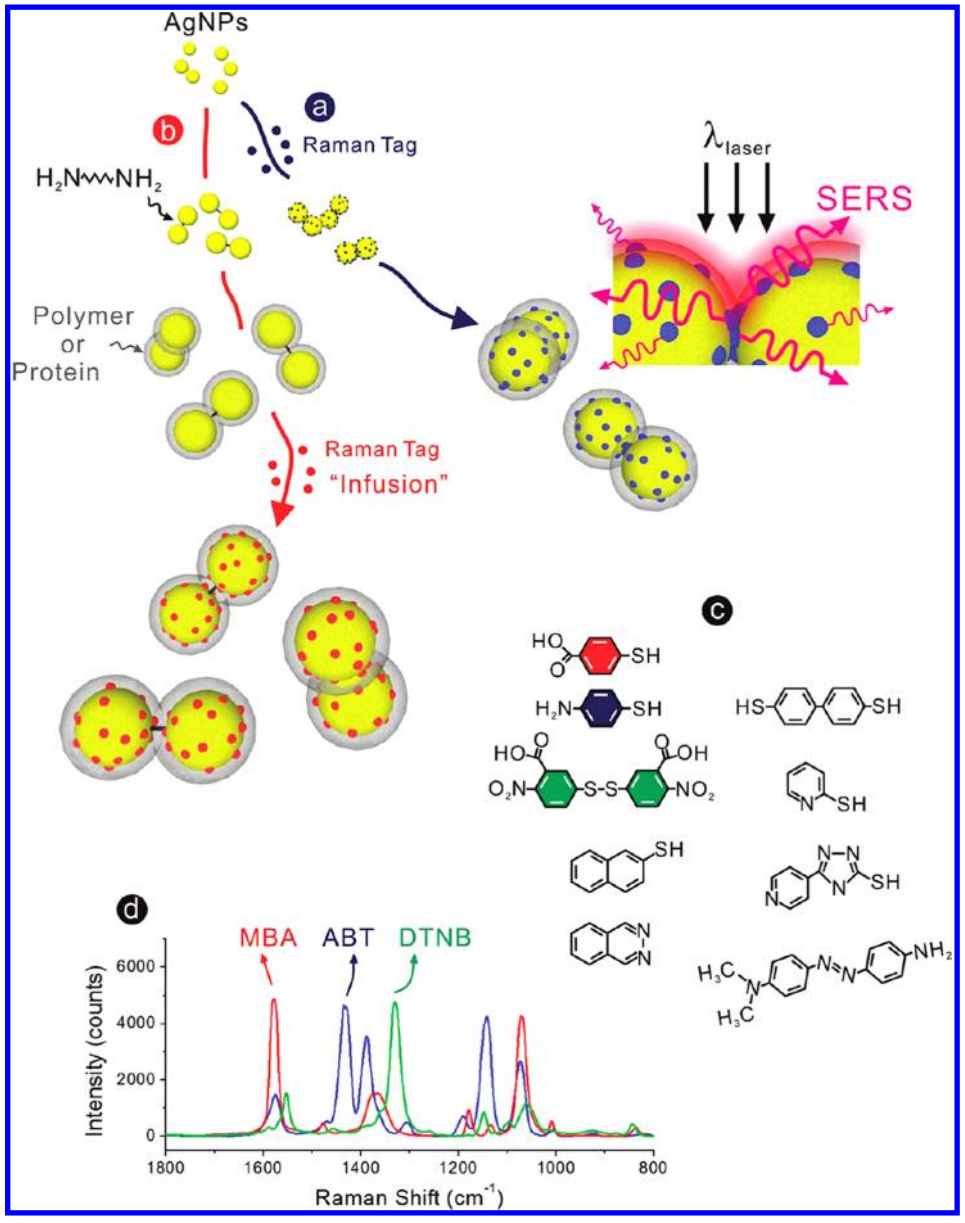

Figure 13. SERS nanocapsule synthesis. (a) Ag nanoparticles are cross-linked with the bifunctional linker 4-aminobenzenethiol (ABT, blue) or (b) 1,6-hexamethylenediamine (HMD, black), each then coated with a layer of PVPA. PEG thiol or streptavidin and bovine serum albumin proteins are then adsorbed (not shown). In part b, the SERS tag (red) is infused through the polymer coat. The inset represents SERS from tags in the junction. (c) Structures of 4-mercaptobenzoic acid (MBA, red), 4-aminobenzenethiol (ABT), 5,5′-dithiobis(2-nitrobenzoic acid) (DTNB), biphenyl-4,4′-dithiol (BPDT), 2-mercaptopyridine (MPY), 2-naphthalenethiol (NPT), 4-amino-5-(4-pyridyl)-4H-1,2,4-triazole-3-thiol (APTT), phthalazine (PHTH), and 4-Amino-4′-dimethylamino azobenzene (DAAB). (d) Color-coded spectra of SERS nanocapsules with MBA and DTNB prepared as in part b and ABT as in part a. Reprinted with permission from ref 109. Copyright 2009 American Chemical Society.

prepared the nanoclusters by random aggregation of metal NPs. Because of the nonuniformity and scarcity of the desired nanostructures, it is difficult to correlate a SERS signal with the exact nanostructure from which it originates.[216] Therefore, producing quantitative, controllable SERS signals and generating a narrow distribution of high enhancement factor values remains tough. To address these problems, a few experimental strategies have been proposed that arrange particles into discrete collections of spatially and symmetrically well-defined aggregates: several reviews of this topic exist,[23,217] so we will illustrate only the most sound and recent examples.

4.1.1.1. Molecularly Bridged Metal Clusters. One way to fabricate controllable NP dimers and small clusters is to use a bifunctional linker bridging Au and Ag NPs together.[191,218] The linker molecules including biphenyl-4,4′-dithiol, 1,4-benzenedithiol, and 6-naphthalenedithiol can form hot spots *in situ* by linking NPs and can simultaneously act as reporters.[109,153,167,219−221] When the SERS enhancement is optimized, the aggregation process is quenched by polymer and protein stabilizers, resulting in SERS substrates (mainly dimers and trimers) with excellent enhancement uniformity, reproducibility, and stability.

Moskovits' group[109] described two strategies involving three stages: linker addition, polymer quenching, and filling the hot spot with analyte. Figure 13a schematically shows the synthesis of tagged clusters by using a bifunctional Raman active linker that possesses terminal thiolate or amino groups (4-aminobenzenethiol, ABT), which can automatically position

dx.doi.org/10.1021/cr300120g | *Chem. Rev.* 2013, 113, 1391−1428

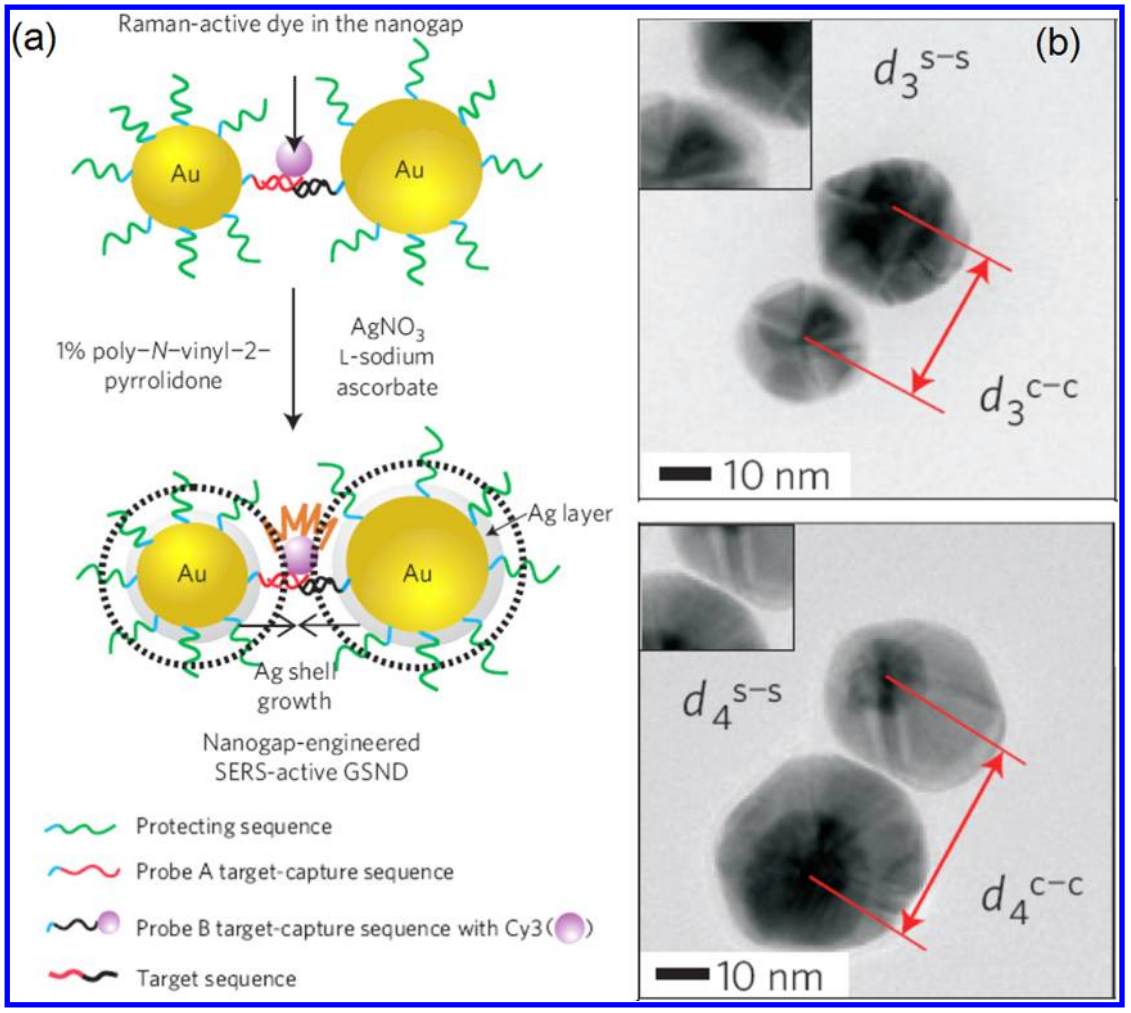

Figure 14. (a) Nanometer-scale silver-shell growth-based gap-engineering in the formation of SERS-active Au@Ag encoded dimers. (b) gold–silver core–shell nanodumbbell (GSNDs) particles with 5 nm (upper) and 10 nm (lower) Ag shell thicknesses. The $d^{s\text{-}s}$ and $d^{c\text{-}c}$ indicate the distances between two particle surfaces and cores, respectively. Reproduced with permission from ref 225. Copyright 2010 Nature Publishing Group.

themselves in hot spots. After sufficient aggregation, polymer is added to quench the reaction.

Figure 13b shows a much more versatile strategy. NP dimers and small aggregates are assembled by using a diamine aggregation agent (1,6-hexamethylenediamine) that can be displaced at a later stage by a molecule of interest without compromising the integrity of the prelinked nanocapsules. Importantly, the diamine has a small Raman cross section and weak binding affinity, allowing the post-infusion and sensing of multiple Raman reporters that may be inefficient aggregation agents in their own right. The polymer-quenching process stabilizes the hot spots between particles, which are accessible by small Raman reporters in a subsequent infiltration step. Figure 13c shows a number of reporters infused into these prelinked nanocapsules.

DNA-assisted assembly of nanodimensional substrates is another successful approach to producing reproducible SERS tags. DNA is a good choice of biological ligand because it has been used successfully to assemble numerous plasmonic nanostructures.[222] Additionally, the length of DNA can be readily controlled and is well understood, and the kinetics of single-DNA molecule hybridization are relevant in biotechnology and nanoscience applications.[223] Qian et al. developed SERS beacons that can be turned on and off by DNA binding and dissociation events.[224] They first functionalized Au NP SERS tags with different thiolated, single-strand DNA probes. When the tags met their complementary DNA-labeled probes, then sequence-specific DNA hybridization brought two or more particles into a desired distance (usually 10–20 nm surface to surface distance), resulting in plasmonic coupling and further enhancement of the Raman signals. This beacon-driven enhancement demonstrated single-base specificity and temperature sensitivity.

More recently, Lim et al.[225] reported a high-yield method for synthesizing SERS-active, Au–Ag core–shell, nanodumbbell (GSND)-type tags via a similar DNA hybridization strategy that resolved two main problems remaining after Qian's work: uncontrollable NP numbers in the nanocomplex and long-distance nanogaps between particles (Figure 14). First, a relatively high yield of structurally reproducible dimetric nanostructures was acquired by using a stoichiometric control over the number of tethering DNA molecules on the Au NP surface and a subsequent magnetic-particle based separation method. Second, the gap between two NPs and the Raman reporter (Cy3) position could be engineered in the range of 3.5 to 1.5 nm wide by forming Ag shells on the surface of the dimeric Au NPs. These programmed nanostructure fabrication and single-DNA detection strategies open avenues for the high-

dx.doi.org/10.1021/cr300120g | Chem. Rev. 2013, 113, 1391–1428

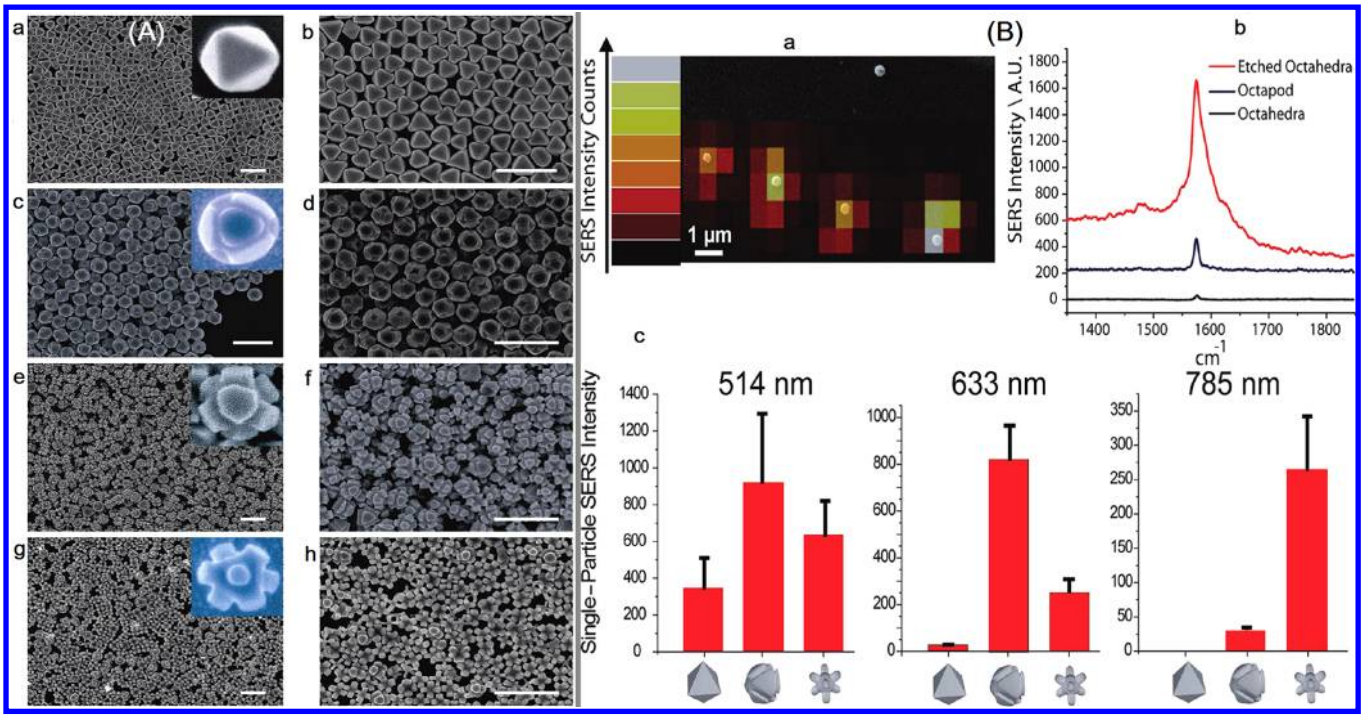

Figure 15. (A) SEM images following the etching progress of the silver octahedral-shaped nanoparticles. (a, b) Octahedra-shaped starting materials showing regular size and shape, which are essential for controlled etching reactions; (c, d) using a small amount of etchant, the edges and corners can be selectively etched leaving gaps of 5−10 nm; (e, f) when exposed to a slightly higher concentration of etching solution, eight distinct arms develop; and (g, h) finally, at relatively high concentrations of etching solution, octapod-shaped nanoparticles are isolated in high yield. All scale bars shown represent 1 μm. (B) Single-particle Raman scattering of benzenethiol at 1584 cm^{-1}. (a) SEM image of isolated, etched particles overlaid with the SERS intensity map; colors are assigned by the relative intensity of the spectrum at 1584 cm^{-1}; (b) representative SERS spectra for each shape obtained during 1 s integration with 633 nm excitation; and (c) average single-particle intensity shown for each particle shape as a function of excitation wavelength. Error bars reflect one standard deviation. Reprinted with permission from ref 226. Copyright 2010 American Chemical Society.

yield synthesis of structurally reproducible SERS tags for bioassays.

4.1.1.2. Modulating Nanosubstrate Morphology via Anisotropic Etching. Reproducible SERS nanosubstrates can also be chemically controlled by a highly anisotropic etching process. Tuning the etchant strength and reaction conditions allows the high-yield, high-purity preparation of new NP shapes that cannot be synthesized by using conventional nanocrystal growth methods.[226] The etching process may introduce modified plasmonic characteristics and significant enhanced Raman-scattering ability, allowing new noble particles to serve as excellent substrates.

Xia's group demonstrated a facile method based upon wet-etching with $Fe(NO_3)_3$ to generate well-defined dimers of Ag nanospheres from a uniform sample of Ag nanocubes.[227] The etching reaction was performed at room temperature in ethanol with the help of PVP. When an aqueous suspension of Ag nanocubes was mixed with a small amount of an aqueous solution of $Fe(NO_3)_3$ in ethanol, the corners and edges of the cubes were truncated to form spheres that then led to the NP dimerization. A SERS enhancement factor of 1.7×10^8 was measured for an individual dimer consisting of 80 nm spheres when 4-methylbenzenethiol was the probe molecule. Mulvihill et al.[226] demonstrated the etching process of silver octahedral-shaped NPs in NH_4OH/H_2O_2 etching solution. As shown in Figure 15, the morphology of the products varied with different amounts of etchant from edges and corners, leaving gaps of 5−10 nm; eight distinct arms develop, and the resultant octapod-shaped NPs form. Enhancement factors for each of these shapes at their optimal excitation wavelength range from 3×10^4 for a single octahedron to 5×10^5 for both the mildly etched octahedra and the octapod structures.

4.1.1.3. Purification of Metal Nanoclusters. Although dimers and small clusters of NPs can be prepared by using multidentate ligands and DNA hybridization, these methods result in the NP-linking molecules being present in the hot spots of the clusters. Therefore, the linker must also be the Raman reporter, increasing the complexity of the system.[131] Etching single crystal NPs is usually done in the presence of polymer, and Raman reporters are required to displace or penetrate into the polymers when preparing SERS tags, limiting the availability of Raman reporter molecules.[131] Fortunately, besides precisely controlled fabrication, homogeneous nanostructure populations can also be realized via postsynthetic sorting. For example, gel electrophoresis[228] and size-exclusion chromatography[229,230] have been used to separate metal NPs by both size and shape. Sedimentation-coefficient differences between NPs of varying size and shape have been exploited for sorting by centrifugation[231] and sedimentation field-flow fractionation.[232] In addition, density gradient centrifugation has proven to be particularly useful for obtaining refined populations of NPs, leading to a specific aggregation state for NP clusters.[233,234]

Colloidal nanocluster spatial isolation techniques offer a more practical and versatile strategy for obtaining precise SERS structure from the monomeric particle's starting material. For example, a study of polymer-coated NP clusters in which centrifugation and filtration were used to remove single-core

dx.doi.org/10.1021/cr300120g | *Chem. Rev.* 2013, 113, 1391−1428

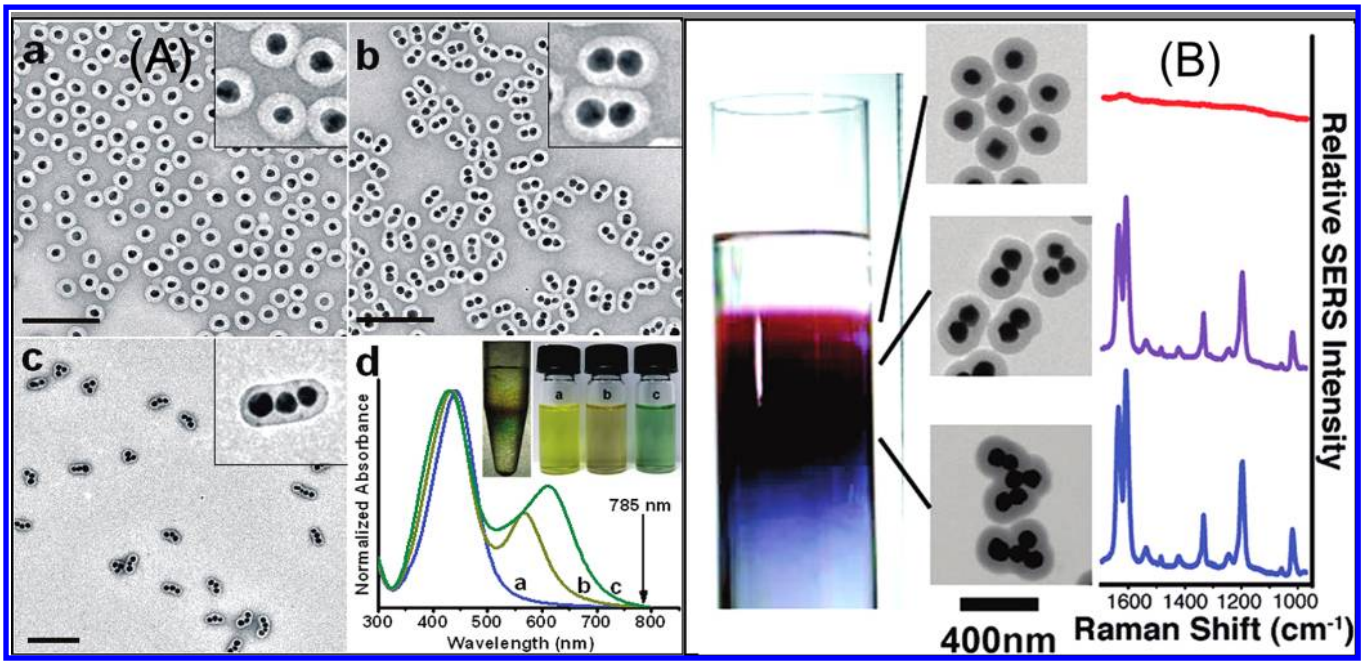

Figure 16. (A) (a–c) TEM images and (d) UV–vis spectra of the samples enriched with Au@Ag monomers (a), dimers (b), and trimers (c). Though often in a bent conformation, the trimers mostly contained only two hot spots. Clear gaps existed within the nanoclusters, and no fusion was observed. The inset in part d shows a typical outcome of the differential centrifugation, where monomers, dimers, and trimers were enriched in distinct yellow, brown, and green bands, respectively. Scale bars: 200 nm. Reprinted with permission from ref 216. Copyright 2010 American Chemical Society. (B) Photograph of a centrifuge tube after centrifugation of the gold core/silica shell SERS tag sample in a surfactant-free aqueous iodixanol linear density gradient (left) and corresponding TEM images of the selected fractions and SERS spectra of Raman reporter 1,2-bis(4-pyridyl)ethylene (right). Reprinted with permission from ref 235. Copyright 2011 American Chemical Society.

NPs and large aggregates, respectively, ultimately yielded samples of primarily multicore-NP clusters with enhanced SERS signals.[109] Another purification example is using differential centrifugation with a high-density CsCl solution (1.9 g cm^{-3}) to distinguish particles (Au@Ag core–shell NP–SERS tags protected with polymer shells) of different sizes (Figure 16A).[216] The resulting nanoclusters led to samples enriched in dimers (85%) and trimers (70%). By analyzing the well-defined nanostructure, it is estimated that each dimeric hot spot would be 700 times as strong as a monomer, and each trimeric hot spot 2100 times as strong per unit area. This centrifugal sorting technique was also used to refine gold core/silica shell SERS tags (Figure 16B).[235] The relatively massive NP clusters are sorted by their sedimentation coefficients via centrifugation in a high-viscosity, density-gradient medium, iodixanol, yielding solutions that contain a preponderance of one aggregation state and a diminished monomer population with the SERS intensity higher than that of the initial solution.

4.1.2. Calibration of SERS Intensities and Enhancements. Signal intensity calibration is always a topic in the quantitative analysis of Raman measurements. Internal standards are often used to calibrate Raman peaks in conventional Raman analysis to adjust for the limitations of Raman instrumental and experimental factors, including changes in laser power, drift in the optical alignment, and variation in the positioning of the sample.[236] However, the same problems remain in SERS-based quantitative assays and are more complicated because SERS signals of analytes strongly depend on their chemical structure and location on the metal substrates (i.e., whether or not they are in hot spots). Overall, three categories of internal standards have been used for quantitative analysis based on SERS substrates: (1) non-SERS-active compounds with unenhanced signals strong enough to be detected in the presence of the surface-enhanced analyte's signal;[237−239] (2) internal standard SAM layers with enhanced signals similar to those of the analyte, with one or more bands in spectrally silent regions;[240] and (3) chemicals with structures similar to those of analytes[241] or an isotopically substituted form of the analyte itself.[242,243] To compare these standards and their detailed applications, please refer to this recent review[244] or this book.[236]

Signal intensity standardization and calibration procedures are also essential for improving the quantitative ability and widespread application of SERS tags. The internal standard calibration method is widely used in SERS tag-based assays. Unlike the SERS substrate-based quantitative method, which uses concrete compounds as standards, the internal standard for SERS tags designed as ion sensors uses "internal standard peaks" originating from the Raman reporters themselves. During the assay process, certain vibrational modes of the Raman reporters are very sensitive to the ion coordination event, leading to regularly changeable peak intensities; however, the peaks of insensitive bonds remain nearly unchanged. The analytes can be quantitatively assayed by analyzing the peak height or peak area ratios.

Zamarion et al.[151] chose 2,4,6-trimercapto-1,3,5-triazine species, a convenient multibridging ion probe, as Raman reporter to detect heavy metal ions. As illustrated in Figure 17A, upon the Hg^{2+} concentration increase in the range of 2×10^{-7} to 2×10^{-6} mol L^{-1}, the ν_{C-S} peaks at 485 and 432 cm^{-1} systematically decreased, consistent with the strong binding of the Hg^{2+} to the thiol groups. Concomitantly, the β_{ring} peak at 973 cm^{-1} gradually increases, suggesting the involvement of the heterocyclic N atom in a bidentate coordination mode to the Hg^{2+} ion. In contrast, adding Cd^{2+} (range, 2.5×10^{-7} to 3×10^{-6} mol L^{-1}) promoted strong enhancement of the ring

dx.doi.org/10.1021/cr300120g | Chem. Rev. 2013, 113, 1391–1428

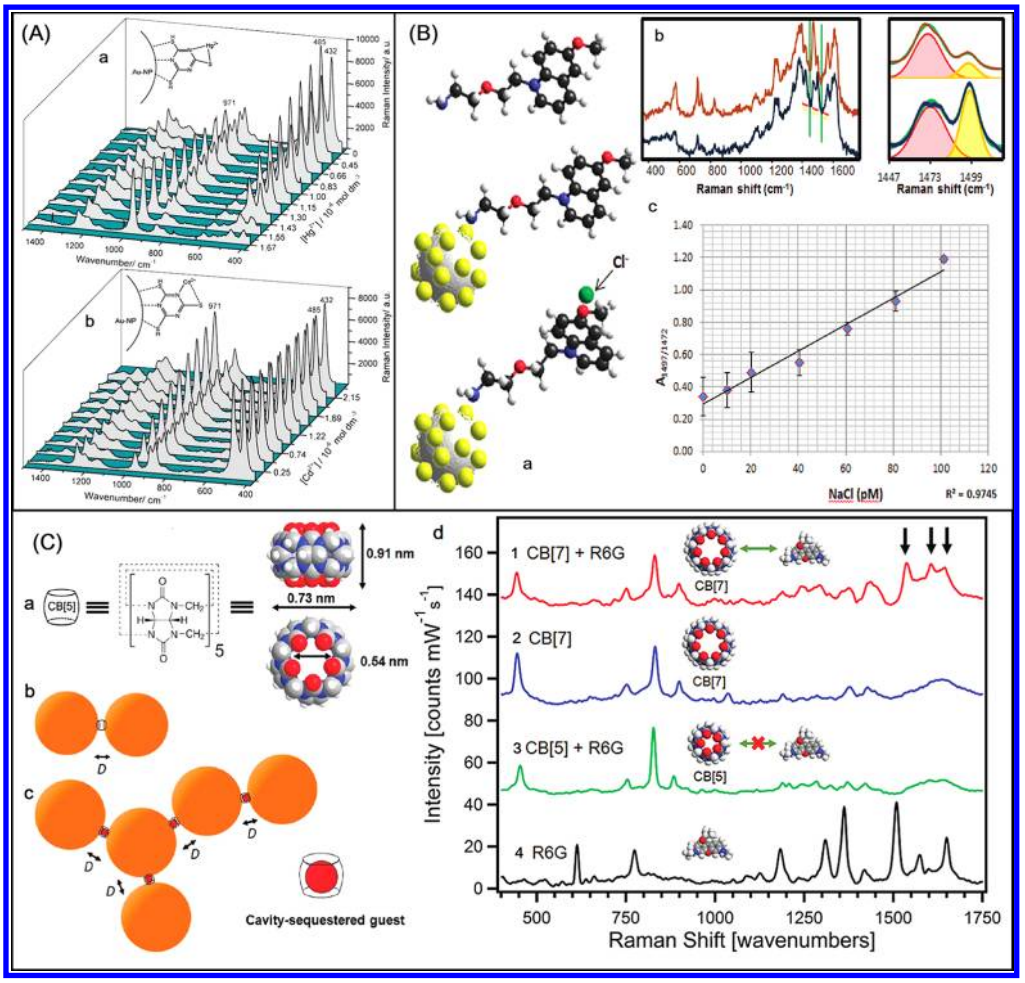

Figure 17. (A) SERS spectral profiles for a 2,4,6-trimercapto-1,3,5-triazine species (TMT)-AuNP aqueous suspension (pH 4.4), recorded at several concentrations of Hg^{2+} ions (a) and Cd^{2+} ions (b). The inset schematic illustrations show the proposed binding mode of metal ions on the TMT-AuNP nanoprobes. Reproduced with permission from ref 151. Copyright 2008 American Chemical Society. (B) (a) Schematic representation of the chloride detection process using amino-MQAE based SERS tags. (b) SERS spectra of 2-(2-(6-methoxyquinoliniumchloride)ethoxy)-ethanamine-hydrochloride (amino-MQAE) (10^{-10} M) with and without chloride (10^{-10} M). Bands where the deconvolution was carried out are highlighted (brown and blue, experimental spectra; green, resulting spectra of coadding peak 1, red, and 2, yellow). (c) Linear plot of the 1497 and 1472 cm^{-1} area ratio as a function of chloride concentration. Error bars represent the standard deviations within five replicated experiments. Reproduced with permission from ref 152. Copyright 2011 American Chemical Society. (C) (a) Cucurbit[5]uril composed of five cyclically arranged glycouril units, with a hydrophobic internal cavity and polar carbonyl portals that bind to the Au surface. (b) AuNPs glued into a dimer by CB[*n*] with portal-to-portal separation rigidly fixed at 0.9 nm. No other binding configuration is possible. (c) CB[*n*] cavity supports selective guest sequestration, leading to the use of AuNP:CB[*n*] aggregates for molecular-recognition-based SERS assays where the CB[*n*] defines the nanojunctions. (d) SERS spectra of (1) CB[7] with R6G, (2) CB[7] alone, and (3) CB[5] with R6G. A bulk Raman spectrum ofR6G is shown (4). Single molecules of R6G sequester in the cavity and get exposed to the intense optical fields on binding with CB[7] but not with CB[5]. Signals from R6G (marked by arrows) are clearly visible with CB[7] and absent with CB[5]. Reproduced with permission from ref 245. Copyright 2011 American Chemical Society.

vibrational peak at 971 cm^{-1}; however, the C−S stretching modes at 485 cm^{-1} and 432 cm^{-1} exhibited only a small decay as a function of the Cd^{2+} concentration. Therefore, plots of the intensity ratios at 432:971 cm^{-1} and 485:971 cm^{-1} versus the concentration of the Hg^{2+} ions and those of the intensity ratios at 971:485 cm^{-1} and 971:432 cm^{-1} versus the concentration of the Cd^{2+} ions can be obtained.

Similarly, Liz-Marzán's group reported a chloride ion detection method based on SERS tags using the chloride-sensitive dye 2-(2-(6-methoxyquinoliniumchloride)ethoxy)-ethanamine-hydrochloride as the Raman reporter.[152] Upon the addition of chloride ions, the peak at 1497 cm^{-1} increases, and the peak at 1472 cm^{-1} decreases; a linear plot can be drawn with the two peaks' area ratio as a function of chloride concentration (Figure 17B). Similar intracellular pH sensors were also designed (see section 3.3.2).

Another internal standard-type in SERS tags can be called "host molecule internal standard". This method is feasible for the following two reasons. First, this kind of molecule can selectively capture the analytes in a stoichiometric relationship through host−guest interactions; thus, it can accurately reflect the amount of targets. Second, the in-pair analyte and host molecule appear at the same hot spot originating from molecular recognition-induced aggregation of host molecule-modified NPs (i.e., they experience the same EM field and signal enhancement). Therefore, the host molecule can be applied to analyte capture and signal-enhancing calibration of metal substrates. A representative example was examined by Mahajan and co-workers.[245] As shown in Figure 17C, they

dx.doi.org/10.1021/cr300120g | *Chem. Rev.* 2013, 113, 1391−1428

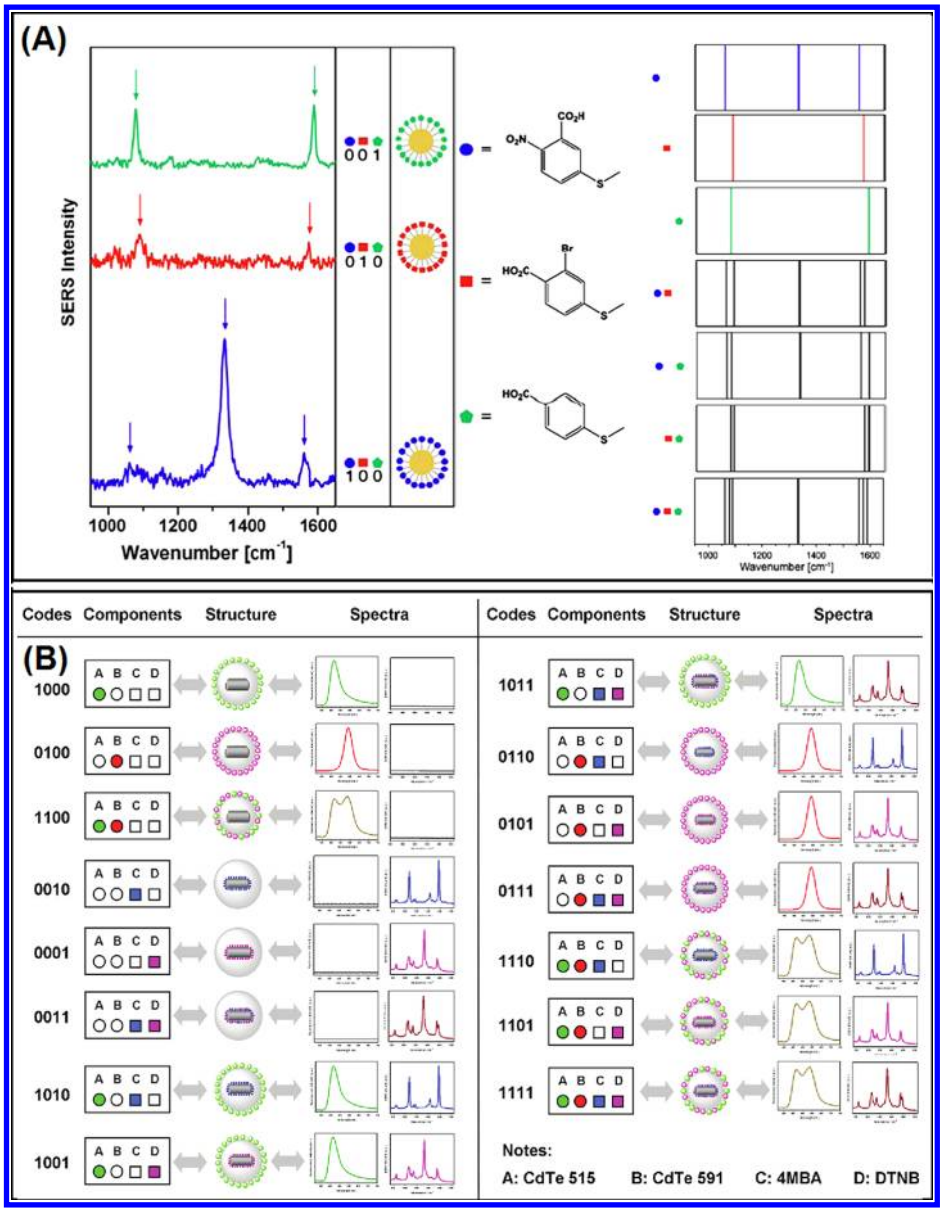

Figure 18. (A) Left: SERS spectra of one-component SAMs on Au NPs and the chemical structures of the SAM molecules. 5,5′-Dithiobis(2-nitrobenzoic acid) (DTNB, blue) has a dominant Raman band at 1333 cm^{-1}, which is assigned to the symmetric nitro stretching vibration. The bands at 1061 and 1558 cm^{-1} are assigned to the aromatic ring vibrations ν_{12} and ν_{8a}. For 2-bromo-4-mercaptobenzoic acid (BMBA, red) and 4-mercaptobenzoic acid (MBA, green), these bands are observed at 1090/1575 cm^{-1} and 1079/1590 cm^{-1}, respectively. Middle: the chemical structure of reporters. Right: bar code diagrams for SERS spectra of one-, two-, and three-component SAMs on Au NPs. Reproduced with permission from ref 125. Copyright 2009 Springer-Verlag. (B) Composition, measured spectra, and codes of the 15 nanoparticles synthesized using the QDs-SERS dual coding method. Reproduced with permission from ref 96. Copyright 2012 American Chemical Society.

selected cucurbit[*n*]urils (CB[*n*]), a kind of macrocyclic host molecule with subnanometer dimensions, to modify Au NPs to act as selectors and Raman reporters. During the assay process with rhodamine 6G (R6G) as model analyte, the host−guest complexation ability of CB[*n*] made it enter the heart of the plasmonic hot spot, with resultant signal enhancement. The *in situ* self-calibrated and reliable signal of R6G could be obtained by comparing its SERS intensity with that of the CB[*n*].

In multiplex immunoassays involving labeling of living subjects, it is generally difficult to introduce internal standards because of several problems associated with strongly absorbing impurity, homogeneity, stability, and spectral overlapping.[246] Therefore, external standards are acquired by using the average SERS intensity value of specific Raman tag bands. To acquire high-quality external standards, the signals should be determined in the optimum experimental condition, acquired within the same sensing media, and applied to all experiments. For example, Woo et al.[246] reported the first quantitative comparisons of multiple protein expression in bronchioalveolar duct junctions. They used three kinds of reporter-labeled SERS tags and calculated the average SERS intensity of characteristic peaks of each tag as external standards.

4.2. Improving Multiplexing Capability

The potential to multiplex with SERS signals is one of its biggest advantages over other optical detection modes (fluorescence for example).[247] We have already discussed several examples of multiplex SERS assays for molecules[110,157]

dx.doi.org/10.1021/cr300120g | *Chem. Rev.* 2013, 113, 1391−1428

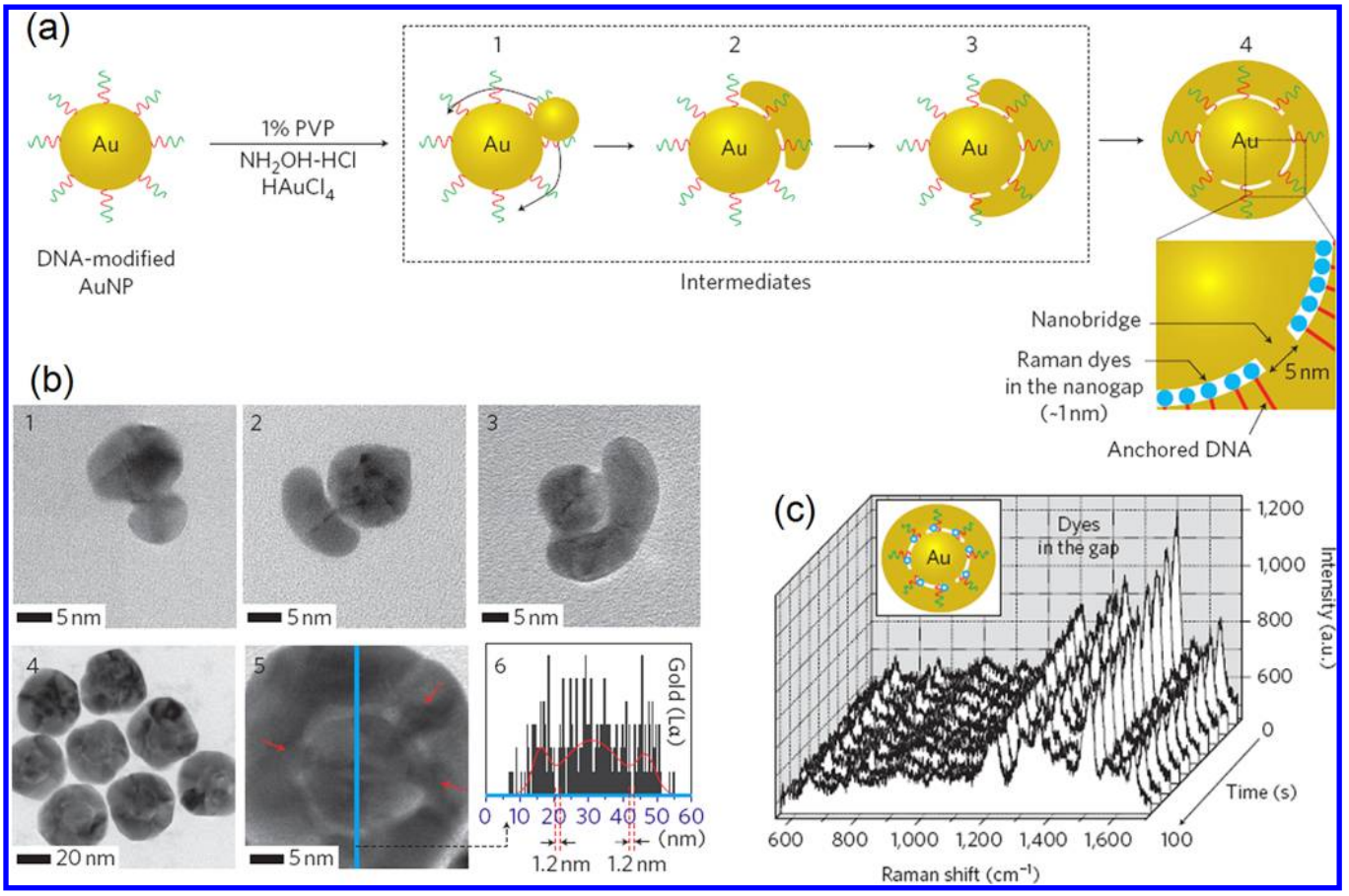

Figure 19. Surface DNA-mediated synthesis and characterization of DNA-anchored nanobridged nanogap particles. (a) Synthetic scheme for the gold nanobridged nanogap particles (Au-NNPs) using DNA-modified gold nanoparticles as templates. (b) HRTEM images of intermediate (panels 1−3) and Au-NNPs (panels 4 and 5). Nanobridges within the Au-NNP are indicated by red arrows in panel 5, and element line mapping and the ~1.2 nm gap in the Au-NNP structure are shown in panel 6. (c) Time-dependent Raman profiles of Au-NNP (carboxy-X-rhodamine, ROXinner). The spectra were acquired with a 633 nm excitation laser, at 300 mW, and for a 10 s exposure for a single spectrum for 100 s, with the same particle concentration (0.5 nM). Reproduced with permission from ref 103. Copyright 2011 Nature Publishing Group.

and living species,[178,213,248] and in the following, we will focus on possible strategies for further expanding this ability.

The narrow, characteristic peaks of the Raman reporters are the foundation of the multiplexing capability of SERS tags. It is relatively easy to find two or three reporters with non-overlapping characteristic peaks to illustrate proof-of-concept multiplexing application. However, when more labeling targets are used, the reporters would be hard to acquire in a random way. Up to now, very few papers reported on the collection and systematical analysis of the SERS profile (including peak position, peak numbers, etc.) of abundant Raman reporters. However, this fundamental work is essential. On the basis of these data, a series of "Raman reporter sets", which are composed of different numbers of reporter molecules with undisturbed SERS signals, could be screened. These established Raman reporter sets will facilitate the synthesis of multicoded tags and make multiplex SERS analysis more feasible in practical applications.

By varying the type and stoichiometry of a Raman reporter in a multicomponent SAM reporter labeled in a one SERS tag system, increasing multiplexing ability of the tags will be obtained. Gellner et al.[125] coated mixed SAMs with up to three different Raman reporter molecules on the surface of the metal colloid. Compared with one-component SAMs, this method allowed the additional parameters of type and stoichiometry of a particular Raman reporter in a multicomponent SAM to be evaluated. As shown in Figure 18A, all one-, two-, and three-component SAMs on Au NSs could be easily discriminated either by their original SERS spectra or by the corresponding bar codes.

Another approach to increase the multiplex ability is to develop dual-mode sensing tags. For instance, after separately modifying two distinct SERS tags with green and red fluorescent dyes, four different Raman reporter/fluorescence dye dual-mode tags will be obtained.[248] This fluorescence-SERS joint-encoding model has been enhanced by using organic−metal−QD hybrid nanoparticles (OMQ NPs).[96] Compared with organic dyes, QDs have narrower emission peaks and can produce more colors. This characteristic ensures a larger encoding capacity. Theoretically, this method can generate multiple codes in a permutation combination manner. When m kinds of QDs and n kinds of SERS reporters are used, the number of available codes increases to $(2^{m+n} - 1)$, which is $[(2^{m+n} - 1)/(2^m - 1)]$ or $[(2^{m+n} - 1)/(2^n - 1)]$ times that obtained by using only fluorescence or SERS spectra. In Figure 18B, 15 codes were attained experimentally with distinguished optical spectral signals by using two fluorescence or two SERS agents.

dx.doi.org/10.1021/cr300120g | Chem. Rev. 2013, 113, 1391−1428

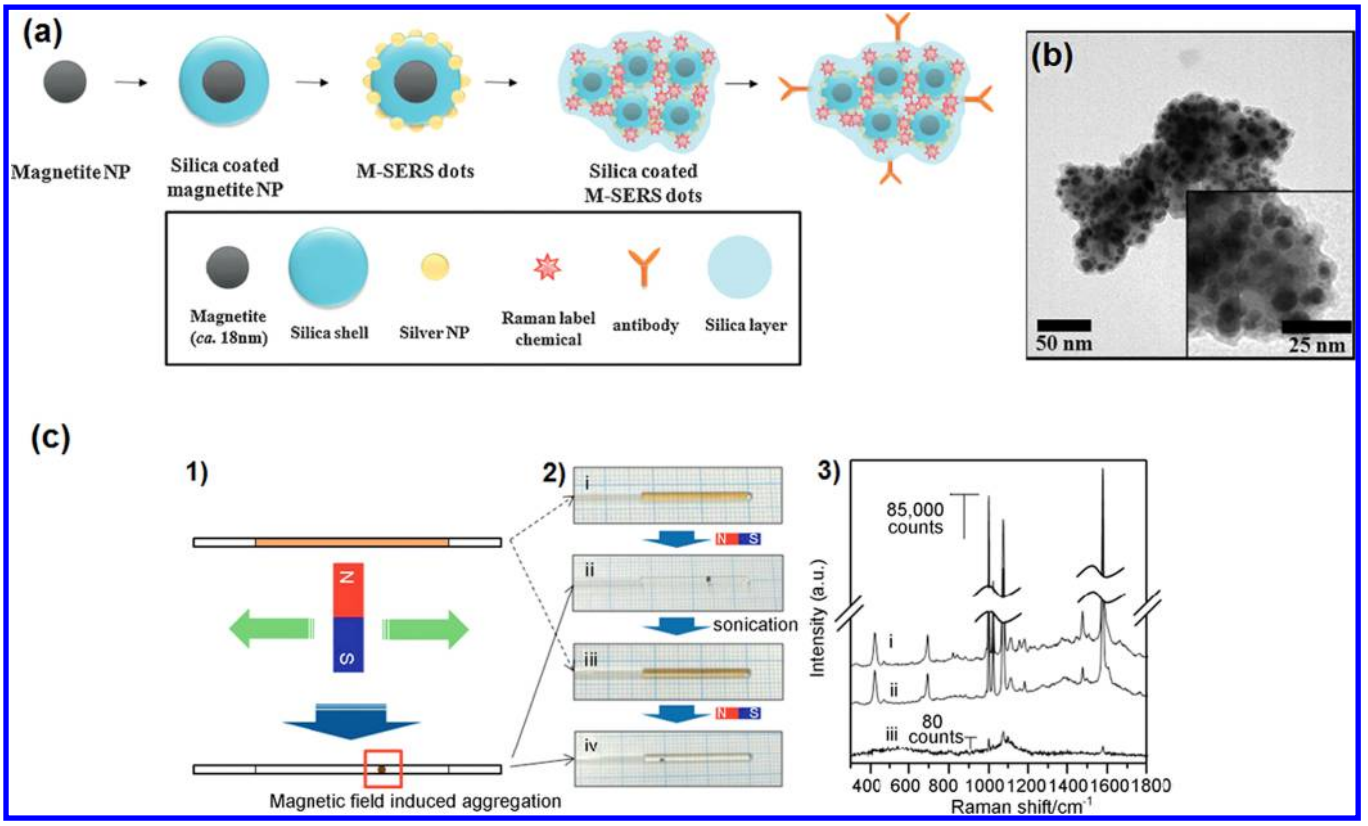

Figure 20. (a) Illustration of synthesis of magnetic active SERS tagging material (M-SERS dots). (b) HR-TEM image of M-SERS dots. (c) Aggregation control of M-SERS dots by magnetic fields. (1) Illustration of aggregation procedure of M-SERS dots. (2) Optical images of M-SERS dots in a capillary. (i) Unaggregated M-SERS dots. (ii) Aggregated M-SERS dots. (iii) Redispersed M-SERS dots after sonication. (iv) Reaggregated M-SERS dots. (3) Raman spectra of M-SERS dots on which 4-ATP molecules are adsorbed: The top two SERS spectra (i, ii) correspond to the aggregated M-SERS dots in steps ii and iv of (2), respectively. The bottom SERS spectra correspond to the unaggregated M-SERS dots in steps i and iii of (2). Acquisition parameters: photoexcitation by the 514.5 nm laser line with 30 mW (i, ii) and 300 mW (iii) at the sample, and signal integration for 60 s. Reproduced with permission from ref 259. Copyright 2010 John Wiley & Sons, Inc.

4.3. Reduced Size for Subcellular Imaging

The Raman mapping approach applies the spectroscopic technique to two dimensions by recording a full SERS spectrum at discrete grid points over a two- or three-dimensional region of a cellular sample.[249] The intensity of a particular Raman band in the SERS tag spectrum can be plotted by using a color gradient or a series of contours, resulting in an "image map" showing the location of the tags over a select physical area as a function of their SERS signal intensity at that particular band.[250] SERS signal intensity depends upon the number of SERS tags within small excitation laser spots (usually less than 200 μm^2), and the biological samples, such as cells and tissues, are intrinsically inhomogeneous. Another problem is that SERS tags in biomedical analysis are too large compared with targeting biological molecules, and any inhomogeneous distribution of the SERS tags superimposed on the inhomogenous molecular distribution on the biological samples will reduce the accuracy of the SERS-based bioimaging and analysis. Thus, controlling the tags into a small size (similar to that of their targets) is essential for accurately revealing the spatial location and number of the biological molecules in subcellular images. However, tags with the typical metal core-reporter shell structure, usually require the use of large Ag or Au NPs (>40 nm) to improve the SERS sensitivity—metal cores that are too small cannot give reliable SERS signals: this becomes a bottleneck to the problem's solution.

A novel SERS tag structure of SERS inside metal nanoshells was recently proposed and showed great potential to overcome this limitation. In contrast to the uncontrollable, small, exterior nanogaps in multimeric nanostructures, this monomeric Raman reporter@metal shell nanostructure provides a uniform, rigid, and larger nanogap area, allowing impressive signal enhancement with a relative small size. Zhang et al.[251] first reported this structure, demonstrating giant SERS enhancement, on the order of 10^{11} to 10^{14}. They embedded the Raman reporter tris(2,2′-bipyridyl)ruthenium(II) chloride into SiO_2 NPs and subsequently coated this reporter-embedded SiO_2 NP with a thin layer of Au metal. Although this SERS phenomenon was discovered with relatively large NPs (70 nm SiO_2), this design of SERS tags offers the versatility of having probe molecules embedded inside the nanoshell and controlling the size and type of the dielectric core. Subsequently, they proposed a modified protocol and synthesized TiO_2-based core−shell NPs as SERS tags that were smaller than 10 nm.[252,253] Three different types of Raman reporter molecules were used to adsorb on the surface of 3 nm TiO_2 NPs, and then the labeled NPs were coated with Au or Ag as the outer shell. Raman detection showed that the resulting small core−shell NPs all had very strong and reproducible SERS signals. Another SERS inside the metal structure was individual Au−Ag bimetallic NPs encapsulated molecules of thiocyanate (SCN^-) as Raman reporters.[254] Au−Ag alloy nanoshells were first synthesized by a galvanic replacement reaction, and SCN^- was then incorpo-

dx.doi.org/10.1021/cr300120g | Chem. Rev. 2013, 113, 1391−1428

rated in the accessible pores at the inner/outer surfaces of the nanoshells. Then the labeled nanoshells were infiltrated with Ag via citrate reduction, filling the core, and entrapping the absorbed Raman reporters in the interior of the core−shell structure.

Sandwich architectures with Raman reporter molecules placed between two layers of noble metals, such as a Au NP@Au shell,[103] a Au NP@Ag shell[100,102] and a Au shell@Ag shell,[101] have been reported recently. For instance, a well-defined, hollow, 1 nm interior gap between a gold core and a gold shell was synthesized with the aid of a DNA bridge.[103] As shown in Figure 19, DNA-modified Au NPs were used as seeds, and the anchored DNA strands in these particles facilitate the formation of the nanobridged nanogap. The precise and quantitative positioning of Raman dyes inside the gap of the resultant particles generates a strong, highly stable, and quantitative SERS signal. Chen's group reported the colloidal deposition of a Ag shell on Au NSs functionalized with MBA, finding that the complex NPs have at least 20 times stronger SERS signals than the already-enhanced SERS signal of MBA on Ag NPs of similar size.[102] Although the signal-enhancing mechanism of these sandwich structures is still not clearly understood, this strategy will undoubtedly lead to the synthesis of a series of ultrasmall, highly uniform, stable SERS tags with quantitative signals for bioimaging applications.

4.4. Development of Multifunctional Nanoplatforms

The emerging multifunctional nanoprobes showed great potential to revolutionize the traditional bioanalysis, imaging, and theragnosis.[255] Recent advancements in engineering SERS tags and the promising benefits of this technology have dictated a shift of focus from the synthesis of single-component probes to the design of complex nanostructures composed of multiple targeting, separation, imaging, and therapeutic modules.

4.4.1. Magnetic SERS Dots. Magnetic NP-based, surface-enhanced Raman spectroscopic dots (M-SERS dots) were developed as a new type of analytical tool for optical labeling and magnetic separation of targeted molecules or cells. The addition of a magnetic functionality to the SERS colloidal platform permits the rapid concentration of the tags, causing magnetic field-induced hot spots within a small region and decreasing the concentration of analyte needed to obtain a meaningful SERS signal.[256]

The combination of magnetic and noble metal NPs is needed to achieve bifunctionality. Spuch-Calvar et al.[257] devised an M-SERS NP system comprising silica-coated magnetic γ-Fe_2O_3 spindle cores coated with a dense monolayer of gold nanorods via a layer-by-layer deposition technique. Hong et al.[258] developed biofunctional Fe_3O_4/ZnO/Au nanorices as SERS tags for rapid and ultrasensitive immunoassays. Jun et al.[259] prepared multifunctional tagging materials for cancer-cell targeting and separation. As illustrated in Figure 20, hybrid NPs composed of an 18-nm magnetic core and a 16-nm-thick silica shell with silver NPs formed on the surface were prepared. After adsorbing simple aromatic compounds as Raman reporters, the NPs were further coated with silica to provide them with chemical and physical stability. The resulting silica-encapsulated M-SERS dots produce strong SERS signals, have magnetic properties, and have been successfully used to target breast cancer cells (SKBR3) and floating leukemia cells (SP2/O).

Gole et al.[260] designed an easy method for one-pot synthesis of M-SERS dots. The procedure involves a microemulsion route for the synthesis of Ag NPs inside a silica shell in the presence of premade iron oxide NPs and the Raman reporter MBA. In the resultant composite structure, both types of NPs are embedded in silica particles. Moreover, the M-SERS dots have also been produced by using silica[261] or polystyrene beads[262] as supports and codepositing silver and magnetic NPs on them.

4.4.2. Multimodal Imaging Dots. Recently there has been an interest in developing multimodal approaches because the combination of different modalities into one system compensates for the deficiencies of any single imaging modality. Several SERS-related multimodal probes have been synthesized and characterized, including nanomaterials suitable for detection by Raman spectrometry, fluorescence, X-ray computed tomography (CT), and MRI.

4.4.2.1. Fluorescent SERS Dots. Because of the sensitivity and convenience of assays, bifunctional dots integrating both SERS and fluorescence moieties have been developed for multiple assays. Despite the excellent multiplex capability of SERS detection, its slow imaging speed is a major obstacle for the fast recognition of specific markers. To resolve this problem, fluorescence-SERS (F-SERS), dual-modal nanoprobes were fabricated. Fluorescence imaging is more intuitive and acquired faster than SERS imaging; therefore, the fluorescence signal can be used as an immediate indicator of molecular recognition, with the SERS signal used subsequently as the signature of specific molecules in multiplex interactions.

Fluorescent tags can be generated in different ways. Cho and co-workers[263] demonstrated the first F-SERS dots by depositing the fluorescent conjugates of 3-aminopropyltriethoxysilane (APS) and fluorescein isothiocyanate (FITC) or Alexa Fluoro 647 on the silica-coated SERS tags via silane chemistry, as done in other works.[248,264] Tian's group conjugated fluorescent molecules such as FITC to organosilica shells of the tags by simple mixing.[265] In another method, electrostatic force aids layer-by-layer deposition used for fluorescent decoration via the interaction between reporter-attached metal nanosubstrates and RBITC-labeled PAH[266,267] or fluorescent QDs.[96,268] RBITC was also reported to directly adsorb onto Ag on silica, polystyrene beads,[146] acting as both Raman reporter and fluorescence generator.

Under certain conditions, F-SERS dots may yield a strong fluorescence background due to the presence of outer layer organic dyes, which interfere with the SERS signal. This problem can be overcome by selecting a longer wavelength laser source (632.8 or 785 nm) for Raman spectrum acquisition because the excitation wavelength is not within the absorption profile of most dyes.

F-SERS tags are widely used in the areas of cancer-cell sensing and *in vivo* imaging, which heavily rely on dual-spectroscopic properties. For instance, tags with different fluorescence and SERS signals were used to detect three cellular proteins that are simultaneously expressed in bronchioalveolar stem cells in the murine lung. The results of quantitative comparisons of multiple protein expression in cells and tissue suggest that immunoassays using F-SERS dots offer significant increases in sensitivity and selectivity.[246] Likewise, Choo's group made F-SERS dots for the duplex imaging of CD24 and CD44 markers that are coexpressed by MDA-MB-231 breast cancer cells.[248] Qian et al. first demonstrated the use of NIR F-SERS dots for purely optical *in vivo* imaging of live mice. NIR dye-functionalized Au NR F-SERS dots were developed for optical *in vivo* imaging.[269] As shown in Figure

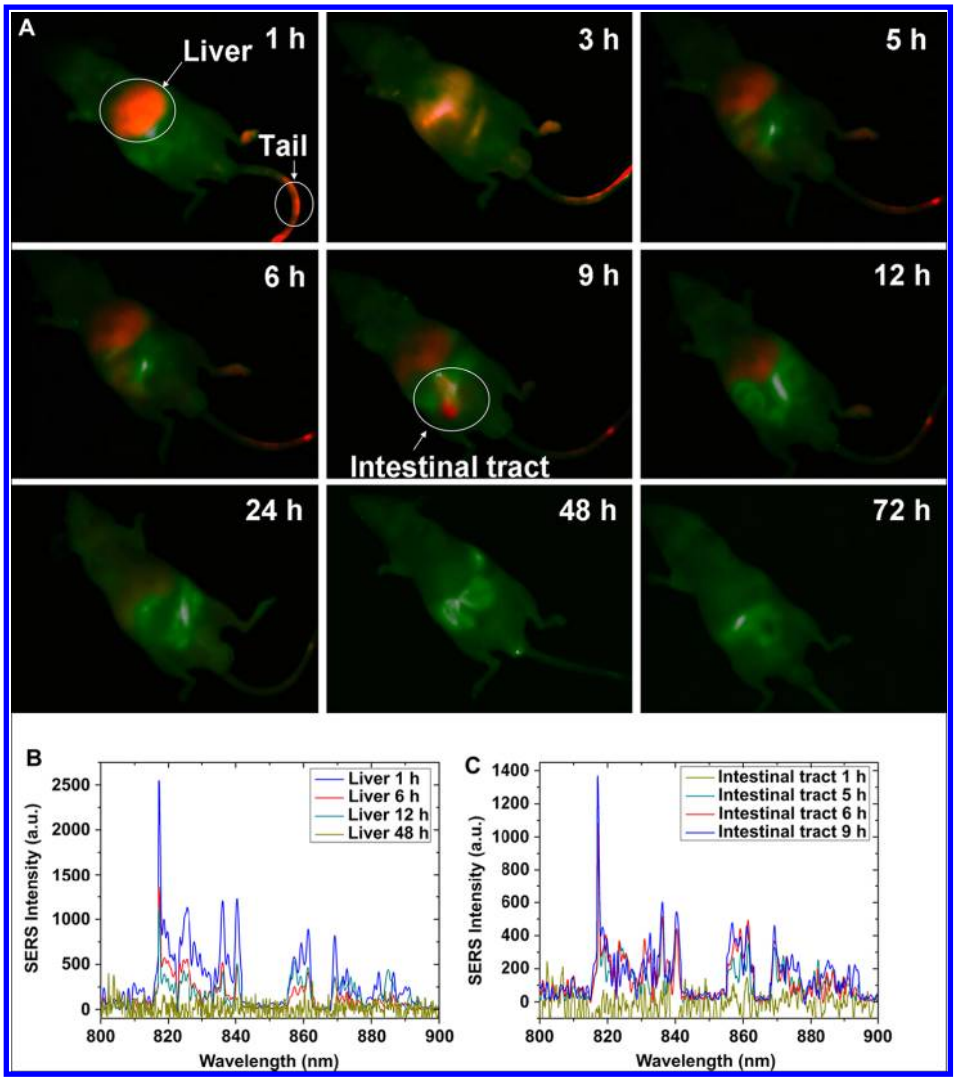

Figure 21. (A) NIR fluorescence imaging (exposure time: 5000 ms) of a nude mouse intravenously injected with PEG-DTTC-GNRs (639 nm) at various time points of postinjection. The NIR fluorescence signal was colored in red, and the background autofluorescence was colored in green. (B) NIR SERS spectra from the liver of the same mouse at various time points (1, 6, 12, and 48 h) postinjection (integrated time: 40,000 ms). As time went by, the intensity of the signals decreased gradually. (C) NIR SERS spectra from the intestinal tract of the same mouse at various time points. Prominent SERS signals were observed at the time points 5, 6, and 9 h, while only noise could be observed at the time point 1 h. Reprinted with permission from ref 269. Copyright 2011 Elsevier.

21, by using a fluorescence *in vivo* imaging system and a Raman spectrometer, the distribution and excretion of iv injected tags in deep tissues of live mice were observed.

4.4.2.2. X-ray Computed Tomography–SERS Dots. Gold has a higher X-ray attenuation coefficient due to it high electron density and atomic number compared to conventionally used iodine compounds, and Au NP-based CT contrast agents have been widely reported for *in vivo* imaging.[270] Inspired by the SERS enhancement ability of Au NPs, Xiao et al.[271] first synthesized multicolor nanotags that combined the imaging functions of SERS and CT.[271] A library of nanotags with six different colors was synthesized for a range of Au NP sizes. An optimum size was established to yield the largest SERS intensity and X-ray attenuation that is higher than that of the iodinated CT contrast agents used in clinics. The results of proof-of-principle *in vivo* imaging with nanotags show the combined dual-modality imaging capability of SERS and CT with a single NP probe (Figure 22A).

4.4.2.3. Magnetic Resonance Imaging–SERS Dots. Magnetic resonance imaging (MRI) is a widespread medical diagnostic modality with high spatial and temporal resolution, unlimited tissue penetration, and tomographic capabilities.[272] SERS capability would be particularly useful if combined with MRI because it is highly sensitive, with signatures distinguishable from those of background tissue. Yigit et al. recently reported a novel nanomaterial that can be used as a bimodal contrast agent for *in vivo* MRI and Raman spectroscopy.[273] The probe consists of MRI-active superparamagnetic iron oxide NPs stably complexed with gold nanostructures, which serve as a substrate for Raman reporters to generate a SERS effect. The synthesized probe produces T_2-weighted contrast and is SERS-active both *in silico* (in aqueous solution) and *in vivo*. Intramuscular administration of the probe decreased the T_2 relaxation time of muscle from 33.4 ± 2.5 to 20.3 ± 2.2 ms. Characteristic SERS peaks were observed consistent with the *in silico* results (Figure 22 B). Gambhir's group[274] recently showed unique triple-modality MRI–photoacoustic–Raman imaging

dx.doi.org/10.1021/cr300120g | *Chem. Rev.* 2013, 113, 1391–1428

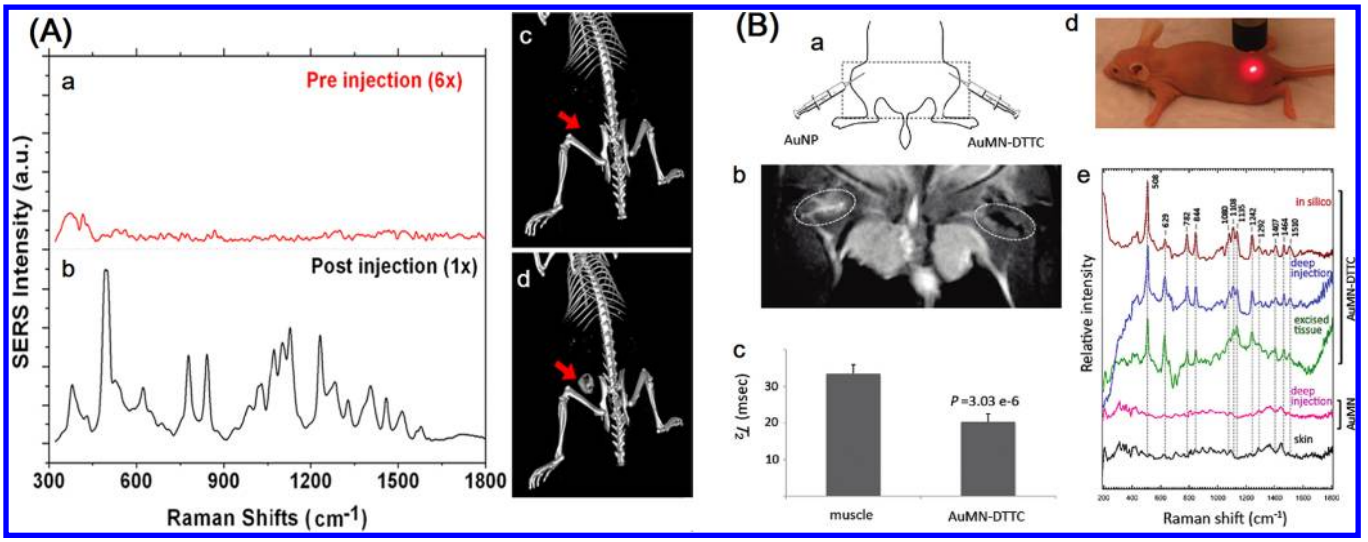

Figure 22. (A) SERS and CT images from subcutaneously injected nanotags (60 nm) in a nude mouse. Parts a and b are recorded Raman spectra, whereas parts c and d are 3D CT images pre- and postinjection, respectively. The arrows in panels c and d point to the site of injection and CT contrast generated. Reprinted with permission from ref 271. Copyright 2010 IOP Publishing Ltd. (B) MRI and Raman spectroscopy *in vivo*. (a) Schematic of the probe injection setup. The experimental AuMN-DTTC probe was injected in the deep right gluteal muscle. A control probe was injected in the contralateral muscle. (b) *In vivo* T_2-weighted MR image of a mouse injected intramuscularly (im) with AuMN-DTTC and the control probe, AuNP. There is a notable loss of signal intensity associated with the site of the AuMN-DTTC injection, confirming the suitability of the probe as an *in vivo* MRI contrast agent. (c) Calculated T_2 values based on multiecho T_2-weighted MRI. The T_2 relaxation time of AuMN-DTTC was significantly lower than those of both noninjected muscle and muscle injected with AuNP (n = 3; Student's t test; $p < 0.05$). (d) A photograph demonstrating the Raman spectroscopy experimental setup. (e) *In vivo* Raman spectra of a mouse injected im with AuMN-DTTC and the control probe, AuMN. The *in vivo* Raman spectrum of muscle injected with AuMN-DTTC has a clear SERS signature, which is indistinguishable from that obtained *ex vivo* and in silico and is absent in skin tissue and in muscle injected with the control probe. Reprinted with permission from ref 273. Copyright 2011 American Chemical Society.

tags which could help delineate the margins of brain tumors in living mice both preoperatively and intraoperatively. The multimodal tags were detected by all three modalities with at least a picomolar sensitivity both in vitro and in living mice. Similar triple-modality imaging tags were also reported with single-walled carbon nanotubes as scaffolds, which were successfully used to label human mesenchymal stem cells for in vivo tracking.[275]

4.4.3. SERS Tag-Based Therapeutic Systems. In recent years, a great deal of attention has been paid to noninvasive photothermal therapy for the selective treatment of tumor cells. This type of therapy utilizes the large absorption cross section of nanomaterials in the NIR region.[276] Owing to its weak absorption by tissues, NIR light can penetrate the skin without much energy loss or damage to normal tissues. Thus, it can be used to treat specific cells targeted by the heat-generating nanomaterials.[277] Taking advantage of NIR light absorbing properties of certain SERS-active noble metal NPs, several researchers have developed multifunctional nanoplatforms for integrated SERS imaging and photothermal therapy.[73,278,279]

von Maltzahn et al.[73] constructed a bifunctional Au NR-based SERS tag *in vivo* imaging and remote-controlled, photothermal heating for cancer treatment. Three NIR-absorbing molecules, IR-792, DTTC, and 3,3′-diethylthiadicarbocyanine (DTDC), were selected as Raman reporters. Each displayed a 10-fold to 10^3-fold higher signal than did molecules with visible absorbance because of the SERRS effect. After intratumoral injection of IR-792-coded NRs into athymic mice bearing bilateral human MDA-MB-435 tumors, evident SERS signals were observed. Upon irradiation with a diode laser (810 nm, 2W cm^2), infrared thermographic maps of mouse surface temperature revealed an increase to 70 °C.

Ray's group[278] used Au nanopopcorn as a heat nanogenerator and constructed a multifunctional system for targeted sensing, nanotherapy, and *in situ* monitoring of photothermal therapy response (Figure 23). The localized heating that occurs during NIR irradiation can cause irreparable damage to the targeted LNCaP human prostate cancer cells. Interestingly, the data allowed linear plotting of percent cancer cell death and SERS intensity change, enabling one to monitor photothermal nanotherapy response during the therapy process. Encouraged by this work, the group designed a novel hybrid nanomaterial using popcorn-shaped, gold nanoparticle-attached, carbon nanotubes for diagnosis and selective photothermal treatment.[280] For SERS detection purposes, they directly incorporated Raman spectroscopic properties (D-band at1340 cm^{-1} and G-band at 1590 cm^{-1}) in individual carbon nanotubes instead of using an organic Raman reporter. After labeling S6 aptamer, the hybrid nanomaterial-based SERS assay was highly sensitive to the targeted human breast cancer cells (SK-BR-3 cell line). Furthermore, 15 min of photothermal therapy with a 120 mW, 785 nm laser was enough to kill the cancer cells.

There have been a few attempts to design a SERS tag–therapeutic drug delivery system that is more versatile in practical application. Fales et al.[281] made DTTC-labeled SERS tags that were further coated with a silica shell containing a methylene blue (MB)-photosensitizing drug. The hybrid tags not only had SERS signaling capability but also showed significant increase in singlet-oxygen generation, causing cytotoxic effects to BT549 breast cancer cells upon laser irradiation. Sailor's group built a cooperative drug delivery system by using AuNRs based SERS tags and the anticancer drugs doxorubicin (DOX) loaded thermal sensitive liposomes.[282] After passive accumulation of iv injected SERS

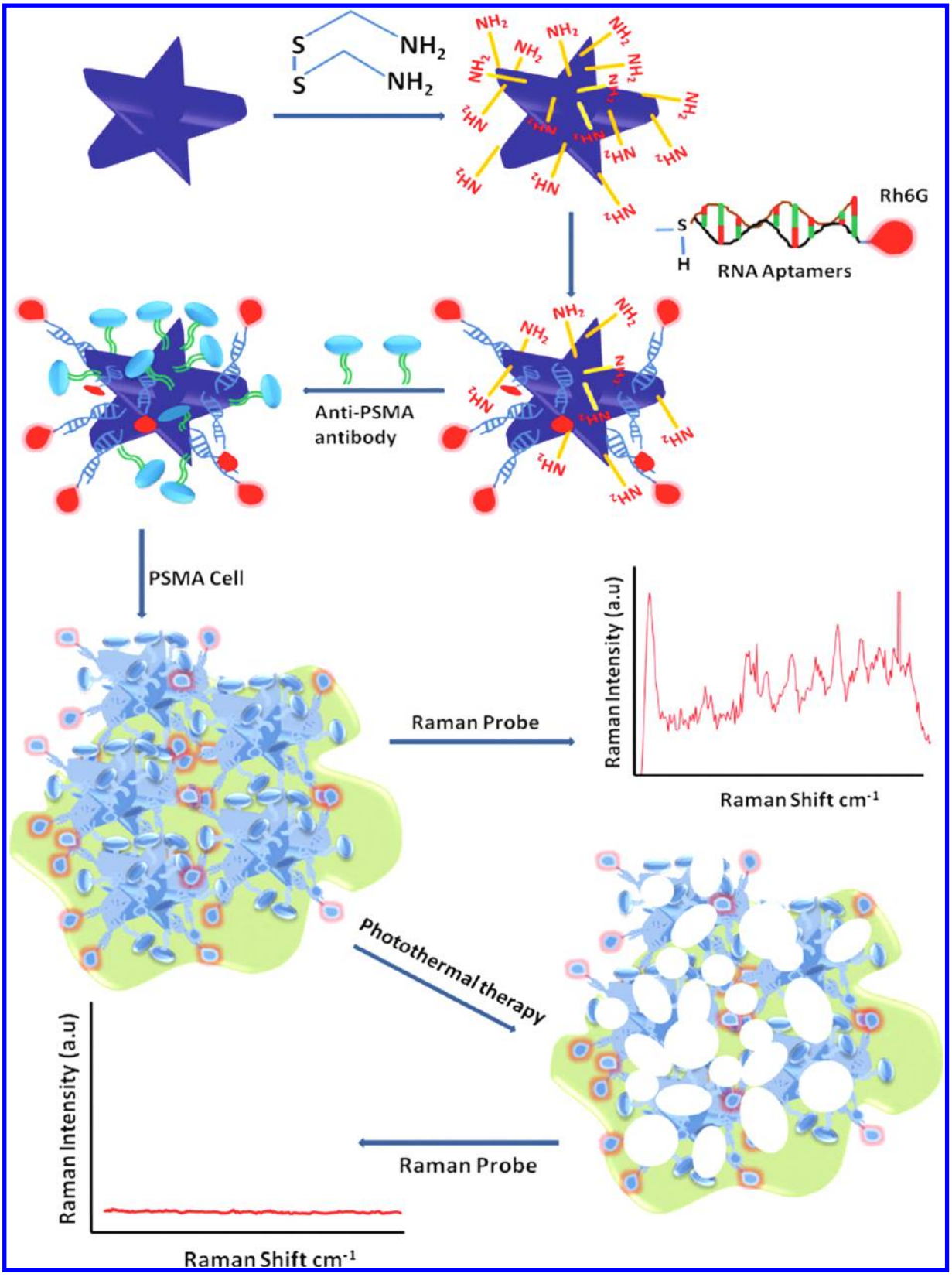

Figure 23. Schematic representation of the synthesis of monoclonal anti-PSMA antibody- and A9 RNA aptamer-conjugated-shaped gold nanoparticles. The third step showed a schematic representation of multifunctional popcorn-shaped gold nanoparticle-based sensing of an LNCaP breast cancer cell line. Reprinted with permission from ref 278. Copyright 2010 American Chemical Society.

tags in the MDA-MB-435 tumor xenografted in the mice, the tumor site was detected with the SERS signal and locally heated through laser irradiation. This localized heat triggered DOX release from liposomes circulating in the body. As a result, tumor growth was significantly suppressed. Wang et al.[283] designed biocompatible triplex Ag@SiO_2@mTiO_2 core−shell

dx.doi.org/10.1021/cr300120g | *Chem. Rev.* 2013, 113, 1391−1428

NPs for simultaneous F-SERS bimodal imaging and drug delivery. In this nanoplatform, a coating of mesoporous titania over SERS tags offered high loading capacity for fluorescence dye and the drug DOX, endowing the material with F-SERS imaging and therapeutic functions in MCF-7 cells. Duan's group developed bioconjugated plasmonic vesicles assembled from SERS-encoded amphiphilic Au NPs for cancer-targeted drug delivery.[284] In acidic intracellular compartments, the vesicles disassembled and allowed intracellular drug release. Simultaneously, the structure disassembling induced dramatic SERS signal decrease, which could serve as independent feedback mechanisms to signal cargo release from the vesicles. These examples show the possibility of developing SERS tag-based hybrid nanomaterials for use as reliable diagnosis and targeted therapy.

4.5. Biocompatibility

Biocompatibility of SERS tags is an important issue in bioanalysis. The first relevant study was performed in live zebrafish embryos after microinjection of MBA labeled Au NSs. No toxicological effect of the tags was found on the subjects.[285] The biocompatibility of PEGylated Raman-active Au NPs was investigated using human cells:[286] No cytotoxicity occurred in either HeLa or HepG2 cells in the acute setting. After prolonged exposures (48 h) at relatively high concentrations (1000 NPs/cell), a minimal amount of cytotoxicity was seen in both cell lines because of increases in cellular oxidative stress. Although few relevant reports exist, the biocompatibility of SERS tags can still be estimated by the biological responses of the nanosubstrates (such as Au and Ag NPs), which have been studied quite extensively using various *in vitro* and *in vivo* model systems.[287−289]

The biocompatibility of SERS-active NPs is dependent on several factors, including metal type, shape, size, and capping materials. Pan et al.[290] examined in detail the size-dependence of toxicity by using gold atomic clusters of 0.8, 1.2, 1.4, and 1.8 nm with 15 nm NPs stabilized by using triphenylphosphine derivatives. According to the MTT assay results, the clusters of 1.4 nm were the most cytotoxic, and the 15 nm NPs were not cytotoxic even at concentrations 100-fold higher than those of the small clusters. In general, ultrasmall Au nanoclusters have greater cytotoxic effects due to their strong endocytosis effectiveness[291] and binding ability to B-form DNA.[292] However, the 30−100 nm Au NPs that are commonly used as SERS substrates cause no noticeable toxicity at concentrations up to 100 mM.[291,293−296]

The biocompatibility of Ag NPs is not as good as that of their gold counterparts because of silver's oxidative nature, which drives genotoxic and cytotoxic outcomes.[297] Carlson et al.[298] determined the ability of Ag NPs (15, 30, and 55 nm) to induce oxidative stress within NR8383 rat alveolar macrophages. All particles were internalized by cells and elicited an increase in reactive oxygen species production, ultimately decreasing cell viability. The responses were size-dependent, with smaller particles exhibiting greater responses. They show a similar law to that of Au NPs.

The shape of NPs affects their cellular response. Chithrani et al.[299] investigated the uptake of negatively charged Au NSs (14, 30, 50, 74, and 100 nm) and Au NRs (14 nm × 40 nm and 14 × 74 nm) by HeLa cells after a 6-h exposure. They found that 50 nm spheres were taken up the fastest by the cells and that spheres were taken up more efficiently than were nanorods with corresponding dimensions.

The cytotoxicity of Au nanoshells is not very different from that of Au NSs. Hirsh et al.[300] and Loo et al.[301] reported the absence of any cytotoxic action by PEG- or immunoglobulin-coated nanoshells on human breast epithelial carcinoma or adenocarcinoma cells. Stern et al.[302] showed the absence of cytotoxicity when human prostate cancer cells were treated with nanoshells for 5−7 days. Liu et al.[303] showed the absence of any cytotoxic effect of nanoshells on human hepatocellular carcinoma cells.

Surface coating is also a key factor that determines the biocompatibility of NPs. The biocompatibility of cytotoxic NPs can be greatly increased by using proper coating materials. A featured example is surface modification-dependent toxicity of Au NRs. Using MTT assays of HeLa cells, Niidome et al.[304] demonstrated that hexadecyltrimethylammonium bromide (CTAB)-coated Au NRs were highly cytotoxic at as low as 0.05 mM (80% of dead cells). However, when CTAB was replaced with PEG-SH, 95% of cells were viable, with the Au NRs concentration being 0.5 mM. Further works demonstrated that the replacement or overcoating of CTAB with nontoxic stabilizers of PSS,[305] PAH,[306] or copolymer poly-(diallyldimethylammonium chloride)/polystyrene sulfonic acid[307] reduced the cytotoxicity of CTAB-stabilized Au NRs.

Surface charge also affects the toxicity of noble metal NPs. Rotello's group[308] investigated the toxicity of 2 nm Au NPs functionalized with either cationic or anionic surface groups in three different cell types. The results suggested that cationic particles are generally toxic at much lower concentrations than anionic particles are, which might result from the electrostatic interaction between the cationic NPs and the negatively charged cell membranes. Moreover, Lu et al.[309] demonstrated that coating PVP polymer on silver NPs prevents toxicity of the powder.

5. CONCLUSIONS AND REMARKS

As newly emerging optical nanoprobes, SERS tags have been synthesized by combining different types of metal nanomaterials, organic Raman reporters, and functional moieties. There has been a considerable amount of research on developing SERS tags for either molecular multiplexed detection or bioimaging at the level of microorganisms, cells, tissues, and living animals. Nevertheless, a number of opportunities and challenges remain. For example, to synthesize SERS tags with higher sensitivity and reproducibility, researchers must be able to fabricate high-performance, single NP-based SERS substrates, precisely control the placement of interparticle hot spots, and generate ultrasmall tags for single-molecule labeling and subcellular imaging.

Most studies have attempted to demonstrate proof-of-concept about SERS tags as novel optical probes. However, in the near future, these tags should make possible biomedical applications from *in vitro* clinical pathology to *in vivo* drug delivery tracing. Therefore, on one hand, engineering SERS-based multifunctional nanoplatforms combining the benefits of multiple imaging, drug loading, and diagnosis capacities will be an important and practical research field. On the other hand, the biocompatibility, toxicity, and long-term stability of nanomaterials in biological systems will undoubtedly be big concerns.[310−312] For instance, the toxicologic effect of SERS tags with different architectures, sizes, Raman reporters, and coatings needs to be deeply researched in parallel with Raman-related optical properties. Additionally, by taking advantage of the multiplex chemical information provided by Raman spectra,

novel biomedical instruments such as Raman-activated flow cytometers for cell sorting[313−315] and miniaturized microfluidic chips[239,316−318] for clinical analysis can be further developed.

AUTHOR INFORMATION

Corresponding Author

*Tel/Fax: +86 535 2109130. E-mail address: lxchen@yic.ac.cn.

Notes

The authors declare no competing financial interest.

Biographies

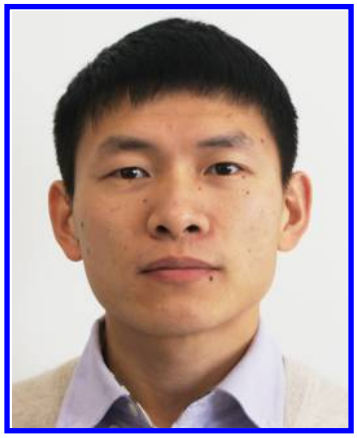

Yunqing Wang received his Ph.D. in Pharmaceutical Analysis from China Pharmaceutical University, Nanjing, China, in 2009. During the same year, he joined the Laboratory of Environmental Microanalysis and Monitoring of Dr. Lingxin Chen at the Yantai Institute of Coastal Zone Research, Chinese Academy of Sciences, as a research assistant. His current research interests focus on the development of quantum dot and noble metal nanoparticle based optical sensors and the applications in bioimaging.

Bing Yan received his Ph.D. from Columbia University in 1990 and carried out postdoctoral research at University of Cambridge, U.K., and University of Texas Medical School in Houston from 1990 to 1993. From 1993 to 2005, he worked at Novartis, Discovery Partners International, and Bristol-Myers Squibb. Now he is a full member at the Department of Chemical Biology and Therapeutics, St. Jude Children's Research Hospital, in Memphis, Tennessee, and professor at Shandong University, China. He serves as Associate Editor for *Journal of Combinatorial Chemistry* published by the American Chemical Society. He is also editor of the book series *Critical Reviews in Combinatorial Chemistry* published by the Francis & Taylor Group. He is interested in understanding the biological activities of nanoparticles, regulation of such activities by modifications of nanoparticle's surface using combinatorial chemistry, and medicinal applications of nanoparticles.

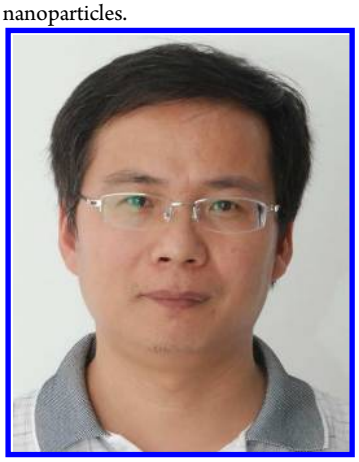

Lingxin Chen received his Ph.D. from the Dalian Institute of Chemical Physics, Chinese Academy of Sciences, China, in 2003. After two years of postdoctoral experience at the Department of Chemistry, Tsinghua University, China, he joined first as a BK21 researcher and then as a research professor at the Department of Applied Chemistry, Hanyang University, Ansan, Korea, in 2006. Now he is a professor in Yantai Institute of Coastal Zone Research, under the program so-called One Hundred Outstanding Young Chinese Scientists, Chinese Academy of Sciences, China. His research interests include study of novel properties of materials such as functionalization nanoparticles for developing nanometer biochemical analysis methods, molecular imprinting based sample pretreatment technology−chromatography (including microfluidic chip) combined technology, and the microbial degradation pollutant mechanism.

ACKNOWLEDGMENTS

We acknowledge financial support from the National Natural Science Foundation of China (Grant No. 21275158, 20975089, 81102415, 21077068, and 21137002), the National Basic Research Program of China (973 Program Grant No. 2010CB933504), the Innovation Projects of the Chinese Academy of Sciences (KZCX2-EW-206), the One Hundred Person Project of the Chinese Academy of Sciences, and the Natural Science Foundation of Shandong Province of China (Grant No. ZR2010BQ012).

REFERENCES

(1) Schlücker, S. *ChemPhysChem* **2009**, *10*, 1344.
(2) Fleischm, M.; Hendra, P. J.; McQuillan, A. J. *Chem. Phys. Lett.* **1974**, *26*, 163.
(3) Albrecht, M. G.; Creighton, J. A. *J. Am. Chem. Soc.* **1977**, *99*, 5215.
(4) Jeanmaire, D. L.; Vanduyne, R. P. *J. Electroanal. Chem.* **1977**, *84*, 1.
(5) Doering, W. E.; Piotti, M. E.; Natan, M. J.; Freeman, R. G. *Adv. Mater.* **2007**, *19*, 3100.
(6) Jarvis, R. M.; Goodacre, R. *Chem. Soc. Rev.* **2008**, *37*, 931.
(7) Qian, X. M.; Nie, S. M. *Chem. Soc. Rev.* **2008**, *37*, 912.
(8) Tripp, R. A.; Dluhy, R. A.; Zhao, Y. P. *Nano Today* **2008**, *3*, 31.
(9) Alvarez-Puebla, R. A.; Liz-Marzán, L. M. *Small* **2010**, *6*, 604.
(10) Xie, W.; Qiu, P.; Mao, C. *J. Mater. Chem.* **2011**, *21*, 5190.
(11) Kneipp, J.; Wittig, B.; Bohr, H.; Kneipp, K. *Theor. Chem. Acc.* **2010**, *125*, 319.
(12) Banholzer, M. J.; Millstone, J. E.; Qin, L.; Mirkin, C. A. *Chem. Soc. Rev.* **2008**, *37*, 885.

(13) Ansari, D. O. Raman-encoded nanoparticles for biomolecular detection and cancer diagnostics. Ph.D. dissertation, Georgia Institute of Technology, Atlanta, September 16, 2008.
(14) Campion, A.; Kambhampati, P. *Chem. Soc. Rev.* **1998**, *27*, 241.
(15) Kneipp, K.; Kneipp, H.; Itzkan, I.; Dasari, R. R.; Feld, M. S. *Chem. Rev.* **1999**, *99*, 2957.
(16) Moskovits, M. *J. Raman Spectrosc.* **2005**, *36*, 485.
(17) Kneipp, K.; Kneipp, H.; Kneipp, J. *Acc. Chem. Res.* **2006**, *39*, 443.
(18) Brus, L. *Acc. Chem. Res.* **2008**, *41*, 1742.
(19) Stiles, P. L.; Dieringer, J. A.; Shah, N. C.; Van Duyne, R. P. *Annu. Rev. Anal. Chem.* **2008**, *1*, 601.
(20) Kneipp, K.; Moskovits, M.; Kneipp, H. *Surface-Enhanced Raman Scattering: Physics and Applications*; Springer: New York, 2006.
(21) Kneipp, K. *Phys. Today* **2007**, *60*, 40.
(22) Lombardi, J. R.; Birke, R. L. *Acc. Chem. Res.* **2009**, *42*, 734.
(23) Guerrini, L.; Graham, D. *Chem. Soc. Rev.* **2012**, *41*, 7085.
(24) Kambhampati, P.; Child, C. M.; Foster, M. C.; Campion, A. *J. Chem. Phys.* **1998**, *108*, 5013.
(25) Kambhampati, P.; Child, C. M.; Campion, A. *J. Chem. Soc., Faraday Trans.* **1996**, *92*, 4775.
(26) Campion, A.; Ivanecky, J. E.; Child, C. M.; Foster, M. *J. Am. Chem. Soc.* **1995**, *117*, 11807.
(27) Michaels, A. M.; Jiang, J.; Brus, L. *J. Phys. Chem. B* **2000**, *104*, 11965.
(28) Nie, S.; Emory, S. R. *Science* **1997**, *275*, 1102.
(29) Kneipp, K.; Wang, Y.; Kneipp, H.; Perelman, L. T.; Itzkan, I.; Dasari, R.; Feld, M. S. *Phys. Rev. Lett.* **1997**, *78*, 1667.
(30) Kneipp, K.; Kneipp, H.; Itzkan, I.; Dasari, R. R.; Feld, M. S. *J. Phys.: Condens. Matter* **2002**, *14*, R597.
(31) Wang, R.; Yu, C. W.; Yu, F. B. A.; Chen, L. X. *TrAC, Trends Anal. Chem.* **2010**, *29*, 1004.
(32) Wang, Y.; Chen, L. *Nanomed.: Nanotechnol. Biol. Med.* **2011**, *7*, 385.
(33) Li, Z. Y.; Xia, Y. *Nano Lett.* **2010**, *10*, 243.
(34) McCreery, R. L. *Raman Spectroscopy for Chemical Analysis*; John Wiley & Sons: New York, 2000.
(35) Lakowicz, J. R. *Principles of Fluorescence Spectroscopy*; Springer: New York, 2006.
(36) Doering, W. E.; Nie, S. *Anal. Chem.* **2003**, *75*, 6171.
(37) Qian, X.; Peng, X. H.; Ansari, D. O.; Yin-Goen, Q.; Chen, G. Z.; Shin, D. M.; Yang, L.; Young, A. N.; Wang, M. D.; Nie, S. *Nat. Biotechnol.* **2008**, *26*, 83.
(38) Zrazhevskiy, P.; Sena, M.; Gao, X. *Chem. Soc. Rev.* **2010**, *39*, 4326.
(39) Frens, G. *Nature, Phys. Sci.* **1973**, *241*, 20.
(40) Cheng, Y.; A, C. S.; Meyers, J. D.; Panagopoulos, I.; Fei, B.; Burda, C. *J. Am. Chem. Soc.* **2008**, *130*, 10643.
(41) Ghosh, P.; Han, G.; De, M.; Kim, C. K.; Rotello, V. M. *Adv. Drug Delivery Rev.* **2008**, *60*, 1307.
(42) Zhang, Q.; Iwakuma, N.; Sharma, P.; Moudgil, B. M.; Wu, C.; McNeill, J.; Jiang, H.; Grobmyer, S. R. *Nanotechnology* **2009**, *20*, 395102.
(43) Lee, P. C.; Meisel, D. *J. Phys. Chem.* **1982**, *86*, 3391.
(44) Leopold, N.; Lendl, B. *J. Phys. Chem. B* **2003**, *107*, 5723.
(45) Link, S.; El-Sayed, M. A. *J. Phys. Chem. B* **1999**, *103*, 4212.
(46) Evanoff, D. D.; Chumanov, G. *J. Phys. Chem. B* **2004**, *108*, 13948.
(47) Abalde-Cela, S.; Aldeanueva-Potel, P.; Mateo-Mateo, C.; Rodríguez-Lorenzo, L.; Alvarez-Puebla, R. A.; Liz-Marzán, L. M. *J. R. Soc., Interface* **2010**, *7* (Suppl 4), S435.
(48) Hodak, J. H.; Martini, I.; Hartland, G. V. *J. Phys. Chem. B* **1998**, *102*, 6958.
(49) Liu, M. Z.; Guyot-Sionnest, P. *J. Phys. Chem. B* **2004**, *108*, 5882.
(50) Talley, C. E.; Jackson, J. B.; Oubre, C.; Grady, N. K.; Hollars, C. W.; Lane, S. M.; Huser, T. R.; Nordlander, P.; Halas, N. J. *Nano Lett.* **2005**, *5*, 1569.
(51) Njoki, P. N.; Lim, I. I. S.; Mott, D.; Park, H. Y.; Khan, B.; Mishra, S.; Sujakumar, R.; Luo, J.; Zhong, C. J. *J. Phys. Chem. C* **2007**, *111*, 14664.
(52) Seney, C. S.; Gutzman, B. M.; Goddard, R. H. *J. Phys. Chem. C* **2009**, *113*, 74.
(53) Sr, E.; Haskins, W. E.; Nie, S. M. *J. Am. Chem. Soc.* **1998**, *120*, 8009.
(54) Lee, S.; Chon, H.; Lee, M.; Choo, J.; Shin, S. Y.; Lee, Y. H.; Rhyu, I. J.; Son, S. W.; Oh, C. H. *Biosens. Bioelectron.* **2009**, *24*, 2260.
(55) Wang, H.; Kundu, J.; Halas, N. J. *Angew. Chem., Int. Ed.* **2007**, *46*, 9040.
(56) Lal, S.; Grady, N. K.; Kundu, J.; Levin, C. S.; Lassiter, J. B.; Halas, N. J. *Chem. Soc. Rev.* **2008**, *37*, 898.
(57) Schwartzberg, A. M.; Oshiro, T. Y.; Zhang, J. Z.; Huser, T.; Talley, C. E. *Anal. Chem.* **2006**, *78*, 4732.
(58) Chon, H.; Lee, S.; Son, S. W.; Oh, C. H.; Choo, J. *Anal. Chem.* **2009**, *81*, 3029.
(59) Ochsenkuhn, M. A.; Jess, P. R. T.; Stoquert, H.; Dholakia, K.; Campbell, C. J. *ACS Nano* **2009**, *3*, 3613.
(60) Rycenga, M.; Wang, Z.; Gordon, E.; Cobley, C. M.; Schwartz, A. G.; Lo, C. S.; Xia, Y. *Angew. Chem., Int. Ed.* **2009**, *48*, 9924.
(61) Fang, J.; Lebedkin, S.; Yang, S.; Hahn, H. *Chem. Commun.* **2011**, *47*, 5157.
(62) Huang, J.; Kim, K. H.; Choi, N.; Chon, H.; Lee, S.; Choo, J. *Langmuir* **2011**, *27*, 10228.
(63) Huang, Y.; Swarup, V. P.; Bishnoi, S. W. *Nano Lett.* **2009**, *9*, 2914.
(64) Jackson, J. B.; Halas, N. J. *Proc. Natl. Acad. Sci. U.S.A.* **2004**, *101*, 17930.
(65) Gellner, M.; Küstner, B.; Schlücker, S. *Vib. Spectrosc.* **2009**, *50*, 43.
(66) Loo, C.; Lin, A.; Hirsch, L.; Lee, M. H.; Barton, J.; Halas, N.; West, J.; Drezek, R. *Technol. Cancer Res. Treat.* **2004**, *3*, 33.
(67) Schwartzberg, A. M.; Olson, T. Y.; Talley, C. E.; Zhang, J. Z. *J. Phys. Chem. B* **2006**, *110*, 19935.
(68) Küstner, B.; Gellner, M.; Schütz, M.; Schöppler, F.; Marx, A.; Ströbel, P.; Adam, P.; Schmuck, C.; Schlücker, S. *Angew. Chem., Int. Ed.* **2009**, *48*, 1950.
(69) Souza, G. R.; Levin, C. S.; Hajitou, A.; Pasqualini, R.; Arap, W.; Miller, J. H. *Anal. Chem.* **2006**, *78*, 6232.
(70) Huang, X. H.; Neretina, S.; El-Sayed, M. A. *Adv. Mater.* **2009**, *21*, 4880.
(71) El-Sayed, M. A. *Acc. Chem. Res.* **2001**, *34*, 257.
(72) Huang, X.; El-Sayed, I. H.; Qian, W.; El-Sayed, M. A. *J. Am. Chem. Soc.* **2006**, *128*, 2115.
(73) von Maltzahn, G.; Centrone, A.; Park, J. H.; Ramanathan, R.; Sailor, M. J.; Hatton, T. A.; Bhatia, S. N. *Adv. Mater.* **2009**, *21*, 3175.
(74) Boca, S. C.; Astilean, S. *Nanotechnology* **2010**, *21*, 235601.
(75) Jiang, L.; Qian, J.; Cai, F.; He, S. *Anal. Bioanal. Chem.* **2011**, *400*, 2793.
(76) Wang, Z.; Zong, S.; Yang, J.; Song, C.; Li, J.; Cui, Y. *Biosens. Bioelectron.* **2010**, *26*, 241.
(77) Park, H.; Lee, S.; Chen, L.; Lee, E. K.; Shin, S. Y.; Lee, Y. H.; Son, S. W.; Oh, C. H.; Song, J. M.; Kang, S. H.; Choo, J. *Phys. Chem. Chem. Phys.* **2009**, *11*, 7444.
(78) Allgeyer, E. S.; Pongan, A.; Browne, M.; Mason, M. D. *Nano Lett.* **2009**, *9*, 3816.
(79) Schütz, M.; Steinigeweg, D.; Salehi, M.; Kömpe, K.; Schlücker, S. *Chem. Commun.* **2011**, *47*, 4216.
(80) Pazos-Pérez, N.; Barbosa, S.; Rodríguez-Lorenzo, L.; Aldeanueva-Potel, P.; Pérez-Juste, J.; Pastoriza-Santos, I.; Alvarez-Puebla, R. A.; Liz-Marzán, L. M. *J. Phys. Chem. Lett.* **2010**, *1*, 24.
(81) Rodríguez-Lorenzo, L.; Alvarez-Puebla, R. A.; Pastoriza-Santos, I.; Mazzucco, S.; Stéphan, O.; Kociak, M.; Liz-Marzán, L. M.; Garcia de Abajo, F. J. *J. Am. Chem. Soc.* **2009**, *131*, 4616.
(82) Rodríguez-Lorenzo, L.; Krpetic, Z.; Barbosa, S.; Alvarez-Puebla, R. A.; Liz-Marzán, L. M.; Prior, I. A.; Brust, M. *Integr. Biol.* **2011**, *3*, 922.

(83) Xie, J.; Zhang, Q.; Lee, J. Y.; Wang, D. I. *ACS Nano* **2008**, *2*, 2473.
(84) Xu, D.; Gu, J.; Wang, W.; Yu, X.; Xi, K.; Jia, X. *Nanotechnology* **2010**, *21*, 375101.
(85) Bechelany, M.; Brodard, P.; Elias, J.; Brioude, A.; Michler, J.; Philippe, L. *Langmuir* **2010**, *26*, 14364.
(86) Jena, B. K.; Mishra, B. K.; Bohidar, S. *J. Phys. Chem. C* **2009**, *113*, 14753.
(87) Yang, M.; Alvarez-Puebla, R.; Kim, H. S.; Aldeanueva-Potel, P.; Liz-Marzán, L. M.; Kotov, N. A. *Nano Lett.* **2010**, *10*, 4013.
(88) Senthil Kumar, P.; Pastoriza-Santos, I.; Rodríguez-González, B.; Javier García de Abajo, F.; Liz-Marzán, L. M. *Nanotechnology* **2008**, *19*, 015606.
(89) Barbosa, S.; Agrawal, A.; Rodríguez-Lorenzo, L.; Pastoriza-Santos, I.; Alvarez-Puebla, R. A.; Kornowski, A.; Weller, H.; Liz-Marzán, L. M. *Langmuir* **2010**, *26*, 14943.
(90) Guerrero-Martinez, A.; Barbosa, S.; Pastoriza-Santos, I.; Liz-Marzán, L. M. *Curr. Opin. Colloid Interface Sci.* **2011**, *16*, 118.
(91) Philip, D.; Gopchandran, K. G.; Unni, C.; Nissamudeen, K. M. *Spectrochim. Acta, A: Mol. Biomol. Spectrosc.* **2008**, *70*, 780.
(92) Pande, S.; Ghosh, S. K.; Praharaj, S.; Panigrahi, S.; Basu, S.; Jana, S.; Pal, A.; Tsukuda, T.; Pal, T. *J. Phys. Chem. C* **2007**, *111*, 10806.
(93) Shen, A. G.; Chen, L. F.; Xie, W.; Hu, J. C.; Zeng, A.; Richards, R.; Hu, J. M. *Adv. Funct. Mater.* **2010**, *20*, 969.
(94) Contreras-Cáceres, R.; Pastoriza-Santos, I.; Alvarez-Puebla, R. A.; Pérez-Juste, J.; Fernández-Barbero, A.; Liz-Marzán, L. M. *Chem.—Eur. J.* **2010**, *16*, 9462.
(95) Shen, A. G.; Guo, J. Z.; Xie, W.; Sun, M. X.; Richards, R.; Hu, J. M. *J. Raman Spectrosc.* **2011**, *42*, 879.
(96) Wang, Z.; Zong, S.; Li, W.; Wang, C.; Xu, S.; Chen, H.; Cui, Y. *J. Am. Chem. Soc.* **2012**, *134*, 2993.
(97) Wu, L.; Wang, Z.; Zong, S.; Huang, Z.; Zhang, P.; Cui, Y. *Biosens. Bioelectron.* **2012**, *38*, 94.
(98) Pinkhasova, P.; Yang, L.; Zhang, Y.; Sukhishvili, S.; Du, H. *Langmuir* **2012**, *28*, 2529.
(99) Rycenga, M.; Hou, K. K.; Cobley, C. M.; Schwartz, A. G.; Camargo, P. H.; Xia, Y. *Phys. Chem. Chem. Phys.* **2009**, *11*, 5903.
(100) Lee, S.; Kim, S.; Choo, J.; Shin, S. Y.; Lee, Y. H.; Choi, H. Y.; Ha, S.; Kang, K.; Oh, C. H. *Anal. Chem.* **2007**, *79*, 916.
(101) Sebba, D. S.; Watson, D. A.; Nolan, J. P. *ACS Nano* **2009**, *3*, 1477.
(102) Feng, Y.; Wang, Y.; Wang, H.; Chen, T.; Tay, Y. Y.; Yao, L.; Yan, Q.; Li, S.; Chen, H. *Small* **2012**, *8*, 246.
(103) Lim, D. K.; Jeon, K. S.; Hwang, J. H.; Kim, H.; Kwon, S.; Suh, Y. D.; Nam, J. M. *Nat. Nanotechnol.* **2011**, *6*, 452.
(104) Bosnick, K. A.; Jiang, J.; Brus, L. E. *J. Phys. Chem. B* **2002**, *106*, 8096.
(105) Halas, N. J.; Lal, S.; Chang, W. S.; Link, S.; Nordlander, P. *Chem. Rev.* **2011**, *111*, 3913.
(106) Driskell, J. D.; Lipert, R. J.; Porter, M. D. *J. Phys. Chem. B* **2006**, *110*, 17444.
(107) Brown, L. O.; Doorn, S. K. *Langmuir* **2008**, *24*, 2277.
(108) Tan, X.; Wang, Z.; Yang, J.; Song, C.; Zhang, R.; Cui, Y. *Nanotechnology* **2009**, *20*, 445102.
(109) Braun, G. B.; Lee, S. J.; Laurence, T.; Fera, N.; Fabris, L.; Bazan, G. C.; Moskovits, M.; Reich, N. O. *J. Phys. Chem. C* **2009**, *113*, 13622.
(110) Su, X.; Zhang, J.; Sun, L.; Koo, T. W.; Chan, S.; Sundararajan, N.; Yamakawa, M.; Berlin, A. A. *Nano Lett.* **2005**, *5*, 49.
(111) Futamata, M.; Yu, Y. Y.; Yanatori, T.; Kokubun, T. *J. Phys. Chem. C* **2010**, *114*, 7502.
(112) Tay, L. L.; Huang, P. J.; Tanha, J.; Ryan, S.; Wu, X.; Hulse, J.; Chau, L. K. *Chem. Commun.* **2012**, *48*, 1024.
(113) Huang, P. J.; Chau, L. K.; Yang, T. S.; Tay, L. L.; Lin, T. T. *Adv. Funct. Mater.* **2009**, *19*, 242.
(114) Jun, B. H.; Kim, J. H.; Park, H.; Kim, J. S.; Yu, K. N.; Lee, S. M.; Choi, H.; Kwak, S. Y.; Kim, Y. K.; Jeong, D. H.; Cho, M. H.; Lee, Y. S. *J. Comb. Chem.* **2007**, *9*, 237.
(115) Kim, K.; Lee, H. B.; Park, H. K.; Shin, K. S. *J. Colloid Interface Sci.* **2008**, *318*, 195.
(116) Li, J. M.; Ma, W. F.; Wei, C. A.; Guo, J.; Hu, J.; Wang, C. C. *J. Mater. Chem.* **2011**, *21*, 5992.
(117) Kim, J. H.; Kim, J. S.; Choi, H.; Lee, S. M.; Jun, B. H.; Yu, K. N.; Kuk, E.; Kim, Y. K.; Jeong, D. H.; Cho, M. H.; Lee, Y. S. *Anal. Chem.* **2006**, *78*, 6967.
(118) Wang, C. G.; Chen, Y.; Wang, T. T.; Ma, Z. F.; Su, Z. M. *Adv. Funct. Mater.* **2008**, *18*, 355.
(119) McNay, G.; Eustace, D.; Smith, W. E.; Faulds, K.; Graham, D. *Appl. Spectrosc.* **2011**, *65*, 825.
(120) Cho, S. J.; Ahn, Y. H.; Maiti, K. K.; Dinish, U. S.; Fu, C. Y.; Thoniyot, P.; Olivo, M.; Chang, Y. T. *Chem. Commun.* **2010**, *46*, 722.
(121) Maiti, K. K.; Dinish, U. S.; Fu, C. Y.; Lee, J. J.; Soh, K. S.; Yun, S. W.; Bhuvaneswari, R.; Olivo, M.; Chang, Y. T. *Biosens. Bioelectron.* **2010**, *26*, 398.
(122) Maiti, K. K.; Samanta, A.; Vendrell, M.; Soh, K. S.; Olivo, M.; Chang, Y. T. *Chem. Commun.* **2011**, *47*, 3514.
(123) Samanta, A.; Maiti, K. K.; Soh, K. S.; Liao, X.; Vendrell, M.; Dinish, U. S.; Yun, S. W.; Bhuvaneswari, R.; Kim, H.; Rautela, S.; Chung, J.; Olivo, M.; Chang, Y. T. *Angew. Chem., Int. Ed.* **2011**, *50*, 6089.
(124) Maiti, K. K.; Dinish, U. S.; Samanta, A.; Vendrell, M.; Soh, K.-S.; Park, S.-J.; Olivo, M.; Chang, Y.-T. *Nano Today* **2012**, *7*, 85.
(125) Gellner, M.; Kompe, K.; Schlücker, S. *Anal. Bioanal. Chem.* **2009**, *394*, 1839.
(126) Schütz, M.; Küstner, B.; Bauer, M.; Schmuck, C.; Schlücker, S. *Small* **2010**, *6*, 733.
(127) Jehn, C.; Küstner, B.; Adam, P.; Marx, A.; Ströbel, P.; Schmuck, C.; Schlücker, S. *Phys. Chem. Chem. Phys.* **2009**, *11*, 7499.
(128) Driskell, J. D.; Kwarta, K. M.; Lipert, R. J.; Porter, M. D.; Neill, J. D.; Ridpath, J. F. *Anal. Chem.* **2005**, *77*, 6147.
(129) Sun, L.; Sung, K. B.; Dentinger, C.; Lutz, B.; Nguyen, L.; Zhang, J.; Qin, H.; Yamakawa, M.; Cao, M.; Lu, Y.; Chmura, A. J.; Zhu, J.; Su, X.; Berlin, A. A.; Chan, S.; Knudsen, B. *Nano Lett.* **2007**, *7*, 351.
(130) Nguyen, C. T.; Nguyen, J. T.; Rutledge, S.; Zhang, J.; Wang, C.; Walker, G. C. *Cancer Lett.* **2010**, *292*, 91.
(131) Martin, L. C.; Larmour, I. A.; Faulds, K.; Graham, D. *Chem. Commun.* **2010**, *46*, 5247.
(132) Potara, M.; Maniu, D.; Astilean, S. *Nanotechnology* **2009**, *20*, 315602.
(133) Merican, Z.; Schiller, T. L.; Hawker, C. J.; Fredericks, P. M.; Blakey, I. *Langmuir* **2007**, *23*, 10539.
(134) Yang, M.; Chen, T.; Lau, W. S.; Wang, Y.; Tang, Q.; Yang, Y.; Chen, H. *Small* **2009**, *5*, 198.
(135) Weng, K. C.; Noble, C. O.; Papahadjopoulos-Sternberg, B.; Chen, F. F.; Drummond, D. C.; Kirpotin, D. B.; Wang, D.; Hom, Y. K.; Hann, B.; Park, J. W. *Nano Lett.* **2008**, *8*, 2851.
(136) Al-Jamal, W. T.; Al-Jamal, K. T.; Tian, B.; Cakebread, A.; Halket, J. M.; Kostarelos, K. *Mol. Pharmaceutics* **2009**, *6*, 520.
(137) Tam, N. C.; Scott, B. M.; Voicu, D.; Wilson, B. C.; Zheng, G. *Bioconjugate. Chem.* **2010**, *21*, 2178.
(138) Ip, S.; MacLaughlin, C. M.; Gunari, N.; Walker, G. C. *Langmuir* **2011**, *27*, 7024.
(139) Tam, N. C.; McVeigh, P. Z.; Macdonald, T. D.; Farhadi, A.; Wilson, B. C.; Zheng, G. *Bioconjugate Chem.* **2012**, *23*, 1726.
(140) Mulvaney, S. P.; Musick, M. D.; Keating, C. D.; Natan, M. J. *Langmuir* **2003**, *19*, 4784.
(141) Brady, C. I.; Mack, N. H.; Brown, L. O.; Doorn, S. K. *Anal. Chem.* **2009**, *81*, 7181.
(142) Li, J. F.; Huang, Y. F.; Ding, Y.; Yang, Z. L.; Li, S. B.; Zhou, X. S.; Fan, F. R.; Zhang, W.; Zhou, Z. Y.; Wu de, Y.; Ren, B.; Wang, Z. L.; Tian, Z. Q. *Nature* **2010**, *464*, 392.
(143) Liu, X.; Knauer, M.; Ivleva, N. P.; Niessner, R.; Haisch, C. *Anal. Chem.* **2010**, *82*, 441.
(144) Chiu, T. C.; Huang, C. C. *Sensors* **2009**, *9*, 10356.
(145) Wang, G.; Wang, Y.; Chen, L.; Choo, J. *Biosens. Bioelectron.* **2010**, *25*, 1859.

(146) Kim, K.; Lee, H. B.; Lee, Y. M.; Shin, K. S. *Biosens. Bioelectron.* **2009**, *24*, 1864.
(147) Lou, T.; Wang, Y.; Li, J.; Peng, H.; Xiong, H.; Chen, L. *Anal. Bioanal. Chem.* **2011**, *401*, 333.
(148) Yin, J.; Wu, T.; Song, J. B.; Zhang, Q.; Liu, S. Y.; Xu, R.; Duan, H. W. *Chem. Mater.* **2011**, *23*, 4756.
(149) Krpetic, Z.; Guerrini, L.; Larmour, I. A.; Reglinski, J.; Faulds, K.; Graham, D. *Small* **2012**, *8*, 707.
(150) Huang, G. G.; Hossain, M. K.; Han, X. X.; Ozaki, Y. *Analyst* **2009**, *134*, 2468.
(151) Zamarion, V. M.; Timm, R. A.; Araki, K.; Toma, H. E. *Inorg. Chem.* **2008**, *47*, 2934.
(152) Tsoutsi, D.; Montenegro, J. M.; Dommershausen, F.; Koert, U.; Liz-Marzán, L. M.; Parak, W. J.; Alvarez-Puebla, R. A. *ACS Nano* **2011**, *5*, 7539.
(153) Fabris, L.; Dante, M.; Nguyen, T. Q.; Tok, J. B. H.; Bazan, G. C. *Adv. Funct. Mater.* **2008**, *18*, 2518.
(154) Xu, S.; Ji, X.; Xu, W.; Li, X.; Wang, L.; Bai, Y.; Zhao, B.; Ozaki, Y. *Analyst* **2004**, *129*, 63.
(155) Wang, Y.; Wei, H.; Li, B.; Ren, W.; Guo, S.; Dong, S.; Wang, E. *Chem. Commun.* **2007**, *48*, 5220.
(156) Wang, Y.; Lee, K.; Irudayaraj, J. *Chem. Commun.* **2010**, *46*, 613.
(157) Chon, H.; Lee, S.; Yoon, S. Y.; Chang, S. I.; Lim, D. W.; Choo, J. *Chem. Commun.* **2011**, *47*, 12515.
(158) Zhang, H.; Harpster, M. H.; Park, H. J.; Johnson, P. A. *Anal. Chem.* **2011**, *83*, 254.
(159) Chen, S.; Yuan, Y.; Yao, J.; Han, S.; Gu, R. *Chem. Commun.* **2011**, *47*, 4225.
(160) Li, J.; Chen, L.; Lou, T.; Wang, Y. *ACS Appl. Mater. Interfaces* **2011**, *3*, 3936.
(161) Senapati, T.; Senapati, D.; Singh, A. K.; Fan, Z.; Kanchanapally, R.; Ray, P. C. *Chem. Commun.* **2011**, *47*, 10326.
(162) Vangala, K.; Yanney, M.; Hsiao, C.-T.; Wu, W. W.; Shen, R.-F.; Zou, S.; Sygula, A.; Zhang, D. *Anal. Chem.* **2010**, *82*, 10164.
(163) Yazgan, N. N.; Boyaci, I. H.; Topcu, A.; Tamer, U. *Anal. Bioanal. Chem.* **2012**, *403*, 2009.
(164) Li, M.; Zhang, J.; Suri, S.; Sooter, L. J.; Ma, D.; Wu, N. *Anal. Chem.* **2012**, *84*, 2837.
(165) Cui, Y.; Ren, B.; Yao, J. L.; Gu, R. A.; Tian, Z. Q. *J. Phys. Chem. B* **2006**, *110*, 4002.
(166) Chen, X.; Liu, H.; Zhou, X.; Hu, J. *Nanoscale* **2010**, *2*, 2841.
(167) Fabris, L.; Schierhorn, M.; Moskovits, M.; Bazan, G. C. *Small* **2010**, *6*, 1550.
(168) Yoon, K. J.; Seo, H. K.; Hwang, H.; Pyo, D.; Eom, I.-Y.; Hahn, J. H.; Jung, Y. M. *Bull. Kor. Chem. Soc.* **2010**, *31*, 1215.
(169) Han, X. X.; Chen, L.; Guo, J.; Zhao, B.; Ozaki, Y. *Anal. Chem.* **2010**, *82*, 4102.
(170) Song, C.; Wang, Z.; Zhang, R.; Yang, J.; Tan, X.; Cui, Y. *Biosens. Bioelectron.* **2009**, *25*, 826.
(171) Wang, G.; Lipert, R. J.; Jain, M.; Kaur, S.; Chakraboty, S.; Torres, M. P.; Batra, S. K.; Brand, R. E.; Porter, M. D. *Anal. Chem.* **2011**, *83*, 2554.
(172) Liu, R.; Liu, B.; Guan, G.; Jiang, C.; Zhang, Z. *Chem. Commun.* **2012**, *48*, 9421.
(173) Kang, T.; Yoo, S. M.; Yoon, I.; Lee, S. Y.; Kim, B. *Nano Lett.* **2010**, *10*, 1189.
(174) Hu, J.; Zhang, C.-y. *Anal. Chem.* **2010**, *82*, 8991.
(175) Kaittanis, C.; Santra, S.; Perez, J. M. *Adv. Drug Delivery Rev.* **2010**, *62*, 408.
(176) Huang, P. J.; Tay, L. L.; Tanha, J.; Ryan, S.; Chau, L. K. *Chem.—Eur. J.* **2009**, *15*, 9330.
(177) Khan, S. A.; Singh, A. K.; Senapati, D.; Fan, Z.; Ray, P. C. *Chem. Commun.* **2011**, *47*, 9444.
(178) Rule, K. L.; Vikesland, P. J. *Environ. Sci. Technol.* **2009**, *43*, 1147.
(179) Charan, S.; Chien, F. C.; Singh, N.; Kuo, C. W.; Chen, P. *Chem.—Eur. J.* **2011**, *17*, 5165.
(180) Wang, Y.; Ravindranath, S.; Irudayaraj, J. *Anal. Bioanal. Chem.* **2011**, *399*, 1271.
(181) Guven, B.; Basaran-Akgul, N.; Temur, E.; Tamer, U.; Boyaci, I. H. *Analyst* **2011**, *136*, 740.
(182) Kneipp, J.; Kneipp, H.; Rajadurai, A.; Redmond, R. W.; Kneipp, K. *J. Raman Spectrosc.* **2009**, *40*, 1.
(183) Kneipp, J.; Kneipp, H.; Wittig, B.; Kneipp, K. *Nanomed.: Nanotechnol., Biol. Med.* **2010**, *6*, 214.
(184) Kneipp, J. *Surf. Enhanced Raman Scattering* **2006**, *103*, 335.
(185) Wu, L. Y.; Ross, B. M.; Hong, S.; Lee, L. P. *Small* **2010**, *6*, 503.
(186) Sha, M. Y.; Xu, H.; Natan, M. J.; Cromer, R. *J. Am. Chem. Soc.* **2008**, *130*, 17214.
(187) Wang, X.; Qian, X.; Beitler, J. J.; Chen, Z. G.; Khuri, F. R.; Lewis, M. M.; Shin, H. J.; Nie, S.; Shin, D. M. *Cancer Res.* **2011**, *71*, 1526.
(188) Kneipp, J.; Kneipp, H.; McLaughlin, M.; Brown, D.; Kneipp, K. *Nano Lett.* **2006**, *6*, 2225.
(189) Kneipp, J.; Kneipp, H.; Kneipp, K. *Chem. Soc. Rev.* **2008**, *37*, 1052.
(190) Kneipp, J.; Kneipp, H.; Rice, W. L.; Kneipp, K. *Anal. Chem.* **2005**, *77*, 2381.
(191) Pallaoro, A.; Braun, G. B.; Reich, N. O.; Moskovits, M. *Small* **2010**, *6*, 618.
(192) Wang, F.; Widejko, R. G.; Yang, Z.; Nguyen, K. T.; Chen, H.; Fernando, L. P.; Christensen, K. A.; Anker, J. N. *Anal. Chem.* **2012**, *84*, 8013.
(193) Wang, Z.; Bonoiu, A.; Samoc, M.; Cui, Y.; Prasad, P. N. *Biosens. Bioelectron.* **2008**, *23*, 886.
(194) Kneipp, J.; Kneipp, H.; Wittig, B.; Kneipp, K. *J. Phys. Chem. C* **2010**, *114*, 7421.
(195) Maclaughlin, C. M.; Parker, E. P.; Walker, G. C.; Wang, C. *Nanomed.: Nanotechnol. Biol. Med.* **2013**, *9*, 55.
(196) Kennedy, D. C.; Duguay, D. R.; Tay, L. L.; Richeson, D. S.; Pezacki, J. P. *Chem. Commun.* **2009**, 6750.
(197) Kneipp, J.; Kneipp, H.; Wittig, B.; Kneipp, K. *Nano Lett.* **2007**, *7*, 2819.
(198) Kennedy, D. C.; Tay, L. L.; Lyn, R. K.; Rouleau, Y.; Hulse, J.; Pezacki, J. P. *ACS Nano* **2009**, *3*, 2329.
(199) Talley, C. E.; Jusinski, L.; Hollars, C. W.; Lane, S. M.; Huser, T. *Anal. Chem.* **2004**, *76*, 7064.
(200) Eliasson, C.; Loren, A.; Engelbrektsson, J.; Josefson, M.; Abrahamsson, J.; Abrahamsson, K. *Spectrochim. Acta, A: Mol. Biomol. Spectrosc.* **2005**, *61*, 755.
(201) Noh, M. S.; Jun, B. H.; Kim, S.; Kang, H.; Woo, M. A.; Minai-Tehrani, A.; Kim, J. E.; Kim, J.; Park, J.; Lim, H. T.; Park, S. C.; Hyeon, T.; Kim, Y. K.; Jeong, D. H.; Lee, Y. S.; Cho, M. H. *Biomaterials* **2009**, *30*, 3915.
(202) Kennedy, D. C.; Hoop, K. A.; Tay, L. L.; Pezacki, J. P. *Nanoscale* **2010**, *2*, 1413.
(203) Schlücker, S.; Küstner, B.; Punge, A.; Bonfig, R.; Marx, A.; Ströbel, P. *J. Raman Spectrosc.* **2006**, *37*, 719.
(204) Lutz, B.; Dentinger, C.; Sun, L.; Nguyen, L.; Zhang, J.; Chmura, A.; Allen, A.; Chan, S.; Knudsen, B. *J. Histochem. Cytochem.* **2008**, *56*, 371.
(205) Lutz, B. R.; Dentinger, C. E.; Nguyen, L. N.; Sun, L.; Zhang, J.; Allen, A. N.; Chan, S.; Knudsen, B. S. *ACS Nano* **2008**, *2*, 2306.
(206) Wang, Y.; Ye, C.; Wu, L.; Hu, Y. *J. Pharm. Biomed. Anal.* **2010**, *53*, 235.
(207) Chen, H.; Wang, Y.; Xu, J.; Ji, J.; Zhang, J.; Hu, Y.; Gu, Y. *J. Fluoresc.* **2008**, *18*, 801.
(208) Dothager, R. S.; Flentie, K.; Moss, B.; Pan, M. H.; Kesarwala, A.; Piwnica-Worms, D. *Curr. Opin. Biotechnol.* **2009**, *20*, 45.
(209) Li, C.; Wang, L. V. *Phys. Med. Biol.* **2009**, *54*, R59.
(210) Zavaleta, C.; de la Zerda, A.; Liu, Z.; Keren, S.; Cheng, Z.; Schipper, M.; Chen, X.; Dai, H.; Gambhir, S. S. *Nano Lett.* **2008**, *8*, 2800.
(211) Aswathy, R. G.; Yoshida, Y.; Maekawa, T.; Kumar, D. S. *Anal. Bioanal. Chem.* **2010**, *397*, 1417.
(212) Keren, S.; Zavaleta, C.; Cheng, Z.; de la Zerda, A.; Gheysens, O.; Gambhir, S. S. *Proc. Natl. Acad. Sci. U.S.A.* **2008**, *105*, 5844.

(213) Zavaleta, C. L.; Smith, B. R.; Walton, I.; Doering, W.; Davis, G.; Shojaei, B.; Natan, M. J.; Gambhir, S. S. *Proc. Natl. Acad. Sci. U.S.A.* **2009**, *106*, 13511.
(214) McQueenie, R.; Stevenson, R.; Benson, R.; Macritchie, N.; McInnes, I.; Maffia, P.; Faulds, K.; Graham, D.; Brewer, J.; Garside, P. *Anal. Chem.* **2012**, *84*, 5968.
(215) Fang, Y.; Seong, N. H.; Dlott, D. D. *Science* **2008**, *321*, 388.
(216) Chen, G.; Wang, Y.; Yang, M.; Xu, J.; Goh, S. J.; Pan, M.; Chen, H. *J. Am. Chem. Soc.* **2010**, *132*, 3644.
(217) Romo-Herrera, J. M.; Alvarez-Puebla, R. A.; Liz-Marzán, L. M. *Nanoscale* **2011**, *3*, 1304.
(218) Maneeprakorn, W.; Malik, M. A.; O'Brien, P. *J. Am. Chem. Soc.* **2010**, *132*, 1780.
(219) Guarrotxena, N.; Bazan, G. C. *Chem. Commun.* **2011**, *47*, 8784.
(220) Guarrotxena, N.; Liu, B.; Fabris, L.; Bazan, G. C. *Adv. Mater.* **2010**, *22*, 4954.
(221) Guarrotxena, N.; Ren, Y.; Mikhailovsky, A. *Langmuir* **2011**, *27*, 347.
(222) Tan, S. J.; Campolongo, M. J.; Luo, D.; Cheng, W. L. *Nat. Nanotechnol.* **2011**, *6*, 268.
(223) Sonnichsen, C.; Reinhard, B. M.; Liphardt, J.; Alivisatos, A. P. *Nat. Biotechnol.* **2005**, *23*, 741.
(224) Qian, X.; Zhou, X.; Nie, S. *J. Am. Chem. Soc.* **2008**, *130*, 14934.
(225) Lim, D. K.; Jeon, K. S.; Kim, H. M.; Nam, J. M.; Suh, Y. D. *Nat. Mater.* **2010**, *9*, 60.
(226) Mulvihill, M. J.; Ling, X. Y.; Henzie, J.; Yang, P. *J. Am. Chem. Soc.* **2010**, *132*, 268.
(227) Li, W.; Camargo, P. H.; Au, L.; Zhang, Q.; Rycenga, M.; Xia, Y. *Angew. Chem., Int. Ed.* **2010**, *49*, 164.
(228) Hanauer, M.; Pierrat, S.; Zins, I.; Lotz, A.; Sonnichsen, C. *Nano Lett.* **2007**, *7*, 2881.
(229) Novak, J. P.; Nickerson, C.; Franzen, S.; Feldheim, D. L. *Anal. Chem.* **2001**, *73*, 5758.
(230) Wei, G. T.; Liu, F. K.; Wang, C. R. *Anal. Chem.* **1999**, *71*, 2085.
(231) Sharma, V.; Park, K.; Srinivasarao, M. *Proc. Natl. Acad. Sci. U.S.A.* **2009**, *106*, 4981.
(232) Contado, C.; Argazzi, R. *J. Chromatogr., A* **2009**, *1216*, 9088.
(233) Qiu, P. H.; Mao, C. B. *Adv. Mater.* **2011**, *23*, 4880.
(234) Chen, G.; Wang, Y.; Tan, L. H.; Yang, M.; Tan, L. S.; Chen, Y.; Chen, H. *J. Am. Chem. Soc.* **2009**, *131*, 4218.
(235) Tyler, T. P.; Henry, A.-I.; Van Duyne, R. P.; Hersam, M. C. *J. Phys. Chem. Lett.* **2011**, *2*, 218.
(236) Schlücker, S. *Surface Enhanced Raman Spectroscopy. Analytical, Biophysical and Life Science Applications*; Wiley: Chichester, West Sussex, U.K., Hoboken, NJ, 2011.
(237) Smejkal, P.; Siskova, K.; Vlckova, B.; Pfleger, J.; Sloufova, I.; Slouf, M.; Mojzes, P. *Spectrochim. Acta, A: Mol. Biomol. Spectrosc.* **2003**, *59*, 2321.
(238) Peron, O.; Rinnert, E.; Toury, T.; Lamy de la Chapelle, M.; Compere, C. *Analyst* **2011**, *136*, 1018.
(239) Lee, S.; Choi, J.; Chen, L.; Park, B.; Kyong, J. B.; Seong, G. H.; Choo, J.; Lee, Y.; Shin, K. H.; Lee, E. K.; Joo, S. W.; Lee, K. H. *Anal. Chim. Acta* **2007**, *590*, 139.
(240) Loren, A.; Engelbrektsson, J.; Eliasson, C.; Josefson, M.; Abrahamsson, J.; Johansson, M.; Abrahamsson, K. *Anal. Chem.* **2004**, *76*, 7391.
(241) Bell, S. E.; Sirimuthu, N. M. *Analyst* **2004**, *129*, 1032.
(242) Stosch, R.; Henrion, A.; Schiel, D.; Guttler, B. *Anal. Chem.* **2005**, *77*, 7386.
(243) Yin, P. G.; Jiang, L.; Lang, X. F.; Guo, L.; Yang, S. *Biosens. Bioelectron.* **2011**, *26*, 4828.
(244) Bell, S. E.; Sirimuthu, N. M. *Chem. Soc. Rev.* **2008**, *37*, 1012.
(245) Taylor, R. W.; Lee, T. C.; Scherman, O. A.; Esteban, R.; Aizpurua, J.; Huang, F. M.; Baumberg, J. J.; Mahajan, S. *ACS Nano* **2011**, *5*, 3878.
(246) Woo, M. A.; Lee, S. M.; Kim, G.; Baek, J.; Noh, M. S.; Kim, J. E.; Park, S. J.; Minai-Tehrani, A.; Park, S. C.; Seo, Y. T.; Kim, Y. K.; Lee, Y. S.; Jeong, D. H.; Cho, M. H. *Anal. Chem.* **2009**, *81*, 1008.
(247) Dougan, J. A.; Faulds, K. *Analyst* **2012**, *137*, 545.
(248) Lee, S.; Chon, H.; Yoon, S. Y.; Lee, E. K.; Chang, S. I.; Lim, D. W.; Choo, J. *Nanoscale* **2012**, *4*, 124.
(249) Gregas, M. K.; Scaffidi, J. P.; Lauly, B.; Vo-Dinh, T. *Appl. Spectrosc.* **2010**, *64*, 858.
(250) Gregas, M. K.; Yan, F.; Scaffidi, J.; Wang, H. N.; Vo-Dinh, T. *Nanomed.: Nanotechnol., Biol. Med.* **2011**, *7*, 115.
(251) Zhang, P.; Guo, Y. *J. Am. Chem. Soc.* **2009**, *131*, 3808.
(252) Li, W.; Guo, Y.; Zhang, P. *J. Phys. Chem. C* **2010**, *114*, 7263.
(253) Li, W.; Miao, X.; Luk, T. S.; Zhang, P. *J. Phys. Chem. C* **2011**, *115*, 3318.
(254) Pinkhasova, P.; Puccio, B.; Chou, T.; Sukhishvili, S.; Du, H. *Chem. Commun.* **2012**, *48*, 9750.
(255) Lee, D. E.; Koo, H.; Sun, I. C.; Ryu, J. H.; Kim, K.; Kwon, I. C. *Chem. Soc. Rev.* **2012**, *41*, 2656.
(256) Contreras-Cáceres, R.; Abalde-Cela, S.; Guardia-Girós, P.; Fernández-Barbero, A.; Pérez-Juste, J.; Alvarez-Puebla, R. A.; Liz-Marzán, L. M. *Langmuir* **2011**, *27*, 4520.
(257) Spuch-Calvar, M.; Rodríguez-Lorenzo, L.; Morales, M. P.; Álvarez-Puebla, R. A.; Liz-Marzán, L. M. *J. Phys. Chem. C* **2009**, *113*, 3373.
(258) Hong, X.; Chu, X.; Zou, P.; Liu, Y.; Yang, G. *Biosens. Bioelectron.* **2010**, *26*, 918.
(259) Jun, B. H.; Noh, M. S.; Kim, J.; Kim, G.; Kang, H.; Kim, M. S.; Seo, Y. T.; Baek, J.; Kim, J. H.; Park, J.; Kim, S.; Kim, Y. K.; Hyeon, T.; Cho, M. H.; Jeong, D. H.; Lee, Y. S. *Small* **2010**, *6*, 119.
(260) Gole, A.; Agarwal, N.; Nagaria, P.; Wyatt, M. D.; Murphy, C. J. *Chem. Commun.* **2008**, *46*, 6140.
(261) Choi, J. Y.; Kim, K.; Shin, K. S. *Vib. Spectrosc.* **2010**, *53*, 117.
(262) Jun, B. H.; Noh, M. S.; Kim, G.; Kang, H.; Kim, J. H.; Chung, W. J.; Kim, M. S.; Kim, Y. K.; Cho, M. H.; Jeong, D. H.; Lee, Y. S. *Anal. Biochem.* **2009**, *391*, 24.
(263) Yu, K. N.; Lee, S. M.; Han, J. Y.; Park, H.; Woo, M. A.; Noh, M. S.; Hwang, S. K.; Kwon, J. T.; Jin, H.; Kim, Y. K.; Hergenrother, P. J.; Jeong, D. H.; Lee, Y. S.; Cho, M. H. *Bioconjugate. Chem.* **2007**, *18*, 1155.
(264) Wang, Z.; Zong, S.; Chen, H.; Wu, H.; Cui, Y. *Talanta* **2011**, *86*, 170.
(265) Cui, Y.; Zheng, X. S.; Ren, B.; Wang, R.; Zhang, J.; Xia, N. S.; Tian, Z. Q. *Chem. Sci.* **2011**, *2*, 1463.
(266) Kim, K.; Lee, Y. M.; Lee, H. B.; Shin, K. S. *Biosens. Bioelectron.* **2009**, *24*, 3615.
(267) Kim, K.; Lee, Y. M.; Lee, H. B.; Shin, K. S. *ACS Appl. Mater. Interfaces* **2009**, *1*, 2174.
(268) Wang, Z. Y.; Wu, H.; Wang, C. L.; Xu, S. H.; Cui, Y. P. *J. Mater. Chem.* **2011**, *21*, 4307.
(269) Qian, J.; Jiang, L.; Cai, F.; Wang, D.; He, S. *Biomaterials* **2011**, *32*, 1601.
(270) Alric, C.; Taleb, J.; Le Duc, G.; Mandon, C.; Billotey, C.; Le Meur-Herland, A.; Brochard, T.; Vocanson, F.; Janier, M.; Perriat, P.; Roux, S.; Tillement, O. *J. Am. Chem. Soc.* **2008**, *130*, 5908.
(271) Xiao, M.; Nyagilo, J.; Arora, V.; Kulkarni, P.; Xu, D.; Sun, X.; Dave, D. P. *Nanotechnology* **2010**, *21*, 035101.
(272) Park, C. W.; Rhee, Y. S.; Vogt, F. G.; Hayes, D., Jr.; Zwischenberger, J. B.; Deluca, P. P.; Mansour, H. M. *Adv. Drug Delivery Rev.* **2011**, *64*, 344.
(273) Yigit, M. V.; Zhu, L.; Ifediba, M. A.; Zhang, Y.; Carr, K.; Moore, A.; Medarova, Z. *ACS Nano* **2011**, *5*, 1056.
(274) Kircher, M. F.; de la Zerda, A.; Jokerst, J. V.; Zavaleta, C. L.; Kempen, P. J.; Mittra, E.; Pitter, K.; Huang, R. M.; Campos, C.; Habte, F.; Sinclair, R.; Brennan, C. W.; Mellinghoff, I. K.; Holland, E. C.; Gambhir, S. S. *Nat. Med.* **2012**, *18*, 829.
(275) Wang, C.; Ma, X.; Ye, S.; Cheng, L.; Yang, K.; Guo, L.; Li, C.; Li, Y.; Liu, Z. *Adv. Funct. Mater.* **2012**, *22*, 2363.
(276) Kim, J.; Park, S.; Lee, J. E.; Jin, S. M.; Lee, J. H.; Lee, I. S.; Yang, I.; Kim, J. S.; Kim, S. K.; Cho, M. H.; Hyeon, T. *Angew. Chem., Int. Ed.* **2006**, *45*, 7754.
(277) Kim, J.; Piao, Y.; Hyeon, T. *Chem. Soc. Rev.* **2009**, *38*, 372.
(278) Lu, W.; Singh, A. K.; Khan, S. A.; Senapati, D.; Yu, H.; Ray, P. C. *J. Am. Chem. Soc.* **2010**, *132*, 18103.

(279) Wu, P.; Gao, Y.; Zhang, H.; Cai, C. *Anal. Chem.* **2012**, *84*, 7692.
(280) Beqa, L.; Fan, Z.; Singh, A. K.; Senapati, D.; Ray, P. C. *ACS Appl. Mater. Interfaces* **2011**, *3*, 3316.
(281) Fales, A. M.; Yuan, H.; Vo-Dinh, T. *Langmuir* **2011**, *27*, 12186.
(282) Park, J. H.; von Maltzahn, G.; Ong, L. L.; Centrone, A.; Hatton, T. A.; Ruoslahti, E.; Bhatia, S. N.; Sailor, M. J. *Adv. Mater.* **2010**, *22*, 880.
(283) Wang, Y.; Chen, L.; Liu, P. *Chem.—Eur. J.* **2012**, *18*, 5435.
(284) Song, J.; Zhou, J.; Duan, H. *J. Am. Chem. Soc.* **2012**, *134*, 13458.
(285) Wang, Y.; Seebald, J. L.; Szeto, D. P.; Irudayaraj, J. *ACS Nano* **2010**, *4*, 4039.
(286) Thakor, A. S.; Paulmurugan, R.; Kempen, P.; Zavaleta, C.; Sinclair, R.; Massoud, T. F.; Gambhir, S. S. *Small* **2011**, *7*, 126.
(287) Murphy, C. J.; Gole, A. M.; Stone, J. W.; Sisco, P. N.; Alkilany, A. M.; Goldsmith, E. C.; Baxter, S. C. *Acc. Chem. Res.* **2008**, *41*, 1721.
(288) Johnston, H. J.; Hutchison, G.; Christensen, F. M.; Peters, S.; Hankin, S.; Stone, V. *Crit. Rev. Toxicol.* **2010**, *40*, 328.
(289) Khlebtsov, N.; Dykman, L. *Chem. Soc. Rev.* **2011**, *40*, 1647.
(290) Pan, Y.; Neuss, S.; Leifert, A.; Fischler, M.; Wen, F.; Simon, U.; Schmid, G.; Brandau, W.; Jahnen-Dechent, W. *Small* **2007**, *3*, 1941.
(291) Jiang, W.; Kim, B. Y.; Rutka, J. T.; Chan, W. C. *Nat. Nanotechnol.* **2008**, *3*, 145.
(292) Semmler-Behnke, M.; Kreyling, W. G.; Lipka, J.; Fertsch, S.; Wenk, A.; Takenaka, S.; Schmid, G.; Brandau, W. *Small* **2008**, *4*, 2108.
(293) Shukla, R.; Bansal, V.; Chaudhary, M.; Basu, A.; Bhonde, R. R.; Sastry, M. *Langmuir* **2005**, *21*, 10644.
(294) de la Fuente, J. M.; Berry, C. C. *Bioconjugate Chem.* **2005**, *16*, 1176.
(295) Gannon, C. J.; Patra, C. R.; Bhattacharya, R.; Mukherjee, P.; Curley, S. A. *J. Nanobiotechnol.* **2008**, *6*, 2.
(296) Cho, W. S.; Cho, M.; Jeong, J.; Choi, M.; Cho, H. Y.; Han, B. S.; Kim, S. H.; Kim, H. O.; Lim, Y. T.; Chung, B. H.; Jeong, J. *Toxicol. Appl. Pharmacol.* **2009**, *236*, 16.
(297) AshaRani, P. V.; Low Kah Mun, G.; Hande, M. P.; Valiyaveettil, S. *ACS Nano* **2009**, *3*, 279.
(298) Carlson, C.; Hussain, S. M.; Schrand, A. M.; Braydich-Stolle, L. K.; Hess, K. L.; Jones, R. L.; Schlager, J. J. *J. Phys. Chem. B* **2008**, *112*, 13608.
(299) Chithrani, B. D.; Ghazani, A. A.; Chan, W. C. *Nano Lett.* **2006**, *6*, 662.
(300) Hirsch, L. R.; Stafford, R. J.; Bankson, J. A.; Sershen, S. R.; Rivera, B.; Price, R. E.; Hazle, J. D.; Halas, N. J.; West, J. L. *Proc. Nat. Acad. Sci. U.S.A.* **2003**, *100*, 13549.
(301) Loo, C.; Lowery, A.; Halas, N.; West, J.; Drezek, R. *Nano Lett.* **2005**, *5*, 709.
(302) Stern, J. M.; Stanfield, J.; Lotan, Y.; Park, S.; Hsieh, J. T.; Cadeddu, J. A. *J. Endourol.* **2007**, *21*, 939.
(303) Liu, S. Y.; Liang, Z. S.; Gao, F.; Luo, S. F.; Lu, G. Q. *J. Mater. Sci. Mater. Med.* **2010**, *21*, 665.
(304) Niidome, T.; Yamagata, M.; Okamoto, Y.; Akiyama, Y.; Takahashi, H.; Kawano, T.; Katayama, Y.; Niidome, Y. *J. Controlled Release* **2006**, *114*, 343.
(305) Leonov, A. P.; Zheng, J.; Clogston, J. D.; Stern, S. T.; Patri, A. K.; Wei, A. *ACS Nano* **2008**, *2*, 2481.
(306) Alkilany, A. M.; Nagaria, P. K.; Hexel, C. R.; Shaw, T. J.; Murphy, C. J.; Wyatt, M. D. *Small* **2009**, *5*, 701.
(307) Hauck, T. S.; Ghazani, A. A.; Chan, W. C. *Small* **2008**, *4*, 153.
(308) Goodman, C. M.; McCusker, C. D.; Yilmaz, T.; Rotello, V. M. *Bioconjugate Chem.* **2004**, *15*, 897.
(309) Lu, W. T.; Senapati, D.; Wang, S. G.; Tovmachenko, O.; Singh, A. K.; Yu, H. T.; Ray, P. C. *Chem. Phys. Lett.* **2010**, *487*, 92.
(310) Mu, Q.; Broughton, D. L.; Yan, B. *Nano Lett.* **2009**, *9*, 4370.
(311) Bai, Y.; Zhang, Y.; Zhang, J.; Mu, Q.; Zhang, W.; Butch, E. R.; Snyder, S. E.; Yan, B. *Nat. Nanotechnol.* **2010**, *5*, 683.
(312) Liu, W.; Wu, Y.; Wang, C.; Li, H. C.; Wang, T.; Liao, C. Y.; Cui, L.; Zhou, Q. F.; Yan, B.; Jiang, G. B. *Nanotoxicology* **2010**, *4*, 319.
(313) Watson, D. A.; Brown, L. O.; Gaskill, D. F.; Naivar, M.; Graves, S. W.; Doorn, S. K.; Nolan, J. P. *Cytometry A* **2008**, *73*, 119.
(314) Jett, J. H. *Cytometry A* **2008**, *73*, 109.
(315) Goddard, G.; Brown, L. O.; Habbersett, R.; Brady, C. I.; Martin, J. C.; Graves, S. W.; Freyer, J. P.; Doorn, S. K. *J. Am. Chem. Soc.* **2010**, *132*, 6081.
(316) Cecchini, M. P.; Hong, J.; Lim, C.; Choo, J.; Albrecht, T.; Demello, A. J.; Edel, J. B. *Anal. Chem.* **2011**, *83*, 3076.
(317) Wang, G.; Lim, C.; Chen, L.; Chon, H.; Choo, J.; Hong, J.; deMello, A. J. *Anal. Bioanal. Chem.* **2009**, *394*, 1827.
(318) Strelau, K. K.; Kretschmer, R.; Moller, R.; Fritzsche, W.; Popp, J. *Anal. Bioanal. Chem.* **2010**, *396*, 1381.